DEUTSCHES ELEKTRONEN-SYNCHROTRON DESY

DESY 74/33
July 1974

Nucleon Resonance Production in e^+e^- Annihilation into $\bar{N}N\pi$

by

A.C. Hirshfeld
Abteilung Physik der Universität Dortmund

G. Kramer
II. Institut für Theoretische Physik der Universität Hamburg

D.H. Schiller
Detusches Elektronen-Synchrotron DESY, Hamburg
and
II. Institut für Theoretische Physik der Universität Hamburg

2 HAMBURG 52 · NOTKESTIEG 1

To be sure that your preprints are promptly included in the
HIGH ENERGY PHYSICS INDEX ,
send them to the following address (if possible by air mail) :

DESY
Bibliothek
2 Hamburg 52
Notkestieg 1
Germany

DESY 74/33
July 1974

Nucleon Resonance Production in e^+e^- Annihilation into $\bar{N}N\pi$

by

A.C. Hirshfeld
Abteilung Physik der Universität Dortmund

G. Kramer
II. Institut für Theoretische Physik der Universität Hamburg

D.H. Schiller
Detusches Elektronen-Synchrotron DESY, Hamburg
and
II. Institut für Theoretische Physik der Universität Hamburg

Abstract

The process $e^+e^- \longrightarrow N\bar{N}x$ is related by crossing to photo- and electroproduction. We relate the quantities of experimental interest in experiments with polarized or unpolarized beams to helicity and thence to invariant amplitudes according to a procedure developed in previous work. The invariant amplitudes are assumed to be dominated, in an appropriate q^2 range, by resonances in the two-body subchannels, of which the nucleon resonances in the pion-nucleon channels are the most important. Using a multipole decomposition of the amplitudes the resonance parameters are related to those measured in photo- and electroproduction. We use a generalized vector meson dominance model for the form factors in order to effect the q^2 - continuation. We calculate various cross-sections, angular distributions, and Dalitz plots in order to show how the results depend on the theoretical assumptions.

I. Introduction

The recent experiments which have been performed with the e^+e^- colliding beam facilities at CEA and SLAC [1] have revealed the gross features of the high energy production of multihadron final states in e^+e^- annihilation. A wealth of theoretical papers have attempted to utilize this data from a hitherto unexplored kinematical region to gain insight into the fundamental questions of photon-hadron interactions. Since the final goal in this area should be to understand the coupling of the virtual photon to hadrons it may be questioned whether the information at hand is really suitable for this purpose. At these high energies the final states are predominantly of high multiplicity, and even were one to measure the exclusive cross sections for these channels it is unclear whether one would be able to disentangle the dynamical mechanisms, which would probably still be masked by statistical effects. Our point of view is therefore that it would be more relevant to concentrate at first on low multiplicity final states, and to obtain precise data on specific channels over a range of energies.

First attempts in this direction have been made by the Orsay and Frascati groups, in measurements of several low-multiplicity mesonic channels [2]. In previous work [3] we have attempted to show how such channels should be analyzed in order to best extract the couplings of the virtual photon. Similar considerations have been presented in ref. [4].

It appears to us that baryonic channels of low multiplicity

should be even more advantageous in this respect as one has here independent information from scattering experiments on the couplings of the baryon resonances. This paper is concerned in particular with the $\bar{N}N\pi$ final state, for which the wealth of information produced by the extensive photoproduction and electroproduction experiments is at our disposal.

The process $e^+e^- \rightarrow \bar{N}N\pi$ (e^+e^- annihilation) is related through analytic continuation in the Mandelstam variables (s,t,u) and q^2 to the processes $e^-N \rightarrow e^-\pi N$ (electroproduction) together with $\gamma N \rightarrow \pi N$ (photoproduction), $\pi N \rightarrow e^+e^-N$ (lepton pair production), and $N\bar{N} \rightarrow \pi e^+e^-$ (nucleon-antinucleon annihilation). For electroproduction and photoproduction one possesses the extensive information already mentioned which includes the estimates of resonance couplings obtained through multipole analyses. Measurements on lepton-pair production are foreseen in the near future.

Despite the fact that from the electroproduction and photoproduction measurements one has some information about the q^2 dependence of the transition form factors $\gamma \rightarrow \bar{N}N^*$ in the space-like region ($q^2 \leq 0$), we still have the problem of continuation to large time-like q^2. Various parametrizations of the q^2-dependence, which are compatible with the available data in the space-like region, produce very different results in the time-like region. We discuss this effect by using various models for the transition form factors.

It is important that we formulate the nucleon resonance production in the framework of the $\bar{N}N\pi$ three-body final state and not of the

quasi two-body state $\bar{N}N^*$ in the narrow width approximation. The main reasons are

(a) since both the $N\pi$ and $\bar{N}\pi$ two-body sub-channels (s and u channel) are physical it is necessary to include coherent interference,

(b) the high spin resonances have strongly varying barrier factors which have been partially determined in the scattering region,

(c) that background effect due to stable one-particle intermediate states (Born terms) can be included.

In section II we consider the kinematics of the processes $e^+e^- \longrightarrow \bar{N}N\pi$. Section III shows how the transition form factors $\gamma \longrightarrow \bar{N}N^*$ may be defined in a fashion consistent with the usage common in analyses of electroproduction, and which is also suitable for use in time-like q^2 region. When these form factors are given, the invariant amplitudes may be constructed using the multipole decomposition. In sect. IV we present the results of calculations of various experimental distributions. We find that the cross sections for the various charge states are large enough to be easily measured with existing storage ring facilities.

II. Kinematics and General Formulae

2.1. Kinematics

We consider electron-positron annihilation into a pion and a nucleon-antinucleon pair in the one-photon-exchange approximation

(fig. 1)

$$e^-(p_-,\lambda_-) + e^+(p_+,\lambda_+) \longrightarrow \gamma_V(q,\lambda) \longrightarrow \bar{N}_1(p_1,\lambda_1) + N_2(p_2,\lambda_2) + \pi(p) \,, \qquad (2.1)$$

where we have indicated in brackets the momenta and helicities of the corresponding particles. Looking at (2.1) as the disintegration channel which results from the scattering channel $N_1 + \gamma_V \rightarrow N_2 + \pi$ by crossing the initial nucleon, we may define the Mandelstam invariants as usual

$$\begin{aligned} s &= (p_2 + p)^2 = (q - p_1)^2 \,, \\ t &= (p_1 + p_2)^2 = (q - p)^2 \,, \\ u &= (p_1 + p)^2 = (q - p_2)^2 \,, \end{aligned} \qquad (2.2)$$

satisfying

$$s + t + u = 2M^2 + m^2 + q^2 \,, \qquad (2.3)$$

where m(M) is the pion (nucleon) mass and $q^2 \geq (m+2M)^2 > 0$ the mass of the virtual time-like photon. The physical regions for the different channels are given by

$$\Phi(s,t,u;q^2) \equiv stu - M^2(q^2-m^2)^2 + (q^2-M^2)(M^2-m^2)t \geq 0 \qquad (2.4)$$

and are shown in fig.2a for $q^2 > 0$, and in fig.2b for $q^2 < 0$. (Note the $s \leftrightarrow u$ symmetry of the boundary curves $\Phi = 0$.) The physical region for our process (2.1) is the usual Dalitz plot for the decay $\gamma_V \rightarrow \bar{N}_1 + N_2 + \pi$. The s, t and u-channel for $q^2 > 0$ could be studied

via time-reversal invariance by observing $\pi + N_2 \to e^+ + e^- + N_1$, $\bar{N}_1 + N_2 \to e^+ + e^- + \pi$ and $\pi + \bar{N}_1 \to e^+ + e^- + N_2$, respectively. For $q^2 < 0$ there is no disintegration region and the s,t,u-channel can be studied experimentally by $e^\pm + N_1 \to e^\pm + \pi + N_2$ (pion electroproduction off nucleons), $e^\pm + \pi \to e^\pm + \bar{N}_1 + N_2$ and $e^\pm + \bar{N}_2 \to e^\pm + \pi + \bar{N}_1$, respectively. Our process (2.1) is thus related to pion electro- and photoproduction by analytic continuation in q^2 from space (light)-like $q^2 \leq 0$ to time-like $q^2 \geq (m+2M)^2$ and crossing of the initial nucleon. Therefore it seems advantageous to parametrize the process (2.1) in terms of quantities already used in pion electroproduction off nucleons.

2.2. Invariant amplitudes

The transition matrix element associated with the diagram of Fig. 1 is

$$T_{fi} = -\frac{e}{q^2}\,\bar{v}(p_+\lambda_+)\,\gamma^\mu\,u(p_-\lambda_-)\,\langle p_1\lambda_1, p_2\lambda_2, p\,|\,J^{em}_\mu(0)\,|\,0\rangle\,, \tag{2.5}$$

where J^{em}_μ is the electromagnetic current of the hadrons. As in electroproduction, we expand $\langle p_1\lambda_1, p_2\lambda_2, p\,|\,J^{em}_\mu(0)\,|\,0\rangle$ in terms of six invariant amplitudes $A_i(s,t,u;q^2)$

$$\langle p_1\lambda_1, p_2\lambda_2, p\,|\,J^{em}_\mu(0)\,|\,0\rangle = \sum_{i=1}^{6} A_i(s,t,u;q^2)\,\bar{u}(p_2\lambda_2)\,M^i_\mu\,v(p_1,\lambda_1)\,, \tag{2.6}$$

where $(a\cdot b \equiv a_\mu b^\mu)$

$$\begin{aligned}
M^1_\mu &= \tfrac{1}{2}\gamma_5\,(\gamma_\mu\, q\cdot\gamma - q\cdot\gamma\,\gamma_\mu)\,,\\
M^2_\mu &= -2\gamma_5\big(P_\mu\, q\cdot(p-\tfrac{1}{2}q) - P\cdot q\,(p-\tfrac{1}{2}q)_\mu\big), \qquad P \equiv \tfrac{1}{2}(p_2-p_1)\\
M^3_\mu &= \gamma_5\,(\gamma_\mu\, q\cdot p - q\cdot\gamma\, p_\mu)\,,\\
M^4_\mu &= 2\gamma_5\,(\gamma_\mu\, q\cdot P - q\cdot\gamma\, P_\mu) - 2M\,M^1_\mu\,,\\
M^5_\mu &= -\gamma_5\,(q_\mu\, q\cdot p - p_\mu\, q^2)\,,\\
M^6_\mu &= \gamma_5\,(q_\mu\, q\cdot\gamma - q^2\,\gamma_\mu)\,.
\end{aligned} \tag{2.7}$$

Each amplitude A_i may be further decomposed in the isotopic spin space as

$$A_i = A_i^{(0)} \tau_\alpha + A_i^{(+)} \delta_{\alpha 3} + A_i^{(-)} \frac{1}{2}(\tau_\alpha \tau_3 - \tau_3 \tau_\alpha), \tag{2.8}$$

where α is the (cartesian) isospin component of the pion. The amplitudes for different final charge states in (2.1) are related to the isospin invariant amplitudes as in electroproduction, namely

$$\begin{aligned} A(\bar{p}n\pi^+) &= \sqrt{2}\left(A^{(0)} + A^{(-)}\right) , \\ A(\bar{p}p\pi^0) &= A^{(0)} + A^{(+)} , \\ A(\bar{n}p\pi^-) &= \sqrt{2}\left(A^{(0)} - A^{(-)}\right) , \\ A(\bar{n}n\pi^0) &= -A^{(0)} + A^{(+)} , \end{aligned} \tag{2.9}$$

and

$$\begin{aligned} A^{(0)} &= A^{\frac{1}{2}S} , \\ A^{(+)} &= \frac{1}{3}\left(A^{\frac{1}{2}V} + 2A^{\frac{3}{2}V}\right) , \\ A^{(-)} &= \frac{1}{3}\left(A^{\frac{1}{2}V} - A^{\frac{3}{2}V}\right) , \end{aligned} \tag{2.10}$$

where the amplitudes A_i^{IS} and A_i^{IV} refer to a given isospin I = 1/2, 3/2 of the final (πN)-subsystem and to the isoscalar (S) and isovector (V) components of the electromagnetic current.

2.3. Cross sections in the helicity frame

To write down the cross section for process (2.1), let us first introduce two conveniently choosen reference frames in the overall c.m.s. ($\vec{q} = 0$), where $\vec{p}_1$, $\vec{p}_2$ and $\vec{p}$ are coplanar (production plane):

a) a system Oxyz with Oz along the beam direction $\vec{p}_-$ and Ox, Oy yet arbitrary, and b) a system OXYZ with OZ along $\vec{p}_1$ and OY along the normal to the production plane. Let the orientation of OXYZ with respect to Oxyz be specified by the Euler angles α, β, γ. Then it has been shown that [3,5]

$$\langle p_1\lambda_1, p_2\lambda_2, p | J^{em}_\sigma(0) | 0 \rangle = \sum_{\lambda=-1}^{+1} D^{1\,*}_{\sigma\lambda}(\alpha,\beta,\gamma)\, \Gamma^{(k)}_{\lambda_1\lambda_2;\lambda}(s,t,u;q^2), \qquad (2.11)$$

where J_σ are the spherical components $J_\pm = \mp(J_x \pm i J_y)/\sqrt{2}$, $J_o = J_z$ (the time component J_t doen't contribute to (2.5) because of current conservation), $D^1_{\sigma\lambda}$ is Wigner's rotation matrix and $\Gamma^{(k)}_{\lambda_1\lambda_2;\lambda}$ are helicity amplitudes describing the decay $Y_V \to \bar{N}_1 N_2 \pi$. Evaluating (2.6) and (2.11) in the frame OXYZ ($\alpha=\beta=\gamma=0$) and equating the results, we obtain the relation between the helicity and invariant amplitudes

$$\Gamma^{(k)}_{\lambda_1\lambda_2;\lambda} = \sum_{i=1}^{6} A_i\, F^i_{\lambda_1\lambda_2;\lambda}\,, \qquad (2.12)$$

where the real coefficients $F^i_{\lambda_1\lambda_2;\lambda}$ are given in Appendix A.

The cross section can now be obtained from [5] by observing that our $\Gamma^{(k)}_{\lambda_1\lambda_2;\lambda}$'s are proportional to the $\Gamma^{\lambda}_{\lambda_1\lambda_2}$'s for convention C-II of ref. [5]. The result for arbitrarily polarized $e^\pm$-beams is thus given by

$$\frac{d^5\sigma^{(h)}}{(d\alpha/2\pi)\,d\cos\beta\,(d\gamma/2\pi)\,dE_1\,dE_2} = \frac{3}{8}\left[(1+Z)(1+\cos^2\beta) + X(\alpha)\sin^2\beta\right]\frac{d^2\sigma_U^{(h)}}{dE_1\,dE_2}$$

$$+\frac{3}{4}(1+Z-X(\alpha))\sin^2\beta\;\frac{d^2\sigma_L^{(h)}}{dE_1\,dE_2} \qquad (2.13)$$

$$+\frac{3}{4}\left\{\left[(1+Z)\sin^2\beta + X(\alpha)(1+\cos^2\beta)\right]\cos 2\gamma + 2Y(\alpha)\cos\beta\sin 2\gamma\right\}\frac{d^2\sigma_T^{(h)}}{dE_1\,dE_2}$$

$$-\frac{3}{\sqrt{2}}\left[(1+Z-X(\alpha))\cos\beta\cos\gamma - Y(\alpha)\sin\gamma\right]\sin\beta\;\frac{d^2\sigma_{IR}^{(h)}}{dE_1\,dE_2}$$

$$+\frac{3}{\sqrt{2}}\left(\xi_x^{(+)} + \xi_x^{(-)}\right)\sin\beta\sin\gamma\;\frac{d^2\sigma_{II}^{(h)}}{dE_1\,dE_2}\quad,$$

where

$$\frac{d^2\sigma_U^{(h)}}{dE_1\,dE_2} = \frac{2\alpha}{12(2\pi)^2(q^2)^2}\sum_{\lambda_1\lambda_2}\left|\Gamma^{(h)}_{\lambda_1\lambda_2;+1}\right|^2\quad,\qquad\left(\alpha=\frac{e^2}{4\pi}=\frac{1}{137}\right)$$

$$\frac{d^2\sigma_L^{(h)}}{dE_1\,dE_2} = \frac{\alpha}{12(2\pi)^2(q^2)^2}\sum_{\lambda_1\lambda_2}\left|\Gamma^{(h)}_{\lambda_1\lambda_2;0}\right|^2\quad,$$

$$\frac{d^2\sigma_T^{(h)}}{dE_1\,dE_2} = \frac{\alpha}{12(2\pi)^2(q^2)^2}\sum_{\lambda_1\lambda_2}\left(\Gamma^{(h)}_{\lambda_1\lambda_2;+1}\,\Gamma^{(h)*}_{\lambda_1\lambda_2;-1}\right),$$

$$\frac{d^2\sigma_{IR}^{(h)}}{dE_1\,dE_2} = \frac{\alpha}{12(2\pi)^2(q^2)^2}\sum_{\lambda_1\lambda_2}\mathrm{Re}\left(\Gamma^{(h)}_{\lambda_1\lambda_2;+1}\,\Gamma^{(h)*}_{\lambda_1\lambda_2;0}\right), \qquad (2.14)$$

$$\frac{d^2\sigma_{II}^{(h)}}{dE_1\,dE_2} = \frac{\alpha}{12(2\pi)^2(q^2)^2}\sum_{\lambda_1\lambda_2}\mathrm{Im}\left(\Gamma^{(h)}_{\lambda_1\lambda_2;+1}\,\Gamma^{(h)*}_{\lambda_1\lambda_2;0}\right).$$

Here $E_1(E_2)$ is the energy of the antinucleon (nucleon) in the overall c.m.s. and X,Y,Z are given by

$$X(\alpha) = \left(\xi_x^{(+)}\xi_x^{(-)} - \xi_y^{(+)}\xi_y^{(-)}\right)\cos 2\alpha + \left(\xi_x^{(+)}\xi_y^{(-)} + \xi_y^{(+)}\xi_x^{(-)}\right)\sin 2\alpha\quad,$$

$$Y(\alpha) = -\left(\xi_x^{(+)}\xi_x^{(-)} - \xi_y^{(+)}\xi_y^{(-)}\right)\sin 2\alpha + \left(\xi_x^{(+)}\xi_y^{(-)} + \xi_y^{(+)}\xi_x^{(-)}\right)\cos 2\alpha\quad, \qquad (2.15)$$

$$Z = \xi_z^{(+)}\xi_z^{(-)}\quad,$$

where the components $\xi^{(\mp)}_{x,y,z}$ of the polarization vectors $\vec{\xi}^{(\mp)}$ (in the corresponding rest frames) of the electron (positron) refer to the frame Oxyz, i.e. $\xi^{(\mp)}_x$, $\xi^{(\mp)}_y$ mean transverse $(\perp \vec{p}_-)$ and $\xi^{(\mp)}_z$ longitudinal $(\parallel \vec{p}_-)$ beam polarization. The cross sections $\sigma^{(h)}_k$ $(k = U, L, T, IR, II)$ on the other hand are labelled according to the polarization of the virtual photon as seen in the frame OXYZ. This follows simply from (2.11), which for $\alpha = \beta = \gamma = 0$ reduces to $\langle p_1\lambda_1, p_2\lambda_2, p | J^{em}_\sigma(0) | 0\rangle = \Gamma^{(h)}_{\lambda_1\lambda_2;\,\lambda=\sigma}$, giving λ the meaning of the polarization with respect to OXYZ of the virtual photon. Thus $\sigma^{(h)}_U$ is the cross section for $\bar{N}_1 N_2 \pi$ production by an unpolarized transverse $(\perp \vec{p}_1)$ virtual photon; $\sigma^{(h)}_L$ by a longitudinal $(\parallel \vec{p}_1)$ virtual photon; $\sigma^{(h)}_T$ by a transverse polarized virtual photon, and $\sigma^{(h)}_{IR}$, $\sigma^{(h)}_{II}$ come from interference between transversely and longitudinally polarized virtual photons.

Note that the (α,β)-distribution as calculated from (2.13) gives the angular distribution of the antinucleon $\bar{N}_1$:

$$\frac{d^2\sigma^{(h)}}{(d\alpha/2\pi)\,d\cos\beta} = \frac{3}{8}\left[(1+I)(1+\cos^2\beta) + X(\alpha)\sin^2\beta\right]\sigma^{(h)}_U + \frac{3}{4}\left(1+I-X(\alpha)\right)\sin^2\beta\;\sigma^{(h)}_L \,, \qquad (2.16)$$

which depends on α only through $X(\alpha)$, i.e. the transverse polarization of both beams. The angle integrated Dalitz plot distribution

$$\frac{d^2\sigma^{(h)}}{dE_1\,dE_2} = (1+I)\left(\frac{d^2\sigma^{(h)}_U}{dE_1\,dE_2} + \frac{d^2\sigma^{(h)}_L}{dE_1\,dE_2}\right) \qquad (2.17)$$

and the total cross section

$$\sigma_{tot}^{(h)} = (1+Z)\left(\sigma_U^{(h)} + \sigma_L^{(h)}\right) \tag{2.18}$$

depend only on the sum $\sigma_U^{(h)} + \sigma_L^{(h)}$, as expected. For unpolarized beams we recover the results of ref. (3).

2.4. Cross sections in the transversity frame

For completeness we give also the relations referring to the case when the normal $\vec{n}$ to the production plane is used as an analyser. Then the transversity amplitudes $\Gamma^{(n)}_{\lambda_1\lambda_2;\lambda}$ instead of the helicity ones $\Gamma^{(h)}_{\lambda_1\lambda_2;\lambda}$ appear in (2.11) and $(\alpha,\beta,\gamma) \to (\alpha',\beta',\gamma')$, where (α',β',γ') give now the orientation with respect to Oxyz of a system OX'Y'Z' with OZ' along the normal $\vec{n} \sim \vec{p}_1 \times \vec{p}_2$ and OX' along $\vec{p}_1$. Since the $\Gamma^{(n)}_{\lambda_1\lambda_2;\lambda}$'s are nothing else than the $\Gamma^{\lambda}_{\lambda_1\lambda_2}$'s for convention C-I of ref. (5), we have the relation

$$\Gamma^{(n)}_{\lambda_1\lambda_2;\lambda} = \sum_{\lambda'} \Gamma^{(h)}_{\lambda_1\lambda_2;\lambda'} \, D^{1}_{\lambda'\lambda}\left(\tfrac{\pi}{2}, \tfrac{\pi}{2}, \pi\right). \tag{2.19}$$

The cross section is then given by

$$\begin{aligned}
\frac{d^5\sigma^{(n)}}{(d\alpha'/2\pi)\, d\cos\beta' \,(d\gamma'/2\pi)\, dE_1 dE_2} &= \frac{3}{8}\left[(1+Z)(1+\cos^2\beta') + X(\alpha')\sin^2\beta'\right] \frac{d^2\sigma_U^{(n)}}{dE_1\, dE_2} \\
&+ \frac{3}{4}\left(1+Z-X(\alpha')\right)\sin^2\beta' \; \frac{d^2\sigma_L^{(n)}}{dE_1 dE_2} \\
&+ \frac{3}{4}\left\{\left[(1+Z)\sin^2\beta' + X(\alpha')(1+\cos^2\beta')\right]\cos 2\gamma' + 2Y(\alpha')\cos\beta'\sin 2\gamma'\right\} \frac{d^2\sigma_{T3}^{(n)}}{dE_1 dE_2} \\
&- \frac{3}{4}\left\{\left[(1+Z)\sin^2\beta' + X(\alpha')(1+\cos^2\beta')\right]\sin 2\gamma' - 2Y(\alpha')\cos\beta'\cos 2\gamma'\right\} \frac{d^2\sigma_{T1}^{(n)}}{dE_1 dE_2} \\
&+ \frac{3}{4}\left(\xi_z^{(+)} + \xi_z^{(-)}\right)\cos\beta' \; \frac{d^2\sigma_{T2}^{(n)}}{dE_1 dE_2} \quad ,
\end{aligned} \tag{2.20}$$

where

$$\frac{d^2\sigma_U^{(n)}}{dE_1 dE_2} = \frac{\alpha}{12(2\pi)^2(q^2)^2} \sum_{\lambda_1\lambda_2} \left(\left| \Gamma^{(n)}_{\lambda_1\lambda_2;+1} \right|^2 + \left| \Gamma^{(n)}_{\lambda_1\lambda_2;-1} \right|^2 \right) ,$$

$$\frac{d^2\sigma_L^{(n)}}{dE_1 dE_2} = \frac{\alpha}{12(2\pi)^2(q^2)^2} \sum_{\lambda_1\lambda_2} \left| \Gamma^{(n)}_{\lambda_1\lambda_2;0} \right|^2 ,$$

$$\frac{d^2\sigma_{T3}^{(n)}}{dE_1 dE_2} = \frac{\alpha}{12(2\pi)^2(q^2)^2} \sum_{\lambda_1\lambda_2} Re \left(\Gamma^{(n)}_{\lambda_1\lambda_2;+1} \Gamma^{(n)*}_{\lambda_1\lambda_2;-1} \right) , \qquad (2.21)$$

$$\frac{d^2\sigma_{T1}^{(n)}}{dE_1 dE_2} = \frac{\alpha}{12(2\pi)^2(q^2)^2} \sum_{\lambda_1\lambda_2} Im \left(\Gamma^{(n)}_{\lambda_1\lambda_2;+1} \Gamma^{(n)*}_{\lambda_1\lambda_2;-1} \right) ,$$

$$\frac{d^2\sigma_{T2}^{(n)}}{dE_1 dE_2} = \frac{\alpha}{12(2\pi)^2(q^2)^2} \sum_{\lambda_1\lambda_2} \left(\left| \Gamma^{(n)}_{\lambda_1\lambda_2;+1} \right|^2 - \left| \Gamma^{(n)}_{\lambda_1\lambda_2;-1} \right|^2 \right) .$$

Here the indices $k = U, L, T1, T2, T3$ of $\sigma_k^{(n)}$ refer to the polarization of the virtual photon as seen in the frame OX'Y'Z': so "longitudinal" ($\lambda=0$) means along the normal $\vec{n}$ and "transverse" ($\lambda=\pm1$) means perpendicular to $\vec{n}$, i.e. in the production plane. The numbers in T1, T2 and T3 mean that the corresponding cross sections are induced by a virtual photon whose transverse polarization is characterized by the Stokes parameter [6] P'_1, P'_2 and P'_3 respectively. These are defined by

$$\rho^{(\gamma)}_{transv.} = \frac{1}{2}\left(1 + \vec{P}'\cdot\vec{\sigma}\right) , \qquad (2.22)$$

where $\rho^{(\gamma)}_{transv.}$ is the transverse part of the density matrix of the virtual photon [5], evaluated in the frame OX'Y'Z'. (*)

(*) Note that in this terminology $\sigma_T^{(h)}$ in (2.14) is induced by P_3 calculated from $\rho^{(\gamma)}_{transv.}$ in the frame OXYZ of subsect. 2.3.

Note that now the (α', β') -distribution gives the angular distribution of the normal to the production plane

$$\frac{d^2\sigma^{(n)}}{(d\alpha'/2\pi)\,d\cos\beta'} = \frac{3}{8}\left[(1+Z)(1+\cos^2\beta') + X(\alpha')\sin^2\beta'\right]\sigma_U^{(n)} + \frac{3}{4}\left(1+Z-X(\alpha')\right)\sin^2\beta'\;\sigma_L^{(n)} + \frac{3}{4}\left(\xi_z^{(+)}+\xi_z^{(-)}\right)\cos\beta\;\sigma_{T2}^{(n)}\,, \tag{2.23}$$

which in contrast to (2.16) depends not only on $\sigma_U^{(n)}$ and $\sigma_L^{(n)}$, but also on $\sigma_{T2}^{(n)}$ if at least one of the $e^{\pm}$-beams is longitudinally polarized.

The angle integrated Dalitz plot distributions have the same form as (2.17) and (2.18).

Finally, using (2.19) in (2.21), we can relate the transversity $\sigma_k^{(n)}$ and helicity $\sigma_k^{(h)}$ cross sections through

$$\begin{aligned}
\sigma_U^{(n)} &= \tfrac{1}{2}\sigma_U^{(h)} - \sigma_T^{(h)} + \sigma_L^{(h)}\,,\\
\sigma_L^{(n)} &= \tfrac{1}{2}\sigma_U^{(h)} + \sigma_T^{(h)}\,,\\
\sigma_{T3}^{(n)} &= \tfrac{1}{4}\sigma_U^{(h)} - \tfrac{1}{2}\sigma_T^{(h)} - \tfrac{1}{2}\sigma_L^{(h)}\,,\\
\sigma_{T1}^{(n)} &= \sqrt{2}\;\sigma_{IR}^{(h)}\,,\\
\sigma_{T2}^{(n)} &= 2\sqrt{2}\;\sigma_{II}^{(h)}\,.
\end{aligned} \tag{2.24}$$

We have

$$\sigma_U^{(n)} + \sigma_L^{(n)} = \sigma_U^{(h)} + \sigma_L^{(h)}\,, \tag{2.25}$$

as expected for the angle integrated cross-section.

III. Dynamical Model for the Invariant Amplitudes

3.1. Born amplitudes

The Born term contributions to the invariant amplitudes are the same as in electroproduction, namely:

$$A_1^{(0,\pm)} = \frac{eg}{2} F_1^{(S,V)}(q^2)\left(\frac{1}{s-M^2} + \eta^{(0,\pm)}\frac{1}{u-M^2}\right),$$

$$A_2^{(0,\pm)} = -\frac{eg}{t-m^2} F_1^{(S,V)}(q^2)\left(\frac{1}{s-M^2} + \eta^{(0,\pm)}\frac{1}{u-M^2}\right),$$

$$A_3^{(0,\pm)} = -\frac{eg}{2} F_2^{(S,V)}(q^2)\left(\frac{1}{s-M^2} - \eta^{(0,\pm)}\frac{1}{u-M^2}\right), \qquad (3.1)$$

$$A_4^{(0,\pm)} = -\frac{eg}{2} F_2^{(S,V)}(q^2)\left(\frac{1}{s-M^2} + \eta^{(0,\pm)}\frac{1}{u-M^2}\right),$$

$$A_5^{(0,\pm)} = -\frac{eg}{2(t-m^2)} F_1^{(S,V)}(q^2)\left(\frac{1}{s-M^2} - \eta^{(0,\pm)}\frac{1}{u-M^2}\right) - \eta_t^{(0,\pm)}\frac{2eg}{q^2(t-m^2)}\left(F_\pi(q^2) - F_1^{(V)}(q^2)\right),$$

$$A_6^{(0,\pm)} = 0,$$

with $\eta^{(0)} = \eta^{(+)} = 1$, $\eta^{(-)} = -1$, $\eta_t^{(0)} = \eta_t^{(+)} = 0$ and $\eta_t^{(-)} = 1$.

For the pion form factor it is sufficient to use naive VMD [7]

$$F_\pi(q^2) = \frac{1}{1 - \frac{q^2}{m_\varrho^2}}. \qquad (3.2)$$

For the nucleon form factors it is well known that this is insufficient. The commonly used dipole parametrization for the electric and magnetic form factors is obviously ill-suited for continuation into the time-like region. It is more reasonable to take here also a parametrization based on some form of vector dominance, and we chose a parametrization due to Felst [8], which has the advantage that besides accounting for the measured data in the space-like region it also extrapolates

through the Frascati point for $e^+e^- \leftrightarrow p\bar{p}$ at $\sqrt{q^2} = 2.1$ GeV [9] as noted in ref. [10]. This parametrization includes besides the ρ,ω and ϕ mesons an effective $\rho''(1500)$ and a $\omega''(1500)$:

$$F_1^{(S)}(q^2) = 2\left(\frac{0.837}{1-q^2/m_\omega^2} - \frac{0.169}{1-q^2/m_\phi^2} - \frac{0.168}{1-q^2/m_{\omega''}^2}\right)$$

$$F_1^{(V)}(q^2) = 2\left(\frac{0.66}{1-q^2/m_\rho^2} - \frac{0.16}{1-q^2/m_{\rho''}^2}\right) \qquad (3.3)$$

$$F_2^{(S)}(q^2) = \frac{1}{M}\left(\frac{2.23}{1-q^2/m_\omega^2} - \frac{3.72}{1-q^2/m_\phi^2} + \frac{1.43}{1-q^2/m_{\omega''}^2}\right)$$

$$F_2^{(V)}(q^2) = \frac{1}{M}\left(\frac{2.97}{1-q^2/m_\rho^2} - \frac{1.12}{1-q^2/m_{\rho''}^2}\right)$$

The electric and magnetic form factors are given by:

$$G_E^{(S)}(q^2) = F_1^{(S)}(q^2) + (q^2/4M^2)\ 2M F_2^{(S)}(q^2)$$

$$G_E^{(V)}(q^2) = F_1^{(V)}(q^2) + (q^2/4M^2)\ 2M F_2^{(V)}(q^2)$$

$$G_M^{(S)}(q^2) = \left(F_1^{(S)}(q^2) + 2M F_2^{(S)}(q^2)\right)/0.88 \qquad (3.4)$$

$$G_M^{(V)}(q^2) = \left(F_1^{(V)}(q^2) + 2M F_2^{(V)}(q^2)\right)/4.70$$

The advantage of working with these form factors is that the threshold condition $G_E(q^2) = G_M(q^2)$ at $q^2 = 4M^2$, which is near the region in which we shall be interested, is automatically fulfilled. The form factors are exhibited in fig. 3 and compared to the dipole form $G_D = (1-q^2/0.71)^{-2}$. For small space-like q^2 values, where data are available, the "scaling law" $G_{E,M}^{(S,V)} \approx G_D$

is approximately satisfied. We notice that in this parametrization the neutron electric form factor G_E^n has a zero at $q^2 \approx -2.5$ GeV^2 and is appreciably different from zero at higher negative q^2. These features would show up in measurements of elastic and quasi-elastic electron-deuteron scattering.

3.2. Multipole amplitudes

The Mandelstam diagram of fig.2a shows that in the kinematical region we are considering, $\sqrt{q^2} \lesssim 4$ GeV^2, the Dalitz plot region for $\gamma \to \bar{N}N\pi$ is rather densely covered by the resonance bands of the s- and u-channel pion-nucleon resonances.(*) This leads us to consider a resonance model for the amplitudes which takes into account the s- and u-channel nucleon resonances. The known t-channel resonances are far away from the physical region and may be safely ignored. Furthermore we shall ignore genuine three-body interactions and higher order rescattering effects (see for example ref. (11)).

Our procedure consisted in the construction of the invariant amplitudes A_i in the electroproduction region $(s \geq (M+m)^2\ ,\ t \leq 0)$, where data is available, from the multipole amplitudes according to (12)

$$A(s,t;q^2) = B^{-1}(s,t;q^2)\, C(s;q^2) \sum_{\ell=0}^{\infty} G_\ell(x)\, M_\ell(s;q^2)\ . \qquad (3.5)$$

B and C are kinematical matrices depending on s,t, and q^2; the G_ℓ's are given in terms of derivatives of the Legendre polynomials in $x = \cos\theta_s$. We then used eq. (3.5) to perform the continuation to the annihilation region : $(M+m)^2 \leq s \leq (\sqrt{q^2}-M)^2$, $4M^2 \leq t \leq (\sqrt{q^2}-m)^2$. The q^2-continuation is controlled by the resonance form factors, which we now discuss.

(*) A resonance of mass m_R lies inside the Dalitz plot if $\sqrt{q^2} \geq (m_R + M)$.

The contribution of an s-channel resonance of mass m_R and width Γ_R to a multipole $\mathcal{M}_\ell = M_\ell, E_\ell$ is parametrized as follows:

$$\mathcal{M}_\ell(s;q^2) = \mathcal{M}_0\, G(q^2) \cdot \frac{m_R \Gamma_R}{m_R^2 - s - i m_R \Gamma} \times \left(\frac{|\vec{p}|}{|\vec{p}_R|}\right)^\ell \left(\frac{|\vec{p}_R|^2 + X_\pi^2}{|\vec{p}|^2 + X_\pi^2}\right)^{\ell/2} \times \left(\frac{|\vec{q}|}{|\vec{q}_R^{(0)}|}\right)^x \left(\frac{|\vec{q}_R^{(0)}|^2 + X_\gamma^2}{|\vec{q}|^2 + X_\gamma^2}\right)^{x/2} . \tag{3.6}$$

Here $\mathcal{M}_0$ is the coupling constant; X_π, X_γ are parameters characterizing the barrier factors at the vertices $R \to N\pi$ and $R \to N\gamma$, respectively; $x = \ell$ for $M_{\ell\pm}$, $E_{\ell+}$ and $x = \ell - 2$ for $E_{\ell-}$ $(\ell \geq 2)$. The widths Γ are

$$\Gamma \equiv \Gamma_R \left(\frac{|\vec{p}|}{|\vec{p}_R|}\right)^{2\ell+1} \left(\frac{|\vec{p}_R|^2 + X_\pi^2}{|\vec{p}|^2 + X_\pi^2}\right)^\ell . \tag{3.7}$$

$\vec{p}$ and $\vec{q}$ are the momentum of the pion and the virtual photon in the resonance rest frame:

$$|\vec{p}| = \frac{1}{2\sqrt{s}} \sqrt{\lambda(s, M^2, m^2)} \quad , \qquad |\vec{q}| = \frac{1}{2\sqrt{s}} \sqrt{\lambda(s, M^2, q^2)} \quad ; \tag{3.8}$$

$|\vec{p}_R|$ is $|\vec{p}|$ evaluated at $s = m_R^2$, $|\vec{q}_R^{(0)}|$ is $|\vec{q}|$ at $s = m_R^2$, $q^2 = 0$.

The Breit-Wigner form (3.6) incorporates the following features: a) it has the correct threshold behavior $|\vec{p}|^{\ell}$ as $|\vec{p}| \to 0$, and $|\vec{q}|^{x}$ as $|\vec{q}| \to 0$; b) the unbounded increase of the threshold factors $|\vec{p}|^{\ell}$ with s, and $|\vec{q}|^{x}$ with s and q^2 is compensated by the barrier factors containing X_π, X_γ. Hence the entire q^2 dependence of $\mathcal{M}_\ell(s;q^2)$ for q^2 away from threshold is given by the form factor $G(q^2)$.

We can also write (3.6) as (*)

$$\mathcal{M}_\ell(s;q^2) = \mathcal{M}_\ell(s;0)\, G(q^2) \left(\frac{|\vec{q}|}{|\vec{q}^{(0)}|}\right)^{x} \left(\frac{|\vec{q}^{(0)}|^2 + X_\gamma^2}{|\vec{q}|^2 + X_\gamma^2}\right)^{x/2}, \tag{3.9}$$

where $\mathcal{M}_\ell(s;0)$ are the photoproduction multipoles:

$$\mathcal{M}_\ell(s;0) = \mathcal{M}_0 \left(\frac{|\vec{p}_R|}{|\vec{p}|}\,\frac{|\vec{q}_R^{(0)}|}{|\vec{q}^{(0)}|}\right)^{1/2} \frac{m_R \left(\Gamma \Gamma_\gamma\right)^{1/2}}{m_R^2 - s - i m_R \Gamma}, \tag{3.10}$$

with

$$\Gamma_\gamma = \Gamma_R \left(\frac{|\vec{q}^{(0)}|}{|\vec{q}_R^{(0)}|}\right)^{2x+1} \left(\frac{|\vec{q}_R^{(0)}|^2 + X_\gamma^2}{|\vec{q}^{(0)}|^2 + X_\gamma^2}\right)^{x} \tag{3.11}$$

in analogy to (3.7) . $|\vec{q}^{(0)}|$ is $|\vec{q}|$ as in (3.8), evaluated at $q^2 = 0$. Eq. (3.10) with $X_\gamma = X_\pi$ is the parametrization

---

(*) In electroproduction [7,13] the last factor in (3.9) is omitted, the large-s dependence of $|\vec{q}|^{x}$ being compensated by taking the factor containing X_π in (3.6) to the power ℓ instead of $\ell/2$.

used by Walker [14] in his multipole analysis of single-pion photoproduction. We can thus in principle take the resonance parameters $(m_R, \Gamma_R, l, x, X_\pi, \mathcal{M}_0)$ from the photoproduction analysis. Continuation to electroproduction or annihilation involves only the form factors $G(q^2)$ of eq. (3.9) for the electric and magnetic multipoles, as well as the additional scalar multipoles which do not contribute in photoproduction.

The resonance parameters we have used in our calculations are listed in Table 1. Except for X_γ they have all been taken from the electroproduction analyses of Devenish and Lyth [7,13]. The couplings $\mathcal{M}_0^{\frac{1}{2}(S)}$, $\mathcal{M}_0^{\frac{1}{2}(V)}$ and $\mathcal{M}_0^{3/2\,(V)}$ correspond to definite isospin states $I = 1/2, 3/2$ of the (π,N) subsystem and to the isoscalar and isovector component of the electromagnetic current. They are related via (3.12) to the couplings $\mathcal{M}_0^{\pi^+n}$, $\mathcal{M}_0^{\pi^0p}$ and $\mathcal{M}_0^{\pi^-p}$ which correspond to specific physical final states and which are tabulated in refs. [7,13]:

$$\mathcal{M}_0^{1/2\,(S)} = \frac{1}{2\sqrt{2}}\left(\mathcal{M}_0^{\pi^+n} + \mathcal{M}_0^{\pi^-p}\right),$$

$$\mathcal{M}_0^{1/2\,(V)} = \frac{3}{2\sqrt{2}}\left(\mathcal{M}_0^{\pi^+n} - \mathcal{M}_0^{\pi^-p}\right), \qquad (3.12)$$

$$\mathcal{M}_0^{3/2\,(V)} = -\frac{3}{\sqrt{2}}\,\mathcal{M}_0^{\pi^+n} = \frac{3}{\sqrt{2}}\,\mathcal{M}_0^{\pi^-p}.$$

Similarly we use the electric and magnetic form factors $G_E^{1/2\,(S)}$, $G_E^{1/2\,(V)}$, $G_M^{1/2\,(S)}$ and $G_M^{1/2\,(V)}$ for resonances of isospin I = 1/2, and $G_E^{3/2\,(S)}$, $G_M^{3/2\,(V)}$ for I = 3/2 resonances. Since there is very little direct information on these form factors, even in the

space-like region, we had recourse to the following two sets of assumptions:

(i) In the interests of simplicity we first use one overall form factor for all the nucleon resonances. As is common in electroproduction analyses, we relate this form factor to one of the nucleon electromagnetic form factors:

$$G_{E,M}^{1/2(S)} = G_{E,M}^{1/2(V)} = G_{E,M}^{3/2(V)} = G_M^{(V)} , \tag{3.13}$$

where $G_M^{(V)}$ is the magnetic isovector nucleon form factor of eq. (3.4). One uses here $G_M^{(V)}$ rather than one of the other nucleon form factors because the only resonance form factor for which some measurements exist, that of the $P_{33}(1236)$, is predominantly due to the magnetic multipole; $G_M^{(V)}$ is actually fairly close to the dipole form G_D in the q^2-range $-3 \leq q^2 \leq 0$ (see fig. 3).

Having set the form factors G according to (3.13) we can now adjust our multipoles to optimal agreement with the electroproduction multipoles of Devenish and Lyth by an appropriate choice of the as yet undetermined parameter X_γ in the q^2 range $-3 \leq q^2 \leq 0$. This choice turns out to be $X_\gamma = 1$ GeV for the $P_{33}(1236)$ resonance, and $X_\gamma = 1.5$ for all others. The smaller value of X_γ for P_{33} implies a faster fall-off of $M_{1+}(s;q^2)$ with q^2 than that of the other resonances; compared to these other resonances, which

fall off in the parametrization of Devenish and Lyth as G_D, the P_{33} falls off as $G_D \times (1 - q^2/4)^{-1}$ for $-3 < q^2 < 0$.

(ii) In a vector dominance model it would be natural to expect different form factors for the isoscalar and isovector components of the electromagnetic current, corresponding to the different vector mesons which control the different channels. To account for this we have considered, besides the choice of form factors of eq. (3.13), also the choice

$$G_{E,M}^{1/2(S)} = G_{E,M}^{(S)} \,, \qquad G_{E,M}^{1/2(V)} = G_{E,M}^{3/2(V)} = G_{E,M}^{(V)} \,, \tag{3.14}$$

where $G_{E,M}^{(S)}$ and $G_{E,M}^{(V)}$ are the isoscalar and isovector nucleon form factors of eq. (3.4).

For the scalar multipoles $S_{\ell\pm}(s;q^2)$ we follow Devenish and Lyth and set $S_\ell = 0$ for all the resonances except P_{33}, for which we take

$$S_{1+}(s;q^2) = -0.05\, M_{1+}(s;q^2) \frac{|\vec{q}|}{|\vec{q}_R^{(0)}|} \left(\frac{|\vec{q}_R^{(0)}|^2 + X_T^2}{|\vec{q}|^2 + X_T^2} \right)^{1/2} , \tag{3.15}$$

where $M_{1+}(s;q^2)$ is the magnetic multipole of P_{33}.

In general we based our calculation on the electroproduction analysis of Devenish and Lyth [7,13]. We are aware of the ambiguities inherent in such analysis, as discussed in detail for example in ref. [15]. For our purposes, however, these more detailed considerations will be important only when data in the annihilation region become available.

3.3. Crossing properties

So far we have only considered the contributions of the s-channel resonances, given by eqs. (3.5) and (3.6). To obtain

the contribution of the u-channel resonances we use the crossing properties of the $A_i^{(0,\pm)}(s,t,u;q^2)$: The u-channel amplitudes $A_i^{(0,\pm)}(u,t;q^2)$ are obtained from the s-channel amplitudes $A_i^{(0,\pm)}(s,t;q^2)$ of eq. (2.10) by substituting u for s. The complete, crossing-symmetric amplitudes are then

$$A_i^{(0,\pm)}(s,t,u;q^2) = A_i^{(0,\pm)}(s,t;q^2) + \eta^{(0,\pm)}\eta_i A_i^{(0,\pm)}(u,t;q^2), \qquad (3.16)$$

where the $\eta^{(0,\pm)}$ are given after eq. (3.1) and $\eta_1 = \eta_2 = \eta_4 = +1$, $\eta_3 = \eta_5 = \eta_6 = -1$.

From the properties of (3.16) under crossing ($s \leftrightarrow u$), or, equivalently, from charge conjugation invariance the following relations follow:

$$\frac{d\sigma}{ds}(e^+e^- \to \bar{p}n\pi^+) = \frac{d\sigma}{du}(e^+e^- \to p\bar{n}\pi^-),$$

$$\frac{d\sigma}{ds}(e^+e^- \to \bar{n}p\pi^-) = \frac{d\sigma}{du}(e^+e^- \to n\bar{p}\pi^+),$$

$$\frac{d\sigma}{ds}(e^+e^- \to \bar{p}p\pi^0) = \frac{d\sigma}{du}(e^+e^- \to p\bar{p}\pi^0), \qquad (3.17)$$

$$\frac{d\sigma}{ds}(e^+e^- \to \bar{n}n\pi^0) = \frac{d\sigma}{du}(e^+e^- \to n\bar{n}\pi^0).$$

Since $ds \sim dE_1$ and $du \sim dE_2$, where E_1 and E_2 are the energies of $\bar{N}_1$ and N_2 in the overall c.m.s., the relations (3.17) imply the equality of the corresponding distributions in E_1 and E_2.

We have also

$$\sigma_{tot}(e^+e^- \to \bar{p}n\pi^+) = \sigma_{tot}(e^+e^- \to \bar{n}p\pi^-). \qquad (3.18)$$

IV. Discussion of Results

Up to now no measurements of the processes $e^+e^- \to \bar{p}p\pi^o$, $\bar{p}n\pi^+$, $\bar{n}p\pi^-$ and $\bar{n}n\pi^o$ have been carried out. We would urge that such measurements be undertaken at Frascati, SLAC, DESY, and Orsay. With cross sections of the order of magnitude which we have estimated such measurements would be well within the capacity of at least some of these laboratories.

4.1. Total cross sections

Our estimates for the total integrated cross sections, $\sigma_{tot} = \sigma_U + \sigma_L$, for the reactions $e^+e^- \to \bar{p}n\pi^+$, $\bar{p}p\pi^o$ and $\bar{n}n\pi^o$ are shown in fig. 4 (solid curves). Figs. 4(a)-(c) are calculated using an overall form factor for all the resonances, as discussed in section III (see (3.13)). In this model the general shape of the total cross sections as a function of q^2 is mainly determined by the contribution of the $P_{33}(1236)$, which reaches a maximum of, e.g., around 4 nb for the $\bar{p}p\pi^o$ final state. To see the effect of the interference between different resonance contributions we have calculated the incoherent sum (dashed curves) of the single resonance contributions (for the $\bar{p}n\pi^+$ and $\bar{p}p\pi^o$ final states). We see that for $\bar{p}n\pi^+$ this effect is sizable, of the order of a factor of two. Figs. 4(d)-(f) show the results of the calculation with different

isoscalar and isovector form factors as given by eq. (3.14). Here we see already in the total cross sections strong effects due to the contributions of the higher resonances, especially in the $\bar{p}n\pi^+$ and $\bar{n}n\pi^o$ channels.

To understand the above structure in detail we exhibit in fig. 5 the contributions of the individual resonances to the cross sections. The hierarchy of the resonances is roughly as in photoproduction; the P_{33}, D_{13}, F_{15} and F_{37} resonances are the most important. The s-wave resonances $S_{11}(1506)$, $S_{31}(1630)$ and $S_{11}(1700)$ are suppressed, although their couplings are not negligible (see Table I). This is due to the effect of the threshold factor (see (3.6)) which enhances resonances with larger ℓ . It is important to note that these factors would by themselves lead to an unbounded rise of the cross sections (for resonances with $\ell > 0$), were their effect not cancelled by the barrier factors in (3.6), which restore the fall-off with increasing q^2 expected for individual resonances due to the form factors. (*)

The contribution of $P_{33}(1236)$ is reduced in $e^+e^- \to \bar{p}n\pi^+$ by roughly a factor of three compared to $\bar{p}p\pi^o$, due to isospin. Since the higher resonances are, for this choice of the resonance form factors, all rather small, they can give rise to appreciable interference effects only in the $\bar{p}n\pi^+$ channel. This is seen in figs. 4(a)-(b).

In the case of different isoscalar and isovector form factors (figs. 5(d)-(f)) we notice that the hierarchy of resonances is somewhat

(*) The neglect of these barrier factors in previous work [3] led to cross sections which rose with q^2.

different than in the case of an overall form factor (figs. 5(a)-(c)). In particular the F_{15} is now rather prominent and takes on values comparable to the P_{33} contribution in $e^+e^- \to \bar{p}n\pi^+$ and $\bar{n}n\pi^o$. In fact in the $\bar{p}n\pi^+$ final state (fig. 4(d)) the F_{15} peak dominates the q^2-dependence of the total cross section.

4.2. Differential cross sections

The study of differential cross sections is much more informative than the integrated cross section. We consider first the Dalitz plot distributions, eq. (2.17). Whereas most of the curves for σ_{tot} show only the contribution of P_{33} as the dominant structure one sees in all the Dalitz plots the contributions of the other resonances as well (at energies above the respective thresholds). For example we show in fig. 6 the $d\sigma/dE_1$ distributions (projections of the Dalitz plots) for the two form factor choices and the four channels $\bar{p}n\pi^+$, $\bar{n}p\pi^-$, $\bar{p}p\pi^o$ and $\bar{n}n\pi^o$, at $\sqrt{q^2} = 3.3$ GeV. Depending on the particular final state one can see the contributions of the first, second, third and fourth resonance regions, with varying relative strengths. For example for $e^+e^- \to \bar{n}p\pi^-$ the resonances of the third region dominate the $d\sigma/dE_1$ distribution, fig. 6(b), even though their contribution is not apparent in the $d\sigma/dE_2$ distribution (which by (3.17) is the same as the $d\sigma/dE_1$ distribution for $e^+e^- \to \bar{p}n\pi^+$), fig. 6(a), and does not show up as a bump in σ_{tot}, fig. 4(a).

Of course in many cases a structure for example in $d\sigma/dE_1$ contains reflections of resonances in the crossed channel $d\sigma/dE_2$ [16]. For instance in fig. 6(g) the sharp structure at low E_1 values for $d\sigma/dE_1(e^+e^- \to \bar{p}p\pi^o)$ is such a reflection. The way in which such

reflections occur is much more transparent if one looks at the full Dalitz plot. For illustration we show in fig. 7(a) and 7(b) the contribution to the Dalitz plot of the single resonances $F_{15}(1690)$ and $S_{11}(1700)$, respectively. One sees that resonances of high angular momentum in one channel produce sharp structures in the other channel near the kinematical boundary, whereas for s-wave resonances this effect does not occur.

In order to get a general impression of the full Dalitz plot if all resonances are included we show in fig. 8 the results for two channels and for the two choices of the resonance form factors.

Further detailed information is contained in the angular distributions (2.13) integrated over E_1 and E_2. We exhibit in fig. 9 the cross sections $\sigma_L^{(k)}$, $\sigma_T^{(k)}$, $\sigma_{IR}^{(k)}$ and $\sigma_{II}^{(k)}$ which determine the angular distributions. These cross sections are large enough to be measured, at least in some energy range, except $\sigma_{II}^{(k)}$ for $e^+e^- \to \bar{p}p\pi^0$ and $e^+e^- \to \bar{n}n\pi^0$ which remain very small over the whole range and which therefore are not included in the figures.

Acknowledgement

We wish to thank Dr. R.C.E. Devenish for instructing us in the art of electroproduction analysis and in the use of his computer program for the construction of the invariant amplitudes. We also thank Dr. W.A. McNeely for helping us to produce the three-dimensional plots with his WAM 715 routine.

Appendix A

We give now the real coefficients $F^{i}_{\lambda_1\lambda_2;\lambda}$ appearing in (2.12) and relating the invariant to the helicity amplitudes for the decay $\gamma_v \to \bar{N}_1 N_2 \pi$ into final particles of masses m_1, m_2 and m, respectively. In terms of the independent variables

$$
\begin{aligned}
W &= \sqrt{q^2} \ , \\
E_1 &= \frac{1}{2W}\left(W^2 + m_1^2 - s\right) \ , \\
E_2 &= \frac{1}{2W}\left(W^2 + m_2^2 - u\right) \ ,
\end{aligned}
\tag{A.1}
$$

the dependent ones

$$
\begin{aligned}
p_i &= \sqrt{E_i^2 - m_i^2} \qquad (i = 1,2) \ , \\
\cos\theta &= \frac{1}{2p_1 p_2}\left[(W - E_1 - E_2)^2 - p_1^2 - p_2^2 - m^2\right] \ ,
\end{aligned}
\tag{A.2}
$$

and the notations

$$
\begin{aligned}
A_{\pm} &= W\left[(E_1+m_1)(E_2+m_2)\right]^{-\frac{1}{2}}\left[p_1(E_2+m_2) \pm p_2(E_1+m_1)\right] \ , \\
B_{\pm} &= W\left[(E_1+m_1)(E_2+m_2)\right]^{-\frac{1}{2}}\left[(E_1+m_1)(E_2+m_2) \pm p_1 p_2\right] \ ,
\end{aligned}
\tag{A.3}
$$

we have:

$$
\begin{aligned}
F^{1}_{++;0} &= \sin\tfrac{\theta}{2}\left\{ A_+ \right\} \\
F^{2}_{++;0} &= \sin\tfrac{\theta}{2}\left\{ \tfrac{1}{2}\left[(W-4E_1)p_2\cos\theta - (W-4E_2)p_1\right] B_+ \right\} \\
F^{3}_{++;0} &= \sin\tfrac{\theta}{2}\left\{ (W-E_1-E_2)A_- + (p_1 + p_2\cos\theta) B_- \right\} \\
F^{4}_{++;0} &= \sin\tfrac{\theta}{2}\left\{ (E_2-E_1)A_- - (m_1+m_2)A_+ + (p_1 - p_2\cos\theta) B_- \right\} \\
F^{5}_{++;0} &= \sin\tfrac{\theta}{2}\left\{ W(p_1 + p_2\cos\theta) B_+ \right\} \\
F^{6}_{++;0} &= \sin\tfrac{\theta}{2}\left\{ - W A_- \right\}
\end{aligned}
\tag{A.4}
$$

$$F^{i}_{--;0} = F^{i}_{++;0} \qquad (i = 1,2,\dots,6) \tag{A.5}$$

$$\begin{aligned}
F^{1}_{+-;0} &= \cos\tfrac{\theta}{2}\{\, A_- \,\} \\
F^{2}_{+-;0} &= \cos\tfrac{\theta}{2}\{\, \tfrac{1}{2}[(W-4E_1)p_2\cos\theta - (W-4E_2)p_1\,]B_- \,\} \\
F^{3}_{+-;0} &= \cos\tfrac{\theta}{2}\{\, (W-E_1-E_2)A_+ + (p_1+p_2\cos\theta)B_+ \,\} \\
F^{4}_{+-;0} &= \cos\tfrac{\theta}{2}\{\, (E_2-E_1)A_+ - (m_1+m_2)A_- + (p_1-p_2\cos\theta)B_+ \,\} \\
F^{5}_{+-;0} &= \cos\tfrac{\theta}{2}\{\, W(p_1+p_2\cos\theta)B_- \,\} \\
F^{6}_{+-;0} &= \cos\tfrac{\theta}{2}\{\, -WA_+ \,\}
\end{aligned} \tag{A.6}$$

$$F^{i}_{-+;0} = -F^{i}_{+-;0} \qquad (i = 1,2,\dots,6) \tag{A.7}$$

$$\begin{aligned}
F^{1}_{++;\pm} &= \sqrt{2}\cos\tfrac{\theta}{2}\{\, A_+ \begin{pmatrix}1\\0\end{pmatrix} \,\} \\
F^{2}_{++;\pm} &= \sqrt{2}\cos\tfrac{\theta}{2}\{\, \tfrac{1}{2}(W-4E_1)p_2\sin^2\tfrac{\theta}{2}\, B_+ \begin{pmatrix}-1\\+1\end{pmatrix} \,\} \\
F^{3}_{++;\pm} &= \sqrt{2}\cos\tfrac{\theta}{2}\{\, (W-E_1-E_2)A_- \begin{pmatrix}1\\0\end{pmatrix} + p_2\sin^2\tfrac{\theta}{2}\, B_- \begin{pmatrix}-1\\+1\end{pmatrix} \,\} \\
F^{4}_{++;\pm} &= \sqrt{2}\cos\tfrac{\theta}{2}\{\, [(E_2-E_1)A_- - (m_1+m_2)A_+] \begin{pmatrix}1\\0\end{pmatrix} + p_2\sin^2\tfrac{\theta}{2}\, B_- \begin{pmatrix}+1\\-1\end{pmatrix} \,\} \\
F^{5}_{++;\pm} &= \sqrt{2}\cos\tfrac{\theta}{2}\{\, Wp_2\sin^2\tfrac{\theta}{2}\, B_+ \begin{pmatrix}-1\\+1\end{pmatrix} \,\} \\
F^{6}_{++;\pm} &= \sqrt{2}\cos\tfrac{\theta}{2}\{\, WA_- \begin{pmatrix}-1\\0\end{pmatrix} \,\}
\end{aligned} \tag{A.8}$$

$$F^{i}_{--;\pm} = -F^{i}_{++;\mp} \qquad (i = 1,2,\dots,6) \tag{A.9}$$

$$F^{1}_{+-;\pm} = \sqrt{2}\,\sin\frac{\theta}{2}\left\{ A_- \begin{pmatrix} -1 \\ 0 \end{pmatrix} \right\}$$

$$F^{2}_{+-;\pm} = \sqrt{2}\,\sin\frac{\theta}{2}\left\{ \frac{1}{2}(W-4E_1)\,p_2\cos^2\frac{\theta}{2}\,B_- \begin{pmatrix} -1 \\ +1 \end{pmatrix} \right\}$$

$$F^{3}_{+-;\pm} = \sqrt{2}\,\sin\frac{\theta}{2}\left\{ (W-E_1-E_2)\,A_+ \begin{pmatrix} -1 \\ 0 \end{pmatrix} + p_2\cos^2\frac{\theta}{2}\,B_+ \begin{pmatrix} -1 \\ +1 \end{pmatrix} \right\}$$

$$F^{4}_{+-;\pm} = \sqrt{2}\,\sin\frac{\theta}{2}\left\{ \left[(E_2-E_1)A_+ - (m_1+m_2)A_-\right] \begin{pmatrix} -1 \\ 0 \end{pmatrix} + p_2\cos^2\frac{\theta}{2}\,B_+ \begin{pmatrix} 1 \\ -1 \end{pmatrix} \right\} \qquad \textbf{(A.10)}$$

$$F^{5}_{+-;\pm} = \sqrt{2}\,\sin\frac{\theta}{2}\left\{ W\,p_2\cos^2\frac{\theta}{2}\,B_- \begin{pmatrix} -1 \\ +1 \end{pmatrix} \right\}$$

$$F^{6}_{+-;\pm} = \sqrt{2}\,\sin\frac{\theta}{2}\left\{ W A_+ \begin{pmatrix} 1 \\ 0 \end{pmatrix} \right\}$$

$$F^{i}_{-+;\pm} = F^{i}_{+-;\mp} \qquad (i=1,2,\ldots,6) \qquad \textbf{(A.11)}$$

References

1. A. Litke et al., Phys. Rev. Lett. 30 (1973) 1189;
B. Richter, report at the Conf. on Lepton-Induced Reactions, Irvine, December 1973;
W. Chinowsky, lecture at the IV. International Conf. on Experimental Meson Spectroscopy, Boston, Mass., April 26-27.

2. J. Le Francois, in Proceedings of the 1971 International Symposium on Electron and Photon Interactions at High Energies, Cornell University, Ithaca N.Y., August 23-27, 1971, p. 51;
A. Zichichi, Why e^+e^- Physics is Fascinating, CERN, 27. February 1974 (to be published in Nuovo Cimento Riv.).

3. A.C. Hirshfeld and G. Kramer, Nucl. Phys. B74 (1974) 241.

4. A. Actor, Cross channel poles and e^+e^- annihilation into three hadrons, Heidelberg University preprint (April 1974).

5. N.M. Avram and D.H. Schiller, Nucl. Phys. B70 (1974) 272.

6. L.D. Landau and E.M. Lifschitz, Relativistische Quantentheorie (Akademie-Verlag, Berlin, 1971), p. 26.

7. R.C.E. Devenish and D.H. Lyth, Phys. Rev. D5 (1972) 47, D6 (1972) 2067.

8. R. Felst, Phenomenological fits to the nucleon electromagnetic form factors based on vector-meson-dominance, preprint DESY 73/56 (November 1973).

9. M. Castellano et al., Nuovo Cimento, 14A (1973) 1.

10. J. Willrodt, Berechnung der Isovektor-Anteile der Formfaktoren des Nukleons mit Hilfe von Dispersionsrelationen im raum- und zeitartigen Bereich, Diplomarbeit, Universität Hamburg (1973).

11. G. Gustafson, Nucl. Phys. B66 (1973) 325

12. F.A. Berends, A. Donnachie and D.L. Weaver, Nucl. Phys. B4 (1967) 1.

13. R.C.E. Devenish and D.H. Lyth, Nucl. Phys. B43 (1972) 228.

14. R.L. Walker, Phys. Rev. 182 (1969) 1729.

15. A. Donnachie, in Proceedings of the 1971 International Symposium on Electron and Photon Interactions at High Energies, Cornell University, Ithaca, N.Y., August 23-27, 1971, p. 73.

16. O. Czyzewski, in Methods in Subnuclear Physics, International School of Elementary Particle Physics, Herceg-Novi 1965, vol. 1, p. 129 (edited by M. Nikolić).

Table I: Resonance parameters entering (3.6)

Resonance	m_R (GeV)	Γ_R (GeV)	$\ell\pm$	X_π (GeV)	X_γ (GeV)	$\sqrt{2}\,E_{0+}^{\frac{1}{2}(s)}$ ($\mu b^{1/2}$)	$\sqrt{2}\,M_{0-}^{\frac{1}{2}(s)}$ ($\mu b^{1/2}$)	$\frac{\sqrt{2}}{3}E_{0+}^{\frac{1}{2}(v)}$ ($\mu b^{1/2}$)	$\frac{\sqrt{2}}{3}M_{0-}^{\frac{1}{2}(v)}$ ($\mu b^{1/2}$)	$\frac{\sqrt{2}}{3}E_{0+}^{\frac{3}{2}(v)}$ ($\mu b^{1/2}$)	$\frac{\sqrt{2}}{3}M_{0-}^{\frac{3}{2}(v)}$ ($\mu b^{1/2}$)
$P_{33}(1236)$	1.232	0.114	1+	0.167	1.0	-	-	-	-	-0.0500	2.4900
$P_{11}(1470)$	1.435	0.200	1-	0.350	1.5	-	0.4630	-	0.4630	-	-
$S_{11}(1506)$	1.506	0.080	0+	0.350	1.5	-0.0750	-	0.7250	-	-	-
$D_{13}(1520)$	1.520	0.102	2-	0.350	1.5	0.0587	0.0862	0.9212	0.3737	-	-
$S_{31}(1630)$	1.630	0.160	0+	0.350	1.5	-	-	-	-	-0.3280	-
$D_{15}(1670)$	1.653	0.134	2+	0.350	1.5	-0.0333	-0.0333	-0.0133	0.1266	-	-
$F_{15}(1690)$	1.690	0.104	3-	0.350	1.5	0.1966	0.0983	0.1966	0.0983	-	-
$S_{11}(1700)$	1.700	0.200	0+	0.350	1.5	0.3280	-	0.3280	-	-	-
$F_{37}(1940)$	1.940	0.200	3+	0.350	1.5	-	-	-	-	0.0031	0.0936
$G_{17}(2190)$	2.190	0.300	4-	0.350	1.5	0.0448	0.0321	0.0448	0.0321	-	-

Figure Captions

Fig. 1: One-photon exchange approximation for $e^+e^- \to \bar{N} N \pi$.

Fig. 2: Physical regions for $\gamma_v(q^2) + N_1 \to \pi + N_2$: (a) for $q^2 > 0$ (annihilation), and (b) for $q^2 < 0$ (electroproduction)

Fig. 3: The isoscalar and isovector form factors (3.4) of the nucleon.

Fig. 4: The coherent (solid curve) and incoherent (dashed curve) total cross sections ($\sigma_{tot} = \sigma_U + \sigma_L$): (a)-(c) for the choice (3.13) of the resonance form factors, and (d)-(f) for the choice (3.14).

Fig. 5: Contribution of the individual resonances to $\sigma_{tot} = \sigma_U + \sigma_L$: (a)-(c) for the choice (3.13) of the resonance form factors, and (d)-(f) for the choice (3.14). The dashed curves (or part of curves) refer to the scale on the left, the solid ones to the scale on the right.

Fig. 6: The Dalitz plot projections $d\sigma_{tot}/dE_1$ at $\sqrt{q^2} = 3.3$ GeV: (a)-(d) for the choice (3.13) of the resonance form factors, and (e)-(h) for the choice (3.14).

Fig. 7: Dalitz plots resulting from calculations using amplitudes which include only the contributions of the single resonances (a) $F_{15}(1690)$ and (b) $S_{11}(1700)$. In this case the choice of the resonance form factor is irrelevant.

Fig. 8: Dalitz plots resulting from calculations using the full amplitudes with all resonances included:(a)-(b) for the choice (3.13) of the resonance form factors, and (c)-(d) for the choice (3.14).

Fig. 9: The cross sections $\sigma_L^{(h)}$, $\sigma_T^{(h)}$, $\sigma_{IR}^{(h)}$ and $\sigma_{II}^{(h)}$: (a)-(d) for the choice (3.13) of the resonance form factors, and (e)-(h) for the choice (3.14).

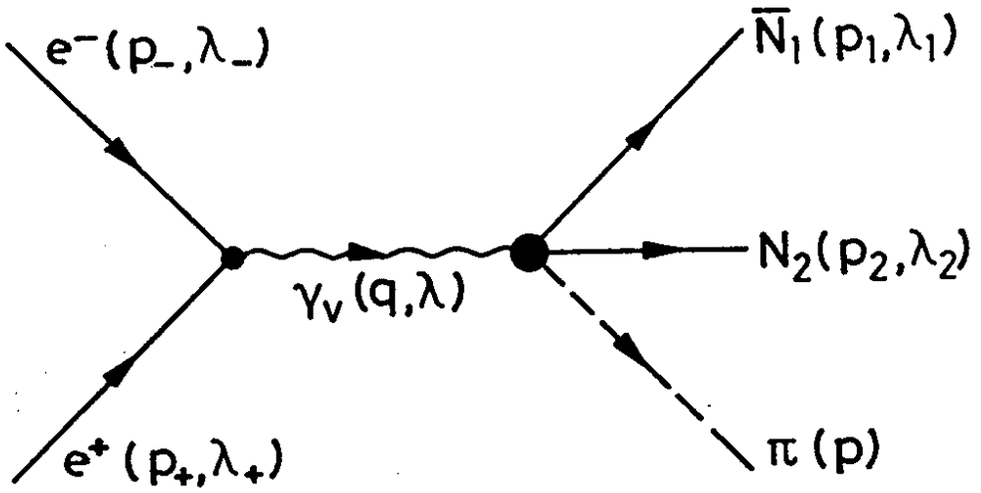
$e^-(p_-,\lambda_-)$
$\bar{N}_1(p_1,\lambda_1)$
$N_2(p_2,\lambda_2)$
$\gamma_V(q,\lambda)$
$e^+(p_+,\lambda_+)$
$\pi(p)$

Fig. 1

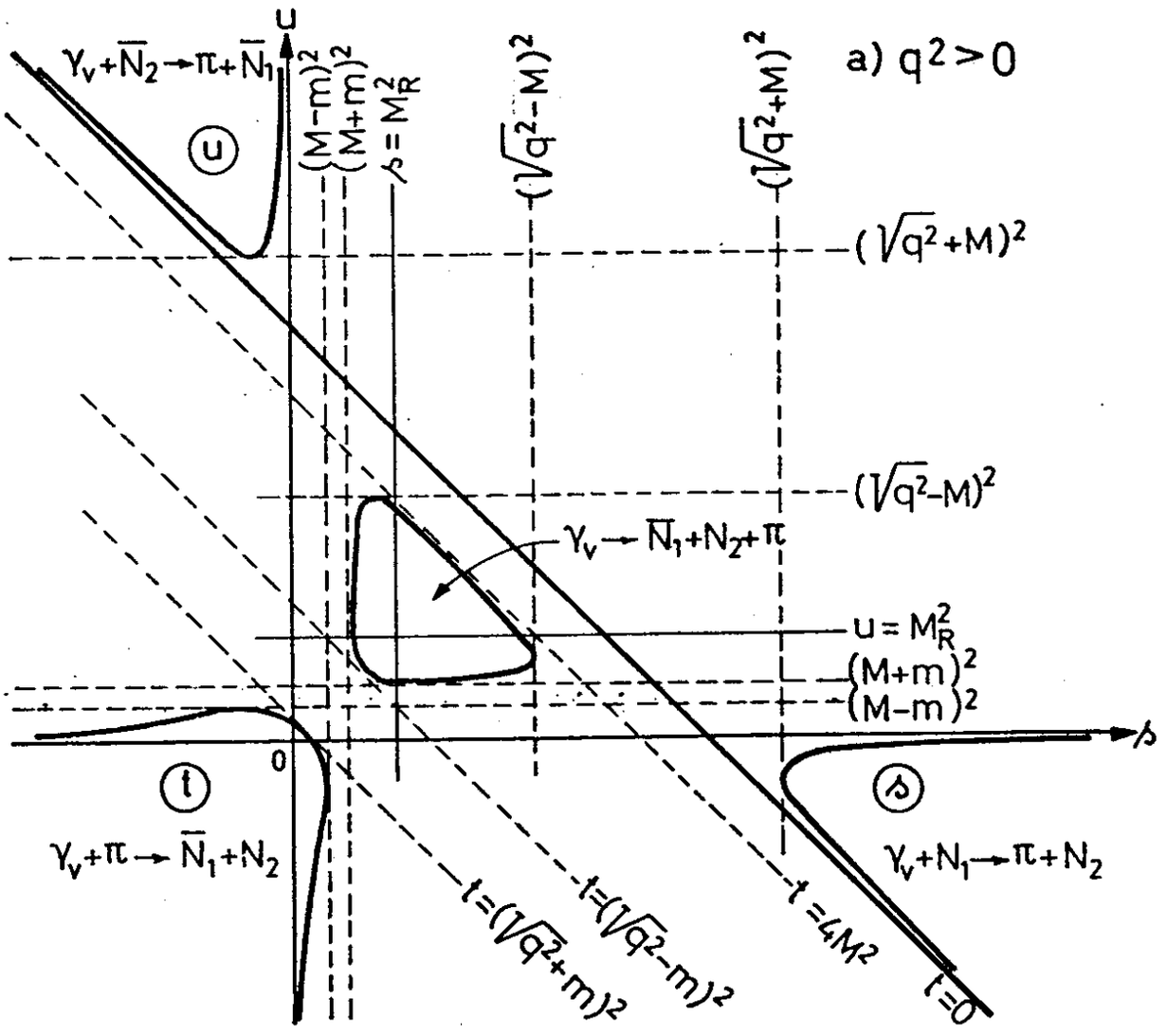
a) $q^2>0$
u
s
$\gamma_v+\bar{N}_2\to\pi+\bar{N}_1$
u
$(M-m)^2$
$(M+m)^2$
$s=M_R^2$
$(\sqrt{q^2}-M)^2$
$(\sqrt{q^2}+M)^2$
$(\sqrt{q^2}+M)^2$
$(\sqrt{q^2}-M)^2$
$\gamma_v\to\bar{N}_1+N_2+\pi$
$u=M_R^2$
$(M+m)^2$
$(M-m)^2$
0
t
t
$\gamma_v+\pi\to\bar{N}_1+N_2$
$\gamma_v+N_1\to\pi+N_2$
$t=(\sqrt{q^2}+m)^2$
$t=(\sqrt{q^2}-m)^2$
$t=4M^2$
$t=0$

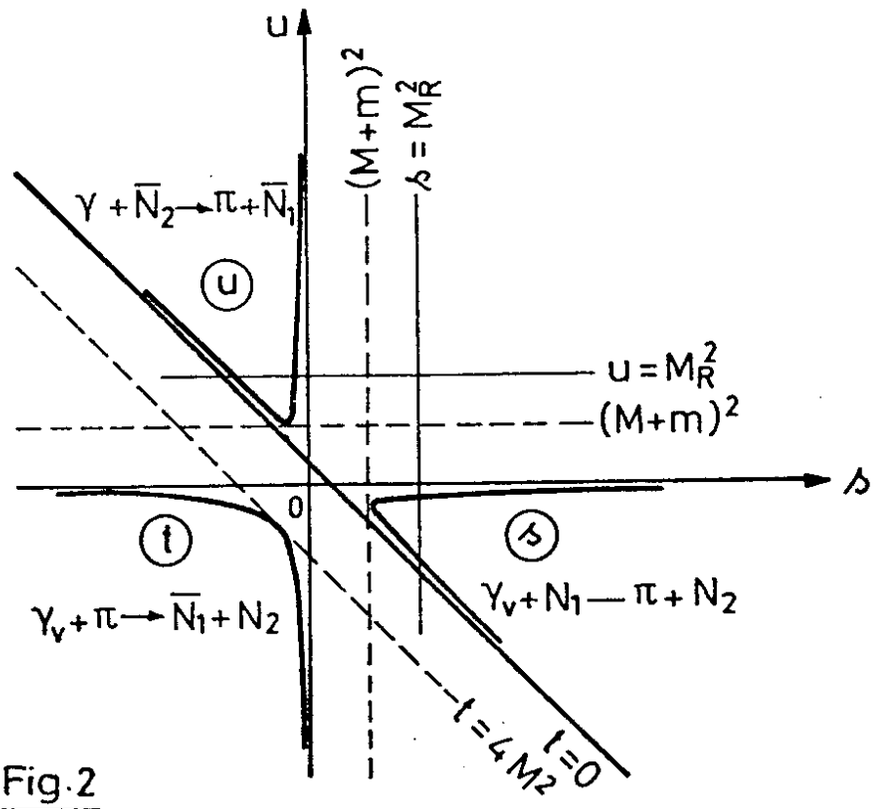
b) $q^2<0$
u
s
$\gamma+\bar{N}_2\to\pi+\bar{N}_1$
u
$(M+m)^2$
$s=M_R^2$
$u=M_R^2$
$(M+m)^2$
0
t
s
$\gamma_v+\pi\to\bar{N}_1+N_2$
$\gamma_v+N_1\to\pi+N_2$
$t=4M^2$
$t=0$

Fig.2

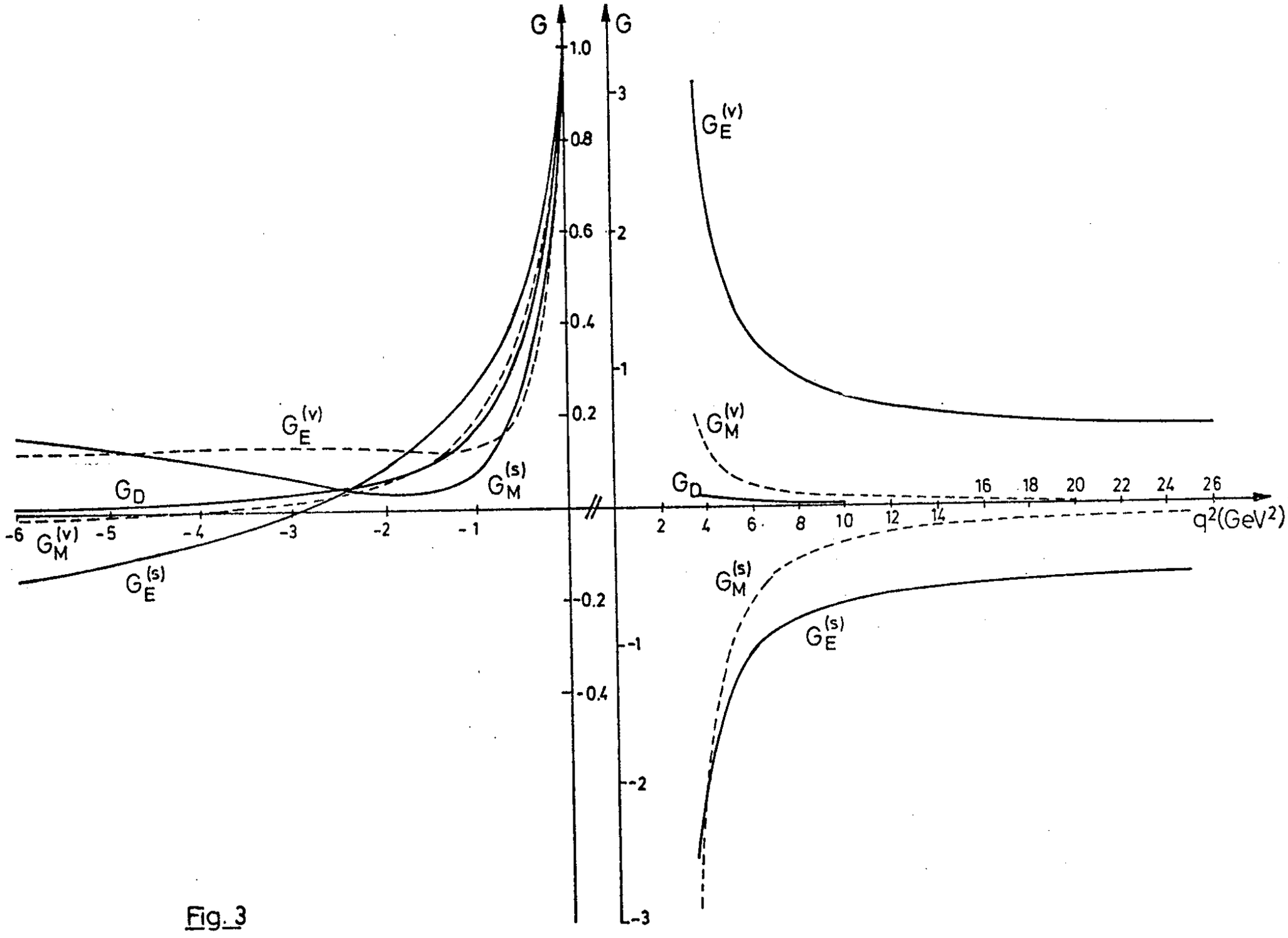
G
G
1.0
0.8
0.6
0.4
0.2
-0.2
-0.4
3
2
1
-1
-2
-3
$G_E^{(v)}$
$G_M^{(v)}$
G_D
$G_M^{(s)}$
$G_E^{(s)}$
-6
-5
-4
-3
-2
-1
2
4
6
8
10
12
14
16
18
20
22
24
26
$q^2(GeV^2)$

Fig. 3

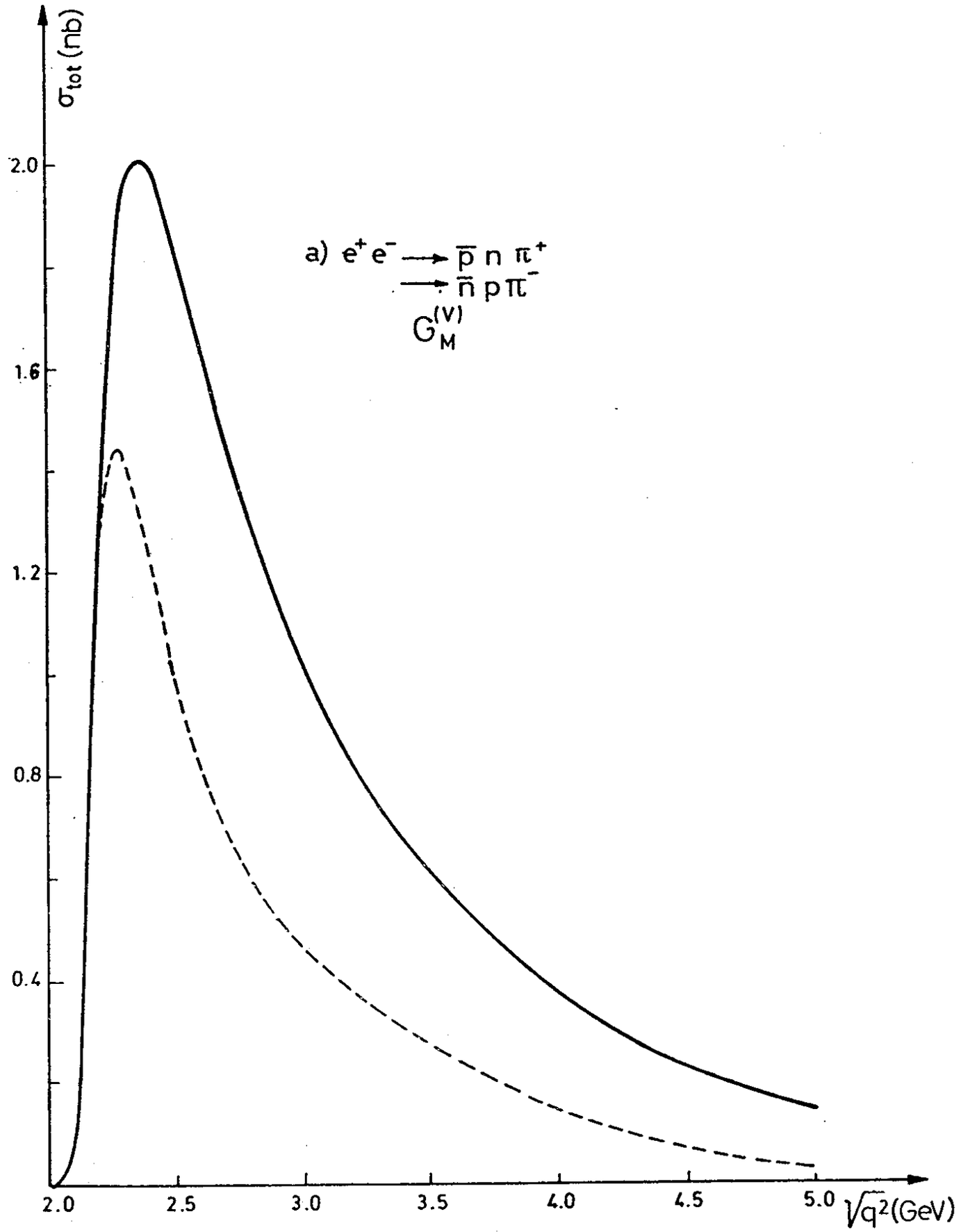
σ_{tot} (nb)
2.0
1.6
1.2
0.8
0.4
a) $e^+e^- \longrightarrow \bar{p}\, n\, \pi^+$
$\longrightarrow \bar{n}\, p\, \pi^-$
$G_M^{(V)}$
2.0
2.5
3.0
3.5
4.0
4.5
5.0
$\sqrt{q^2}$(GeV)

Fig.4

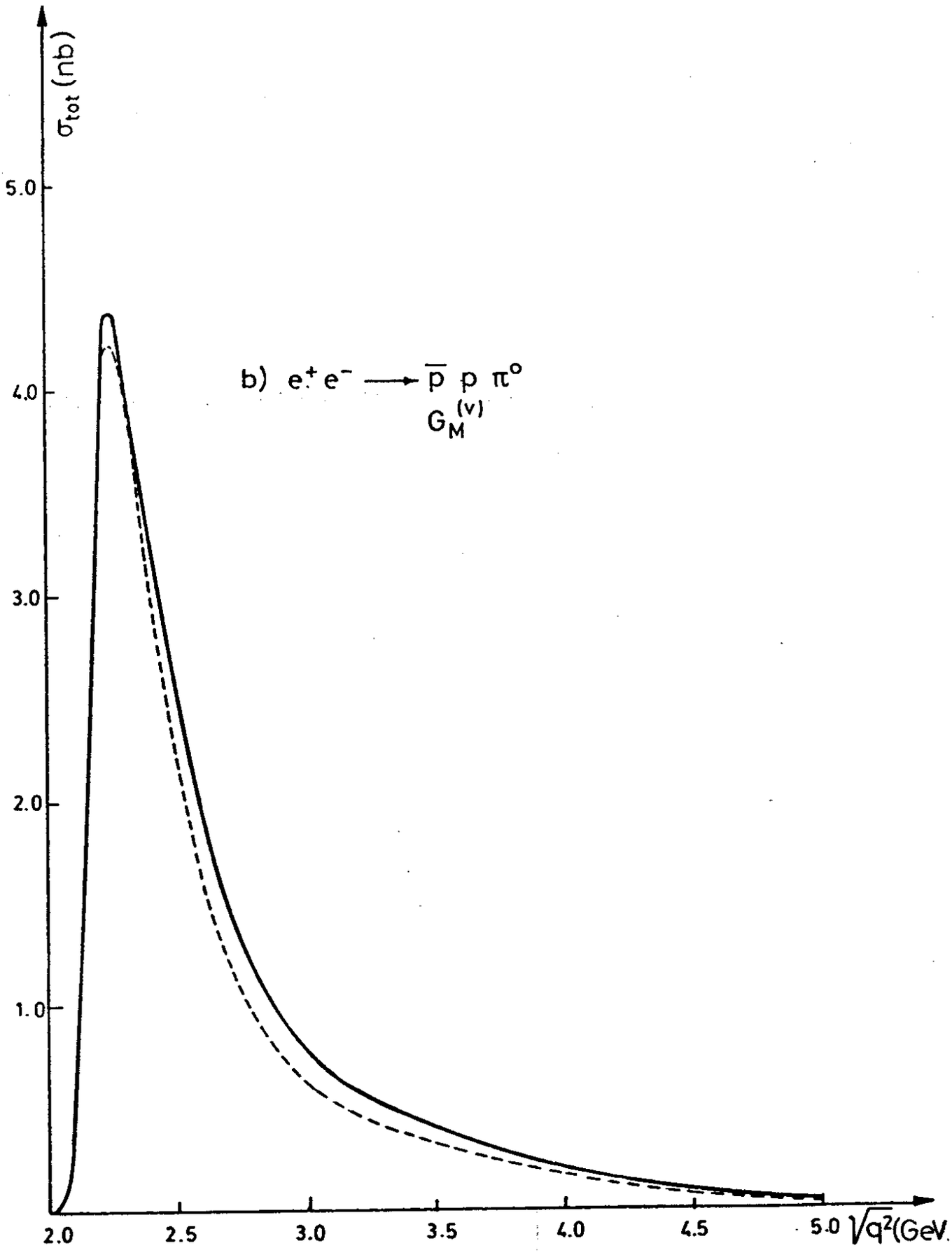
σ_{tot} (nb)
5.0
4.0
3.0
2.0
1.0
b) $e^+e^- \longrightarrow \bar{p}\ p\ \pi^0$
$G_M^{(v)}$
2.0
2.5
3.0
3.5
4.0
4.5
5.0 $\sqrt{q^2}$(GeV.

Fig.4

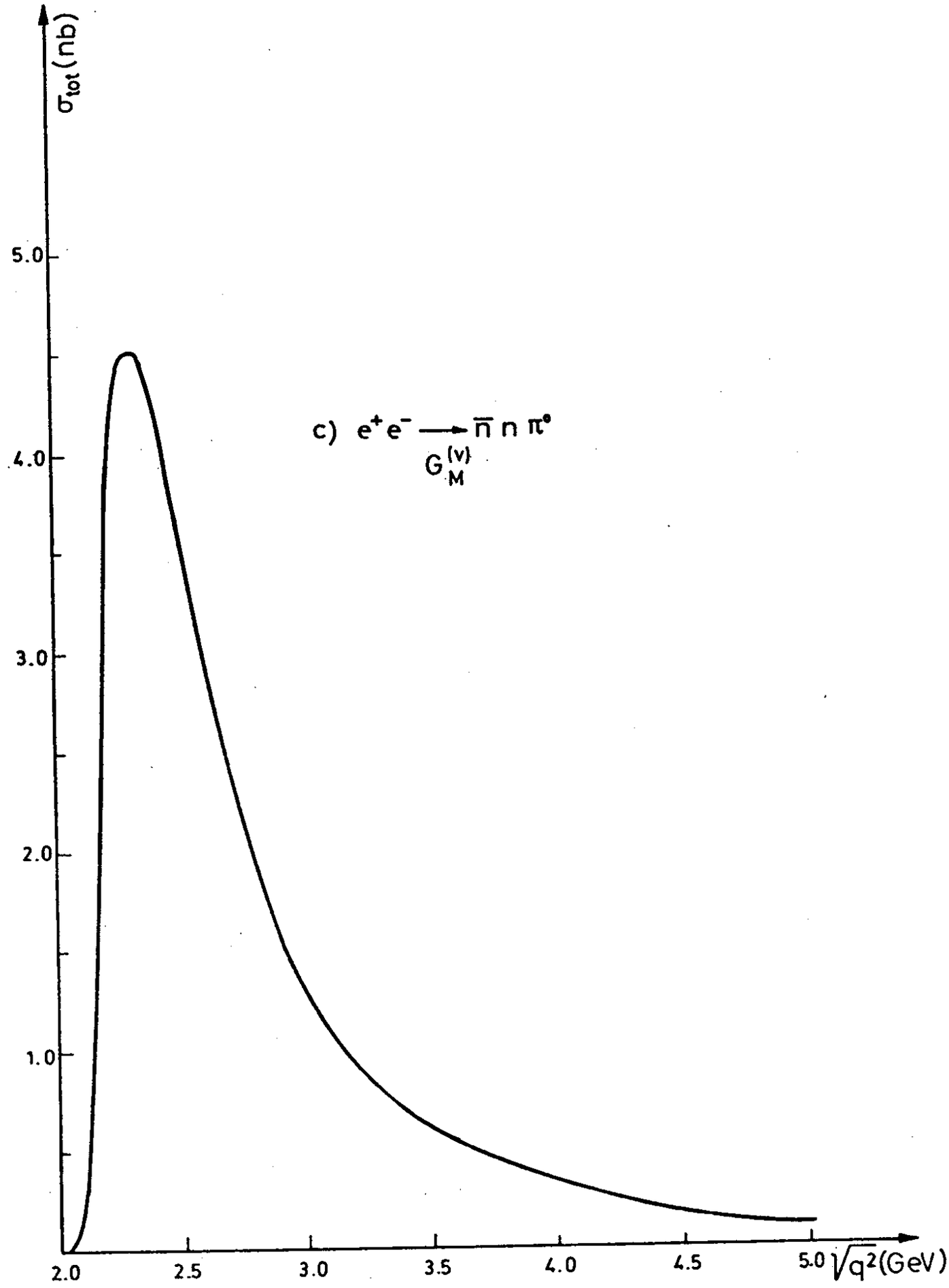
σ_{tot} (nb)
5.0
4.0
3.0
2.0
1.0
c) $e^+e^- \longrightarrow \bar{n}\, n\, \pi^0$
$G_M^{(v)}$
2.0
2.5
3.0
3.5
4.0
4.5
5.0
$\sqrt{q^2}$(GeV)

Fig.4

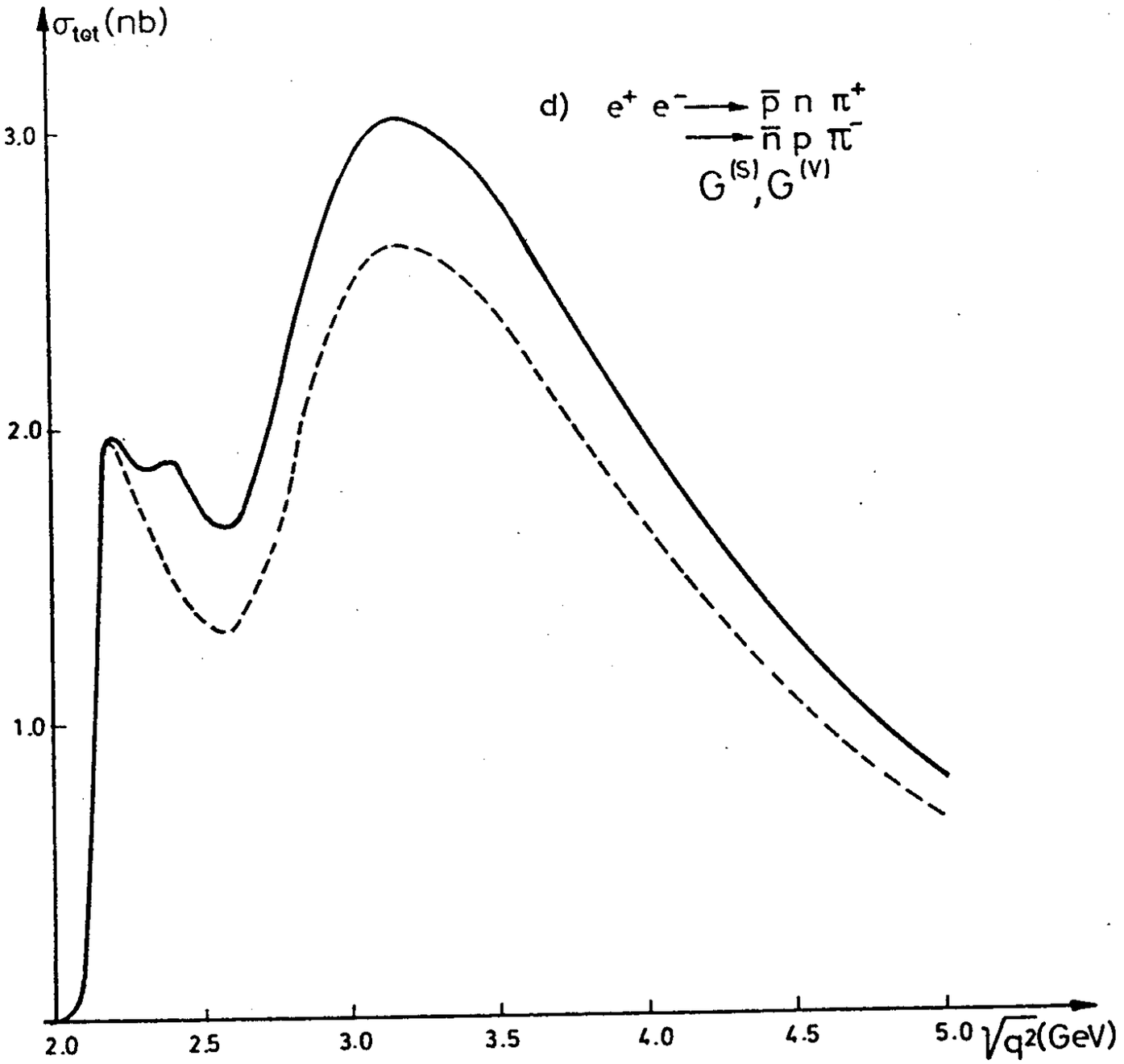
σ_{tot}(nb)
d) $e^+ e^- \longrightarrow \bar{p}\, n\, \pi^+$
$\longrightarrow \bar{n}\, p\, \pi^-$
$G^{(S)}, G^{(V)}$
3.0
2.0
1.0
2.0
2.5
3.0
3.5
4.0
4.5
5.0
$\sqrt{q^2}$(GeV)

Fig.4

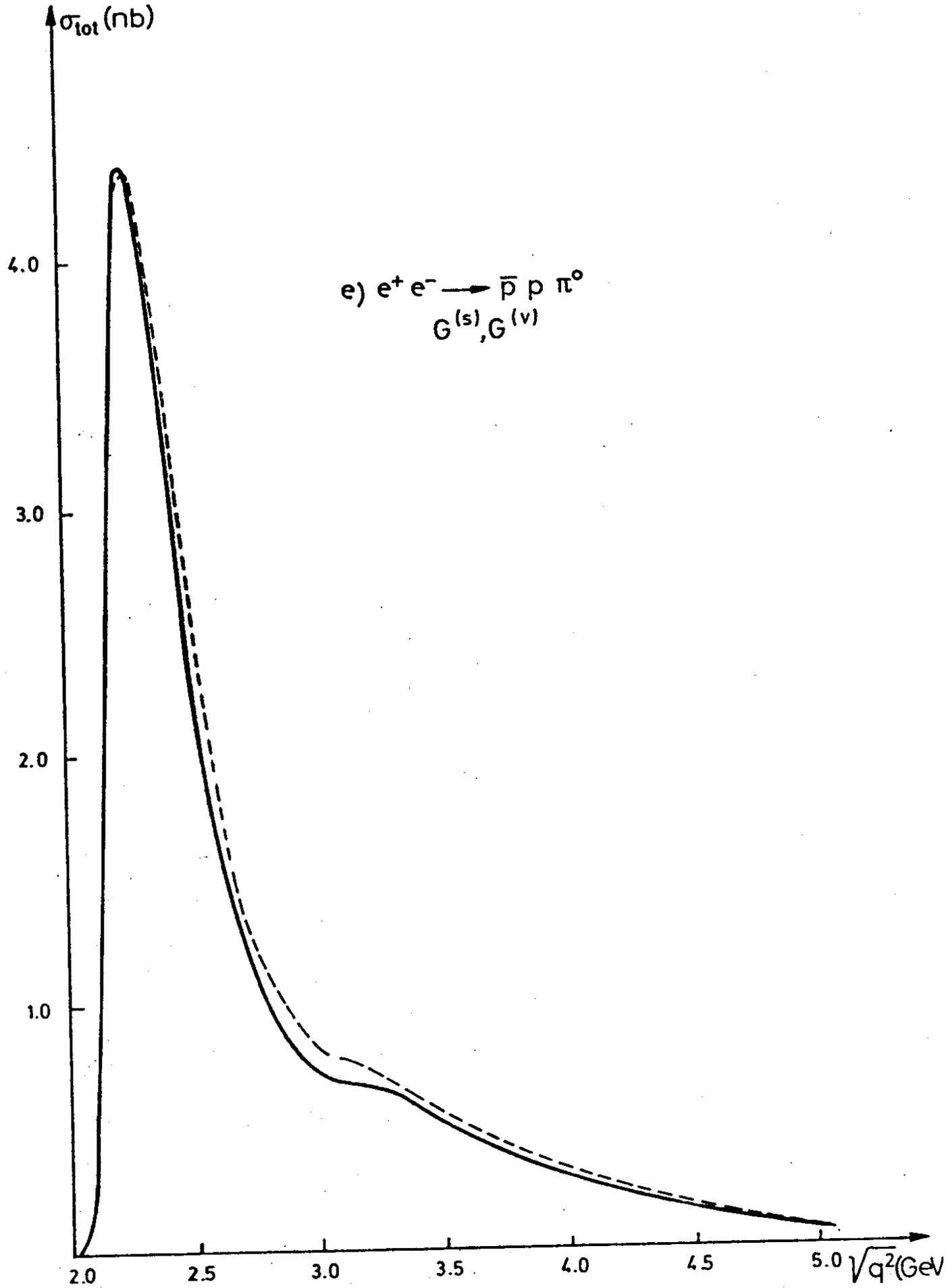
σ_{tot} (nb)
4.0
3.0
2.0
1.0
e) $e^+ e^- \longrightarrow \bar{p}\ p\ \pi^\circ$
$G^{(s)}, G^{(v)}$
2.0
2.5
3.0
3.5
4.0
4.5
5.0
$\sqrt{q^2}$(GeV

Fig.4

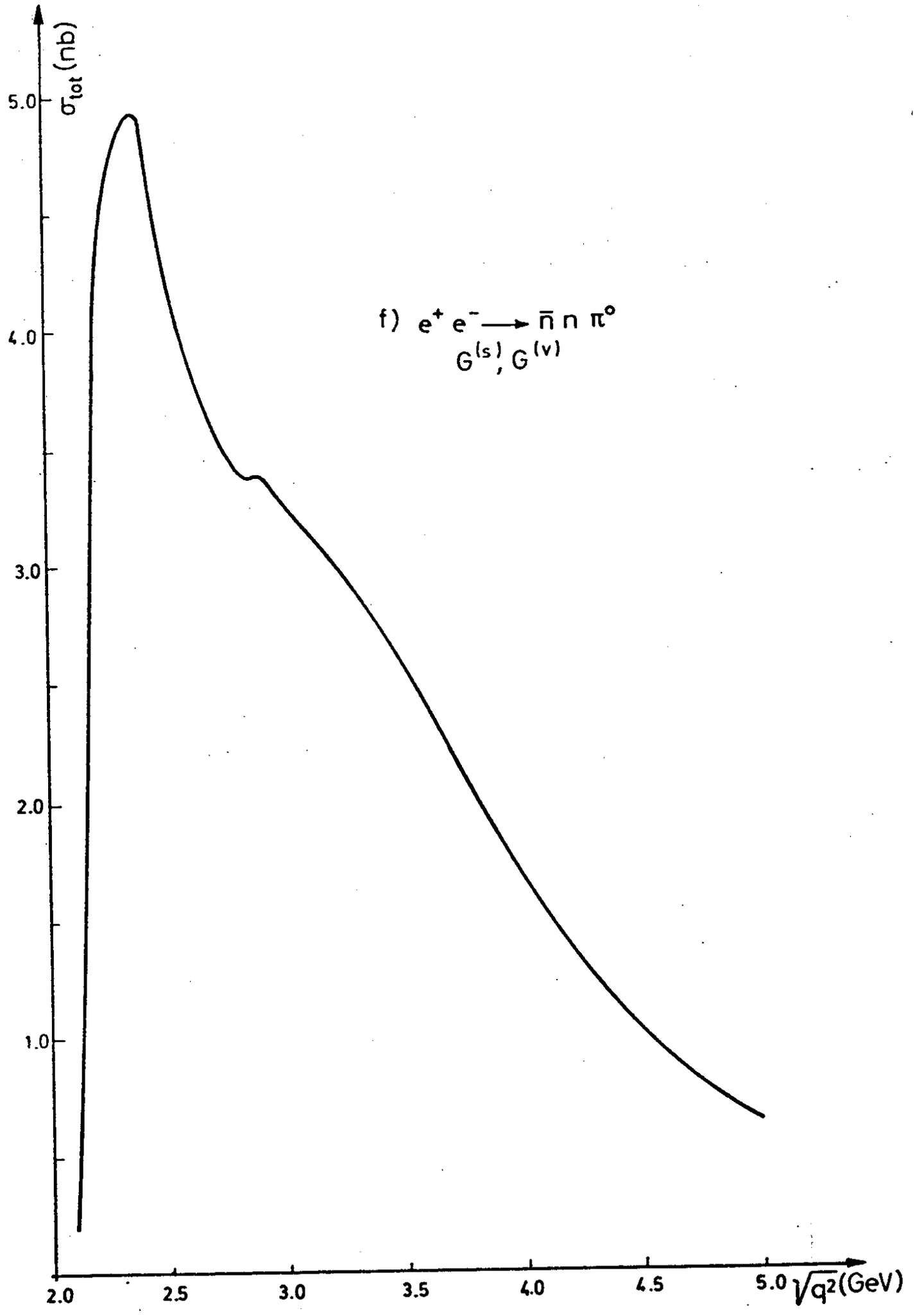
σ_{tot} (nb)
5.0
4.0
3.0
2.0
1.0
f) $e^+ e^- \longrightarrow \bar{n}\, n\, \pi^\circ$
$G^{(s)}, G^{(v)}$
2.0
2.5
3.0
3.5
4.0
4.5
5.0
$\sqrt{q^2}$(GeV)

Fig. 4

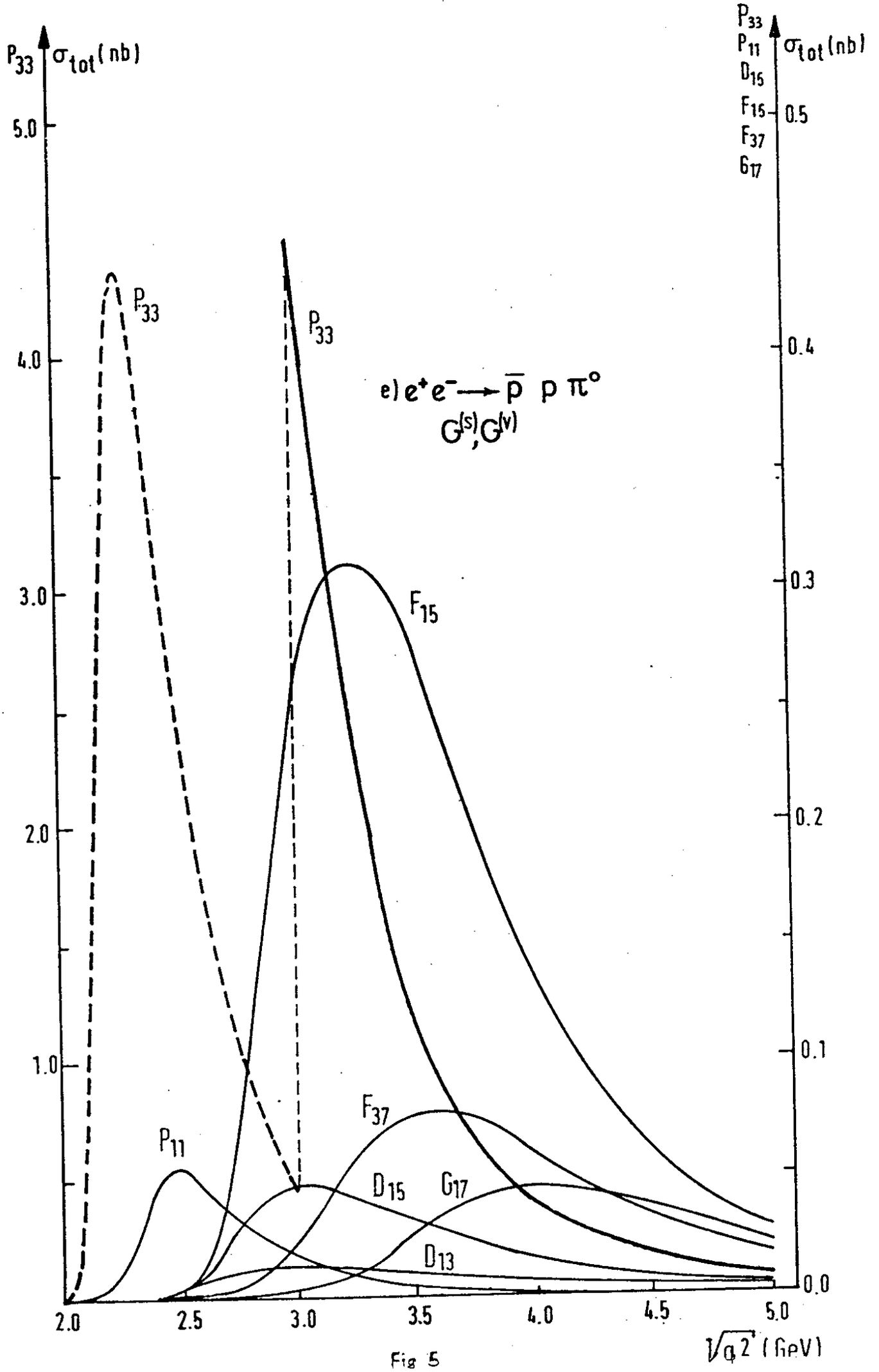
P33 σtot (nb)
5.0
4.0
3.0
2.0
1.0
P33
P33
P11
F15
F37
D15
G17
D13
e) e+e− → p̄ p π°
G(s), G(v)
P33
P11
D15
F15
F37
G17
σtot (nb)
0.5
0.4
0.3
0.2
0.1
0.0
2.0
2.5
3.0
3.5
4.0
4.5
5.0
√q2 (GeV)

Fig 5

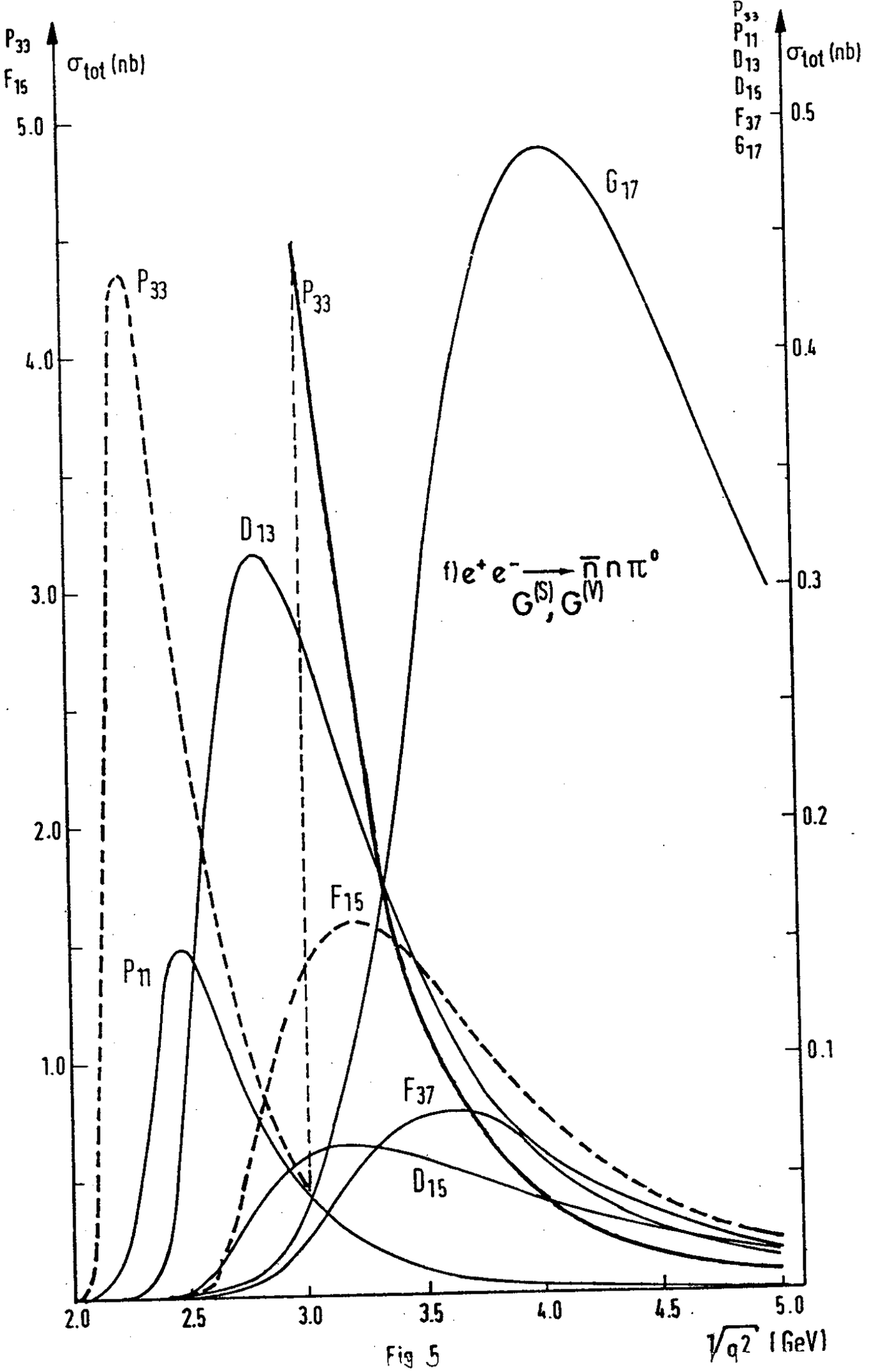
P33
F15
σtot (nb)
5.0
4.0
3.0
2.0
1.0
P33
P11
D13
D15
F37
G17
σtot (nb)
0.5
0.4
0.3
0.2
0.1
G17
P33
P33
D13
f) e+ e- → n̄ n π°
G(S), G(M)
F15
P11
F37
D15
2.0
2.5
3.0
3.5
4.0
4.5
5.0
√q² (GeV)

Fig 5

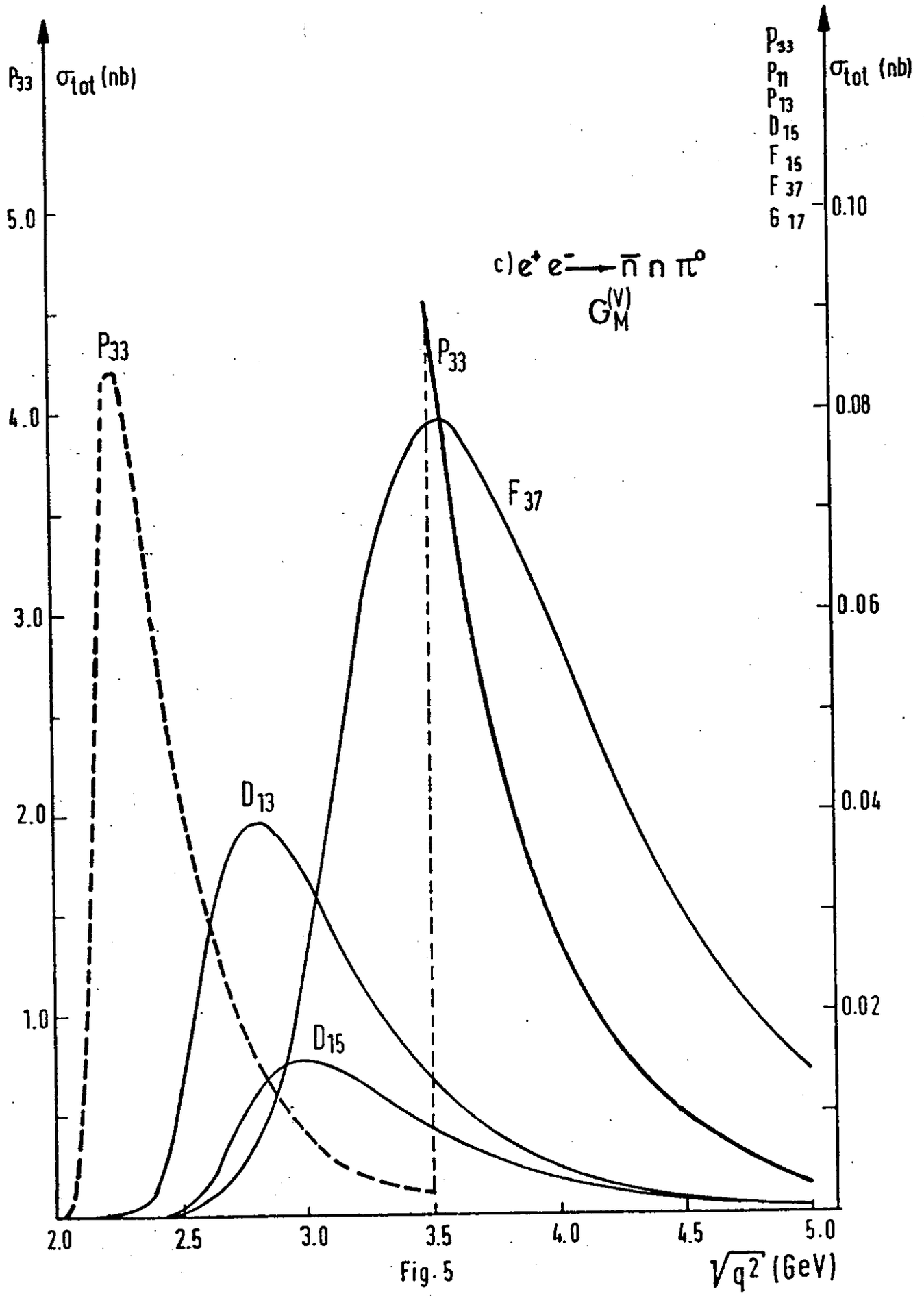
P33
σtot (nb)
P33
Pπ
P13
D15
F15
F37
G17
σtot (nb)
c) e+ e− → n̄ n π°
G(V)M
P33
P33
F37
D13
D15
5.0
4.0
3.0
2.0
1.0
0.10
0.08
0.06
0.04
0.02
2.0
2.5
3.0
3.5
4.0
4.5
5.0
√q2 (GeV)

Fig. 5

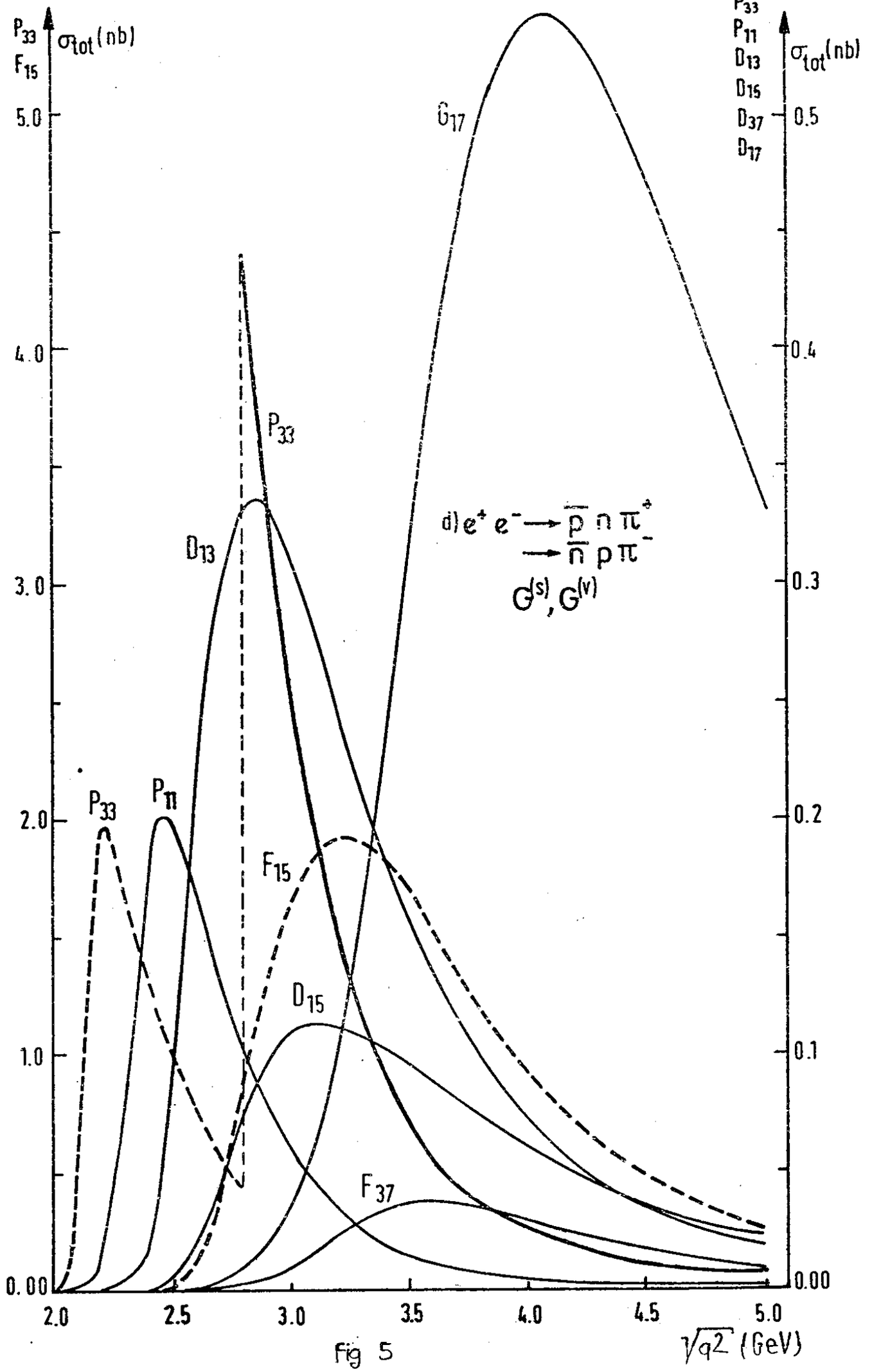
P_{33}
F_{15}
σ_{tot} (nb)
5.0
4.0
3.0
2.0
1.0
0.00
P_{33}
P_{11}
D_{13}
D_{15}
D_{37}
D_{17}
σ_{tot} (nb)
0.5
0.4
0.3
0.2
0.1
0.00
G_{17}
P_{33}
D_{13}
P_{33}
P_{11}
F_{15}
D_{15}
F_{37}
d) $e^+ e^- \rightarrow \bar{p} n \pi^+$
$\rightarrow \bar{n} p \pi^-$
$G^{(s)}, G^{(v)}$
2.0
2.5
3.0
3.5
4.0
4.5
5.0
$\sqrt{q^2}$ (GeV)

Fig 5

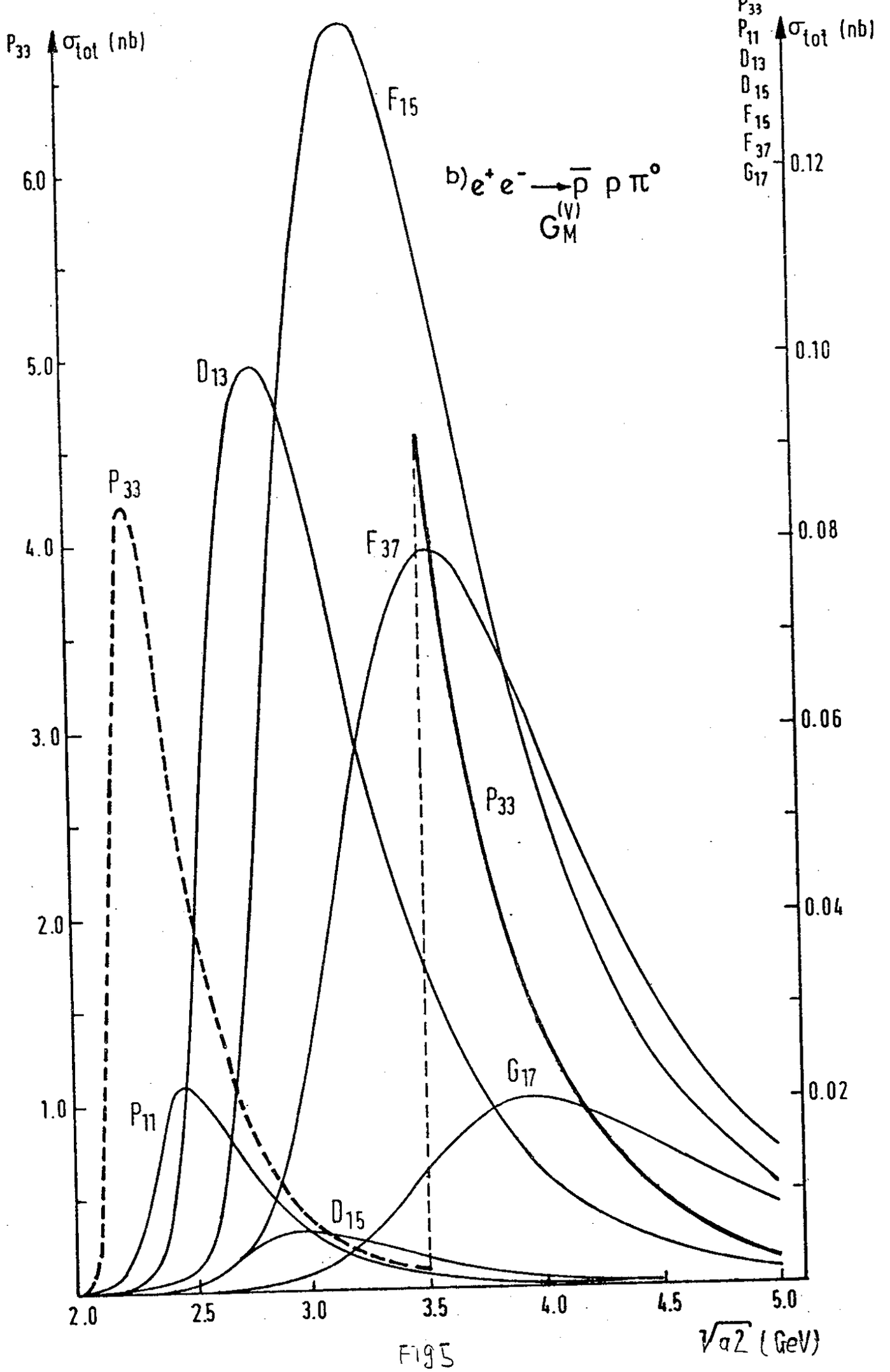
P33
σtot (nb)
F15
b) e+ e- → p̄ p π°
G(V)M
D13
P33
F37
P33
P11
D15
G17
P33
P11
D13
D15
F15
F37
G17
σtot (nb)
6.0
5.0
4.0
3.0
2.0
1.0
0.12
0.10
0.08
0.06
0.04
0.02
2.0
2.5
3.0
3.5
4.0
4.5
5.0
√q2 (GeV)

Fig 5

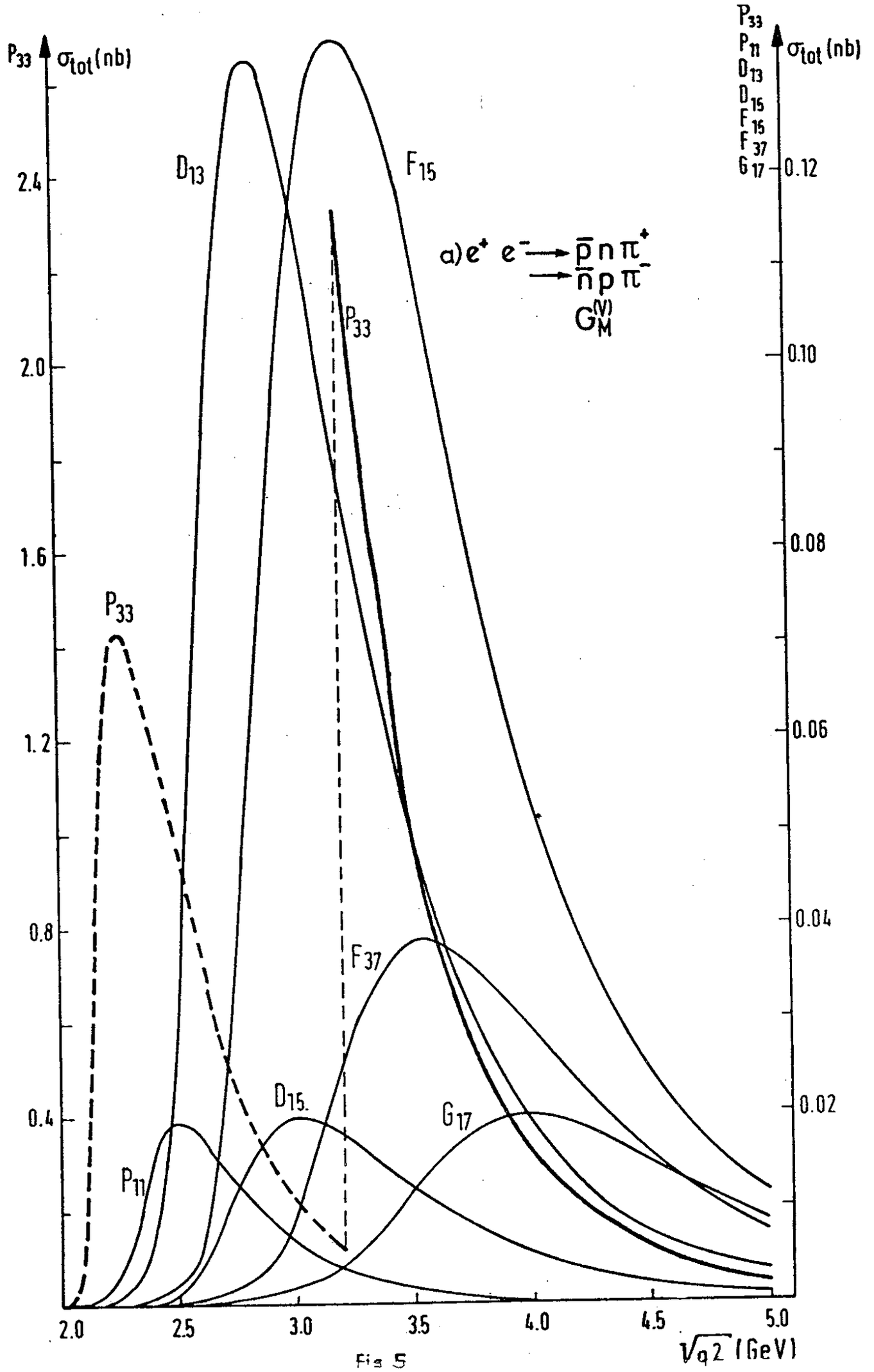
P33
σtot (nb)
2.4
2.0
1.6
1.2
0.8
0.4
D13
F15
P33
P33
P11
D15.
F37
G17
a) e+ e− → p̄ n π+
→ n̄ p π−
G(V)M
P33
P11
D13
D15
F15
F37
G17
σtot (nb)
0.12
0.10
0.08
0.06
0.04
0.02
2.0
2.5
3.0
3.5
4.0
4.5
5.0
√q2 (GeV)

Fig 5

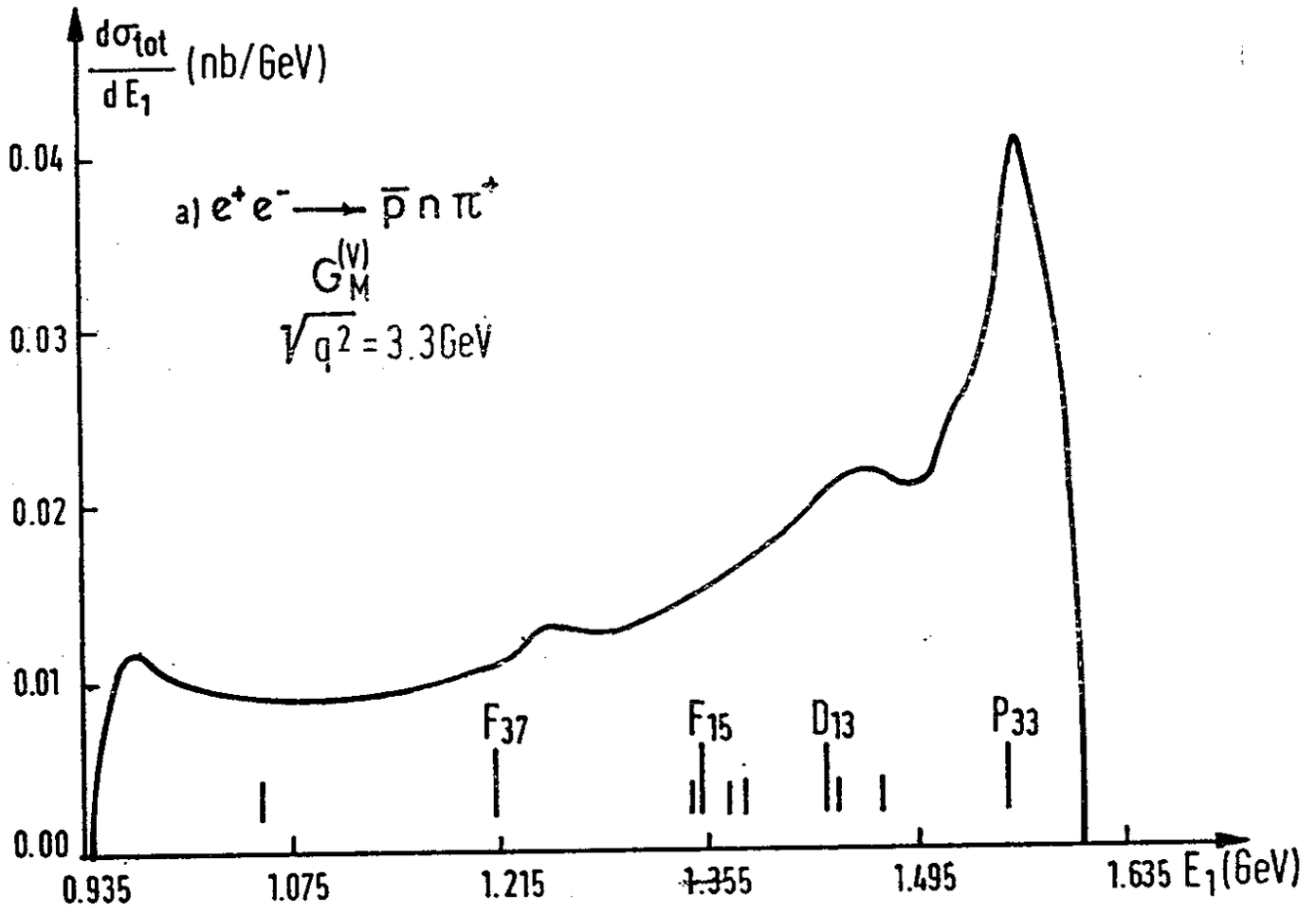
$\frac{d\sigma_{tot}}{dE_1}$ (nb/GeV)
0.04
0.03
0.02
0.01
0.00
a) $e^+e^- \longrightarrow \bar{p}n\pi^+$
$G_M^{(V)}$
$\sqrt{q^2} = 3.3$GeV
F_{37}
F_{15}
D_{13}
P_{33}
0.935
1.075
1.215
1.355
1.495
1.635 E_1(GeV)

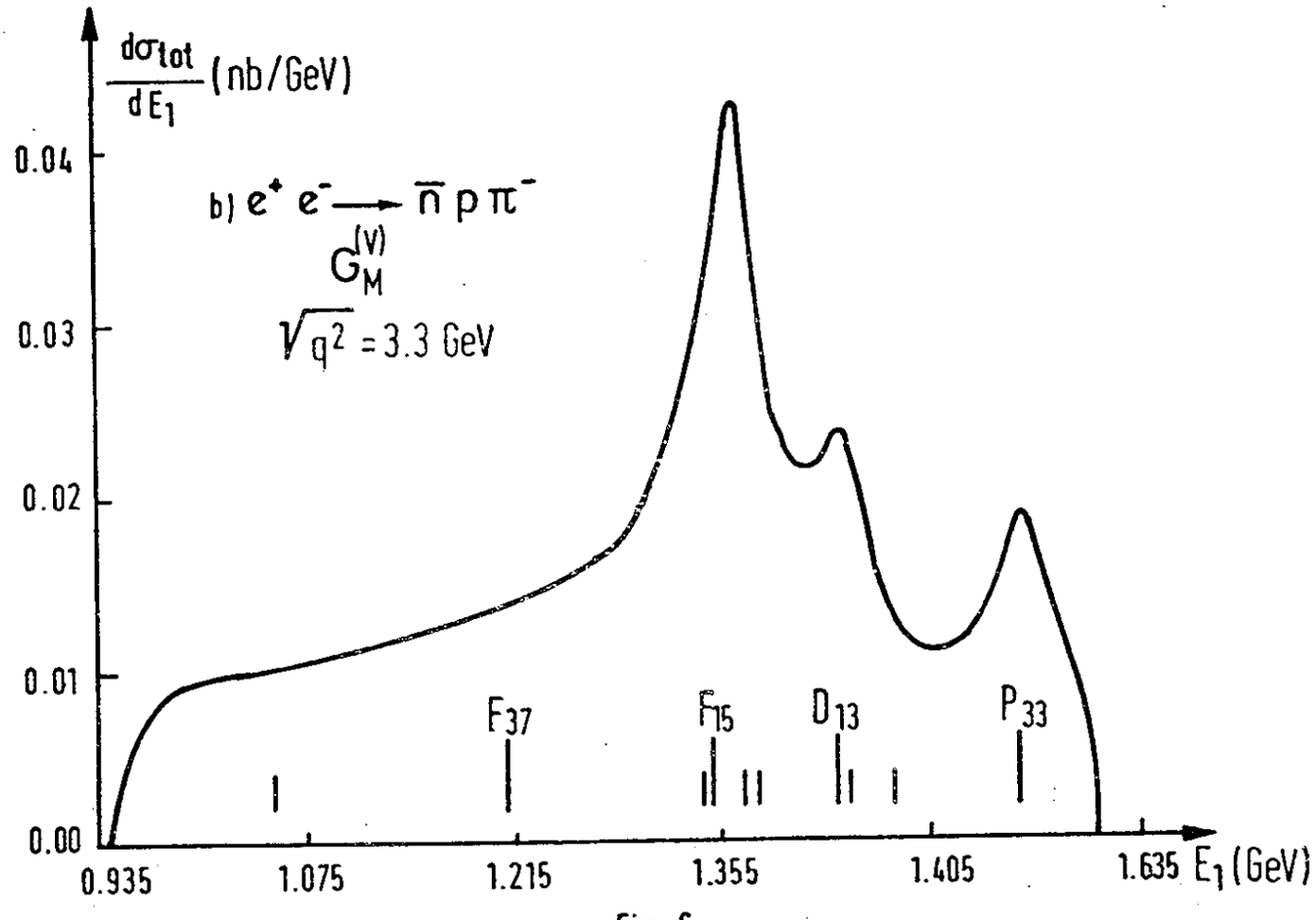
$\frac{d\sigma_{tot}}{dE_1}$ (nb/GeV)
0.04
0.03
0.02
0.01
0.00
b) $e^+e^- \longrightarrow \bar{n}p\pi^-$
$G_M^{(V)}$
$\sqrt{q^2} = 3.3$ GeV
F_{37}
F_{15}
D_{13}
P_{33}
0.935
1.075
1.215
1.355
1.405
1.635 E_1(GeV)

Fig. 6

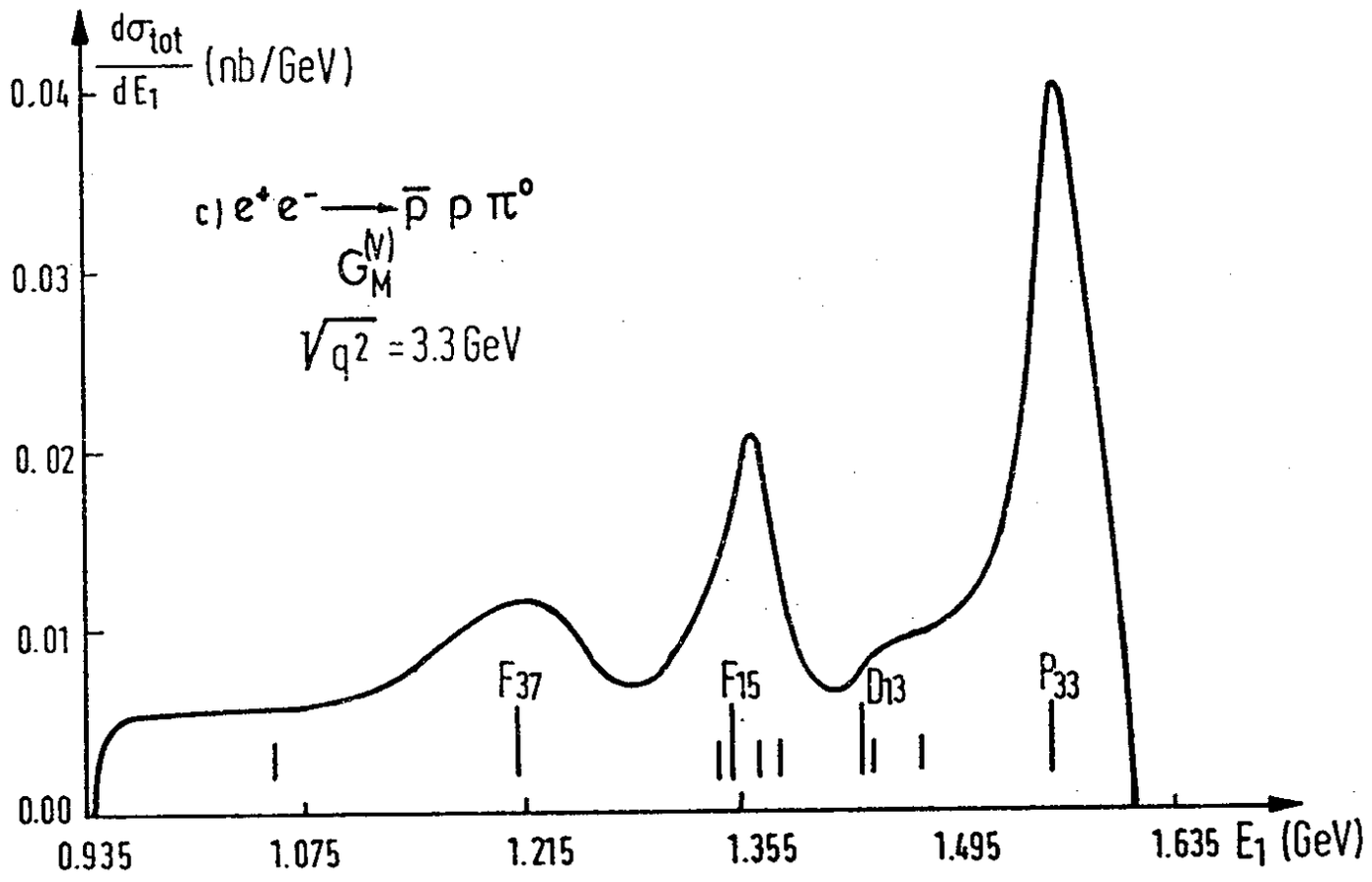
$\frac{d\sigma_{tot}}{dE_1}$ (nb/GeV)
0.04
0.03
0.02
0.01
0.00
c) $e^+e^- \longrightarrow \bar{p}\, p\, \pi^0$
$G_M^{(V)}$
$\sqrt{q^2} = 3.3$ GeV
F_{37}
F_{15}
D_{13}
P_{33}
0.935
1.075
1.215
1.355
1.495
1.635 E_1 (GeV)

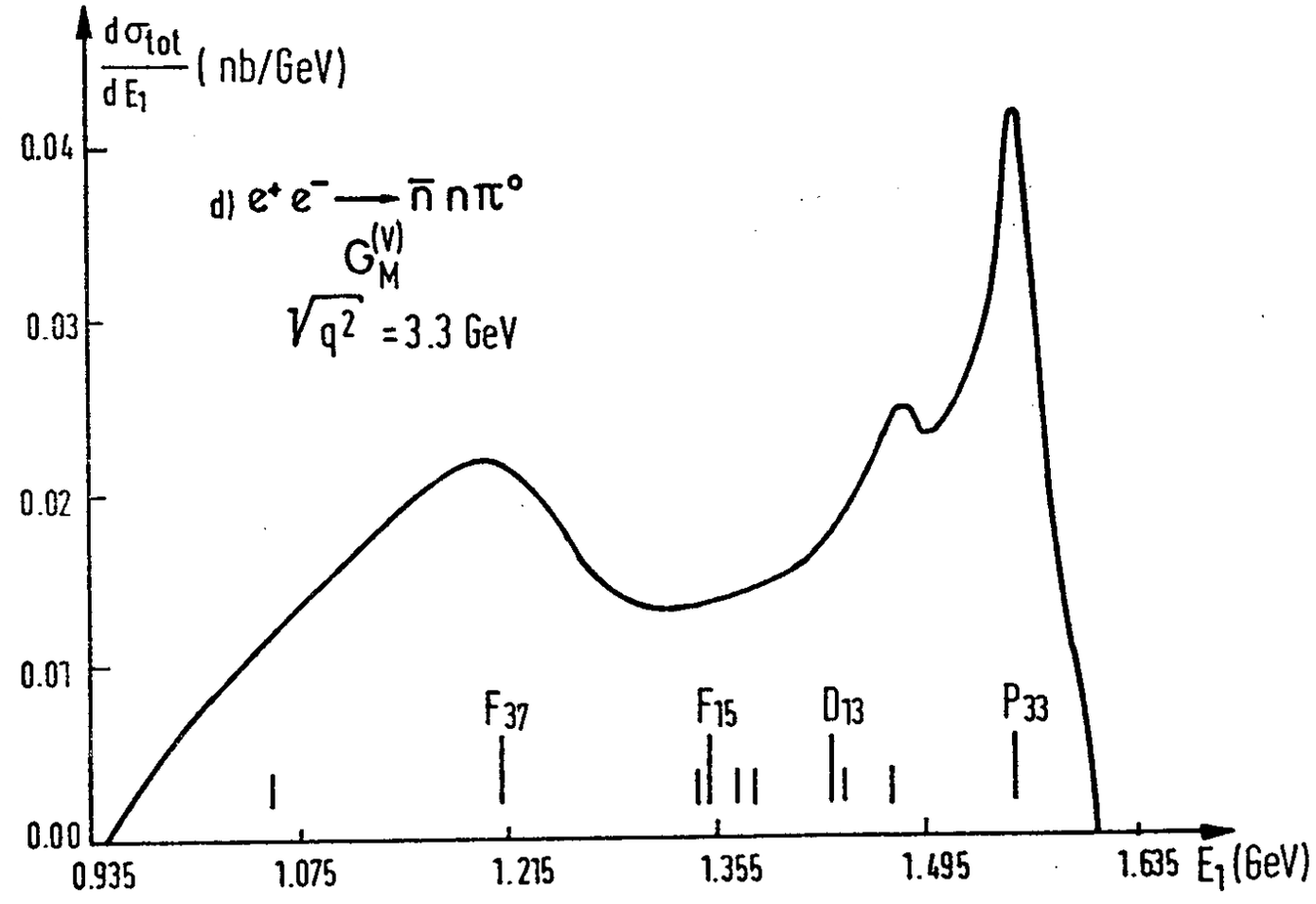
$\frac{d\sigma_{tot}}{dE_1}$ (nb/GeV)
0.04
0.03
0.02
0.01
0.00
d) $e^+e^- \longrightarrow \bar{n}\, n\, \pi^0$
$G_M^{(V)}$
$\sqrt{q^2} = 3.3$ GeV
F_{37}
F_{15}
D_{13}
P_{33}
0.935
1.075
1.215
1.355
1.495
1.635 E_1 (GeV)

Fig. 6

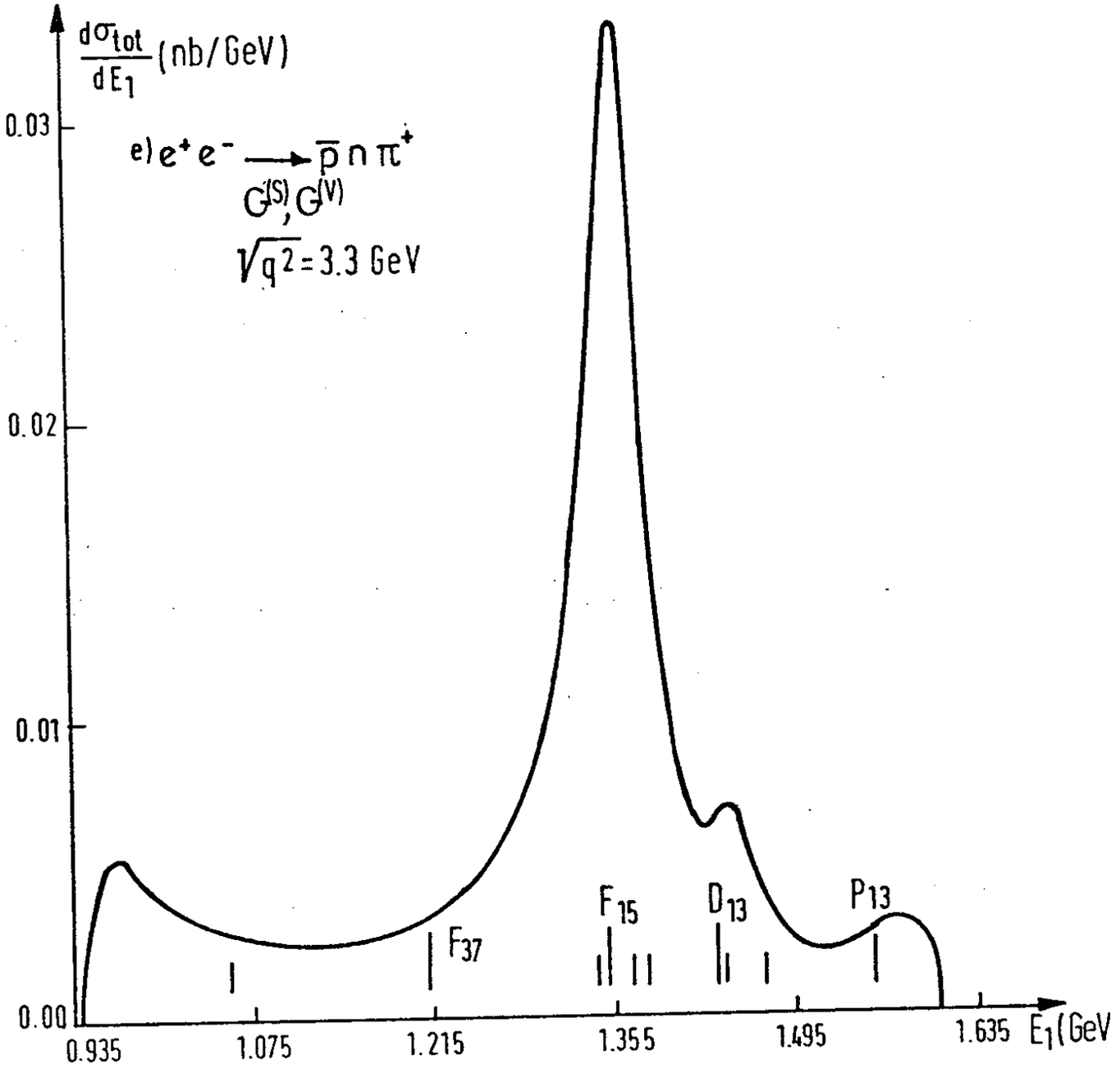
$\frac{d\sigma_{tot}}{dE_1}$ (nb/GeV)
0.03
0.02
0.01
0.00
e) $e^+e^- \longrightarrow \bar{p}\, n\, \pi^+$
$G^{(S)}, G^{(V)}$
$\sqrt{q^2} = 3.3$ GeV
F_{37}
F_{15}
D_{13}
P_{13}
0.935
1.075
1.215
1.355
1.495
1.635
E_1(GeV)

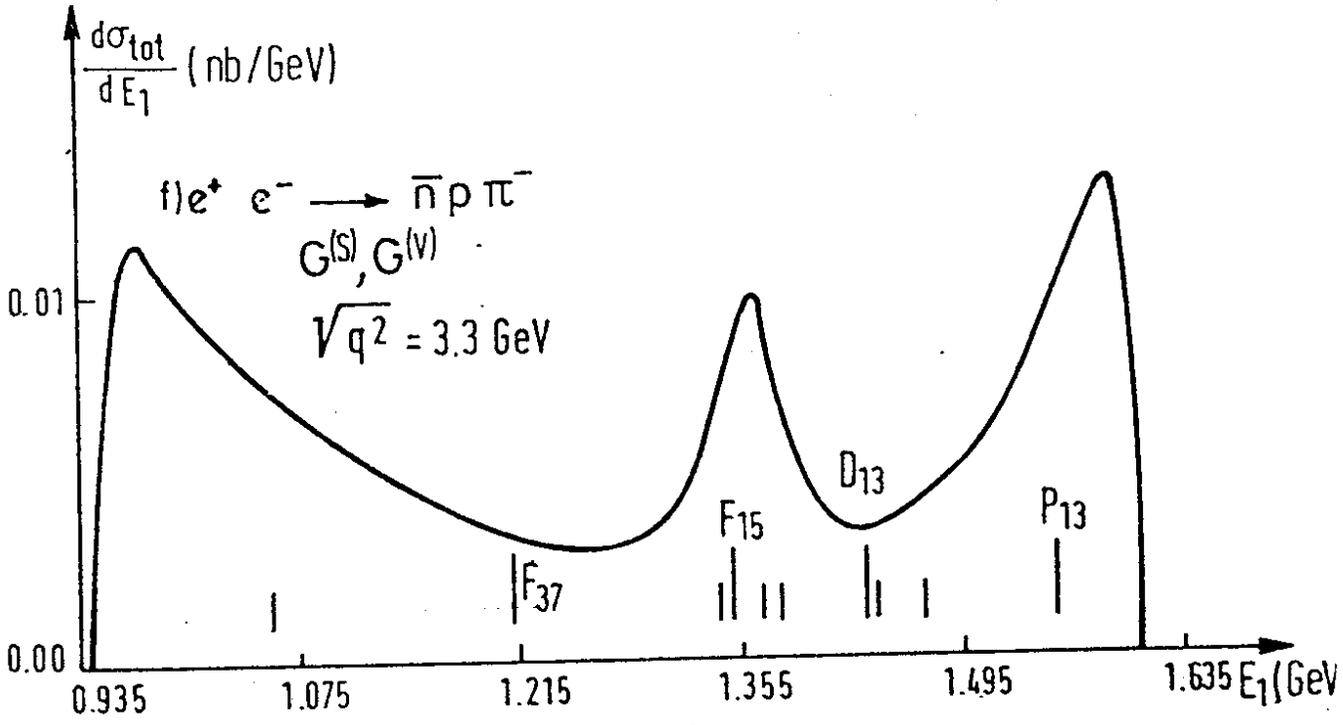
$\frac{d\sigma_{tot}}{dE_1}$ (nb/GeV)
0.01
0.00
f) $e^+ e^- \longrightarrow \bar{n}\, p\, \pi^-$
$G^{(S)}, G^{(V)}$
$\sqrt{q^2} = 3.3$ GeV
F_{37}
F_{15}
D_{13}
P_{13}
0.935
1.075
1.215
1.355
1.495
1.635
E_1(GeV)

Fig. 6

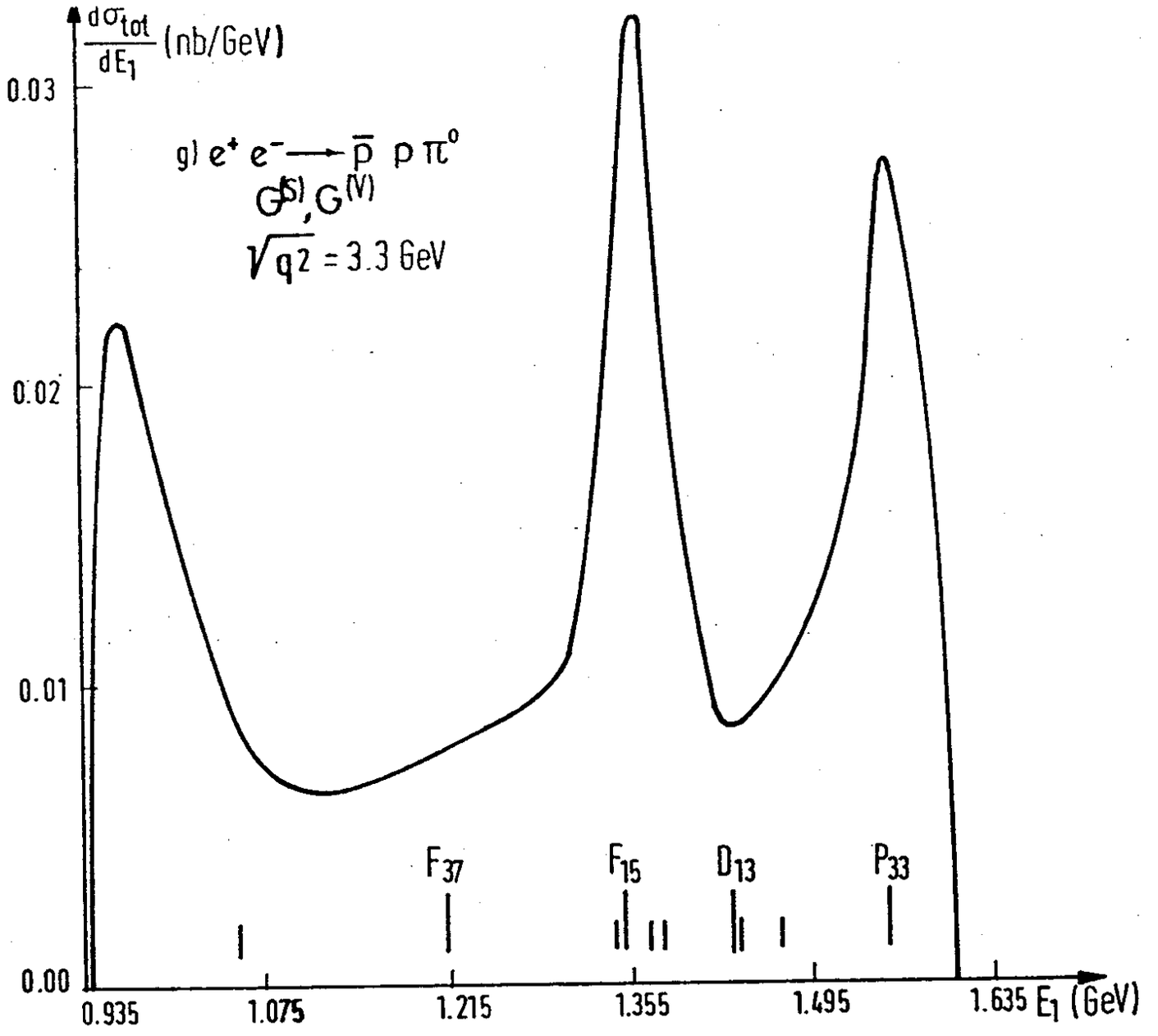
$\frac{d\sigma_{tot}}{dE_1}$ (nb/GeV)
0.03
0.02
0.01
0.00
g) $e^+ e^- \longrightarrow \bar{p}\, p\, \pi^0$
$G^{(S)}, G^{(V)}$
$\sqrt{q^2} = 3.3$ GeV
F_{37}
F_{15}
D_{13}
P_{33}
0.935
1.075
1.215
1.355
1.495
1.635 E_1 (GeV)

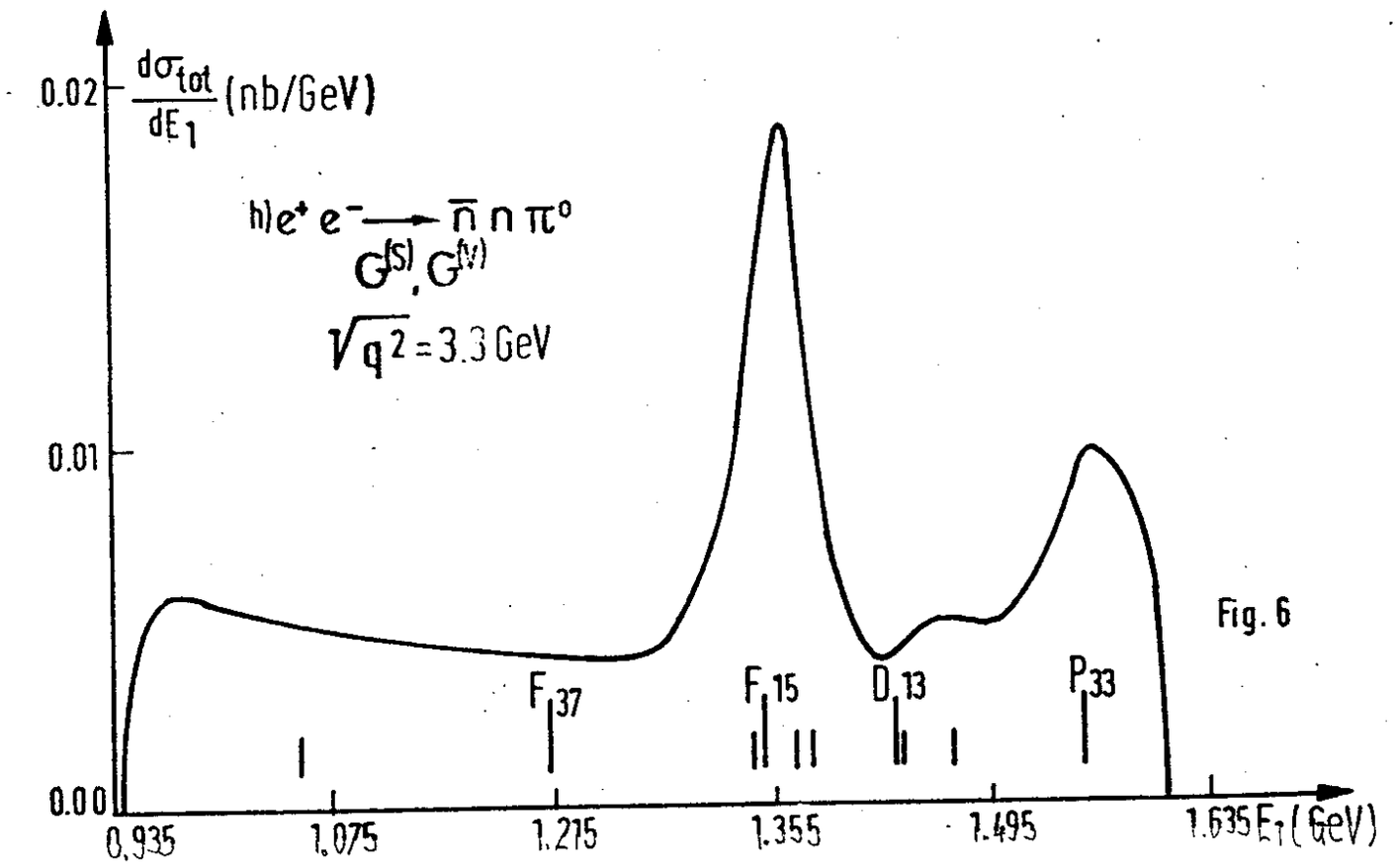
$\frac{d\sigma_{tot}}{dE_1}$ (nb/GeV)
0.02
0.01
0.00
h) $e^+ e^- \longrightarrow \bar{n}\, n\, \pi^0$
$G^{(S)}, G^{(V)}$
$\sqrt{q^2} = 3.3$ GeV
F_{37}
F_{15}
D_{13}
P_{33}
0.935
1.075
1.215
1.355
1.495
1.635 E_1 (GeV)

Fig. 6

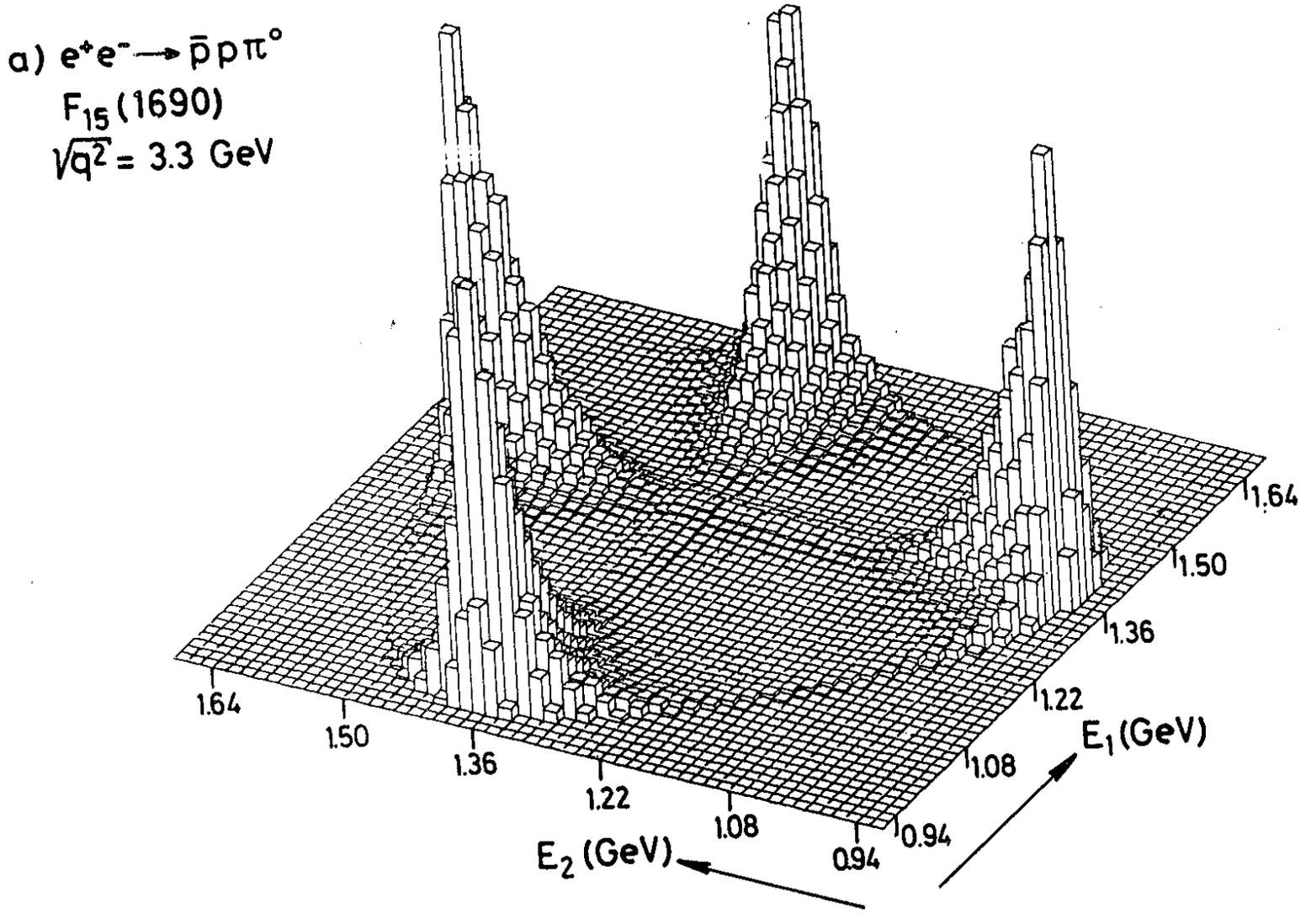
a) $e^+e^- \rightarrow \bar{p}p\pi^0$
$F_{15}(1690)$
$\sqrt{q^2} = 3.3$ GeV
1.64
1.50
1.36
1.22
1.08
0.94
E_2 (GeV)
1.64
1.50
1.36
1.22
1.08
0.94
E_1 (GeV)

Fig. 7

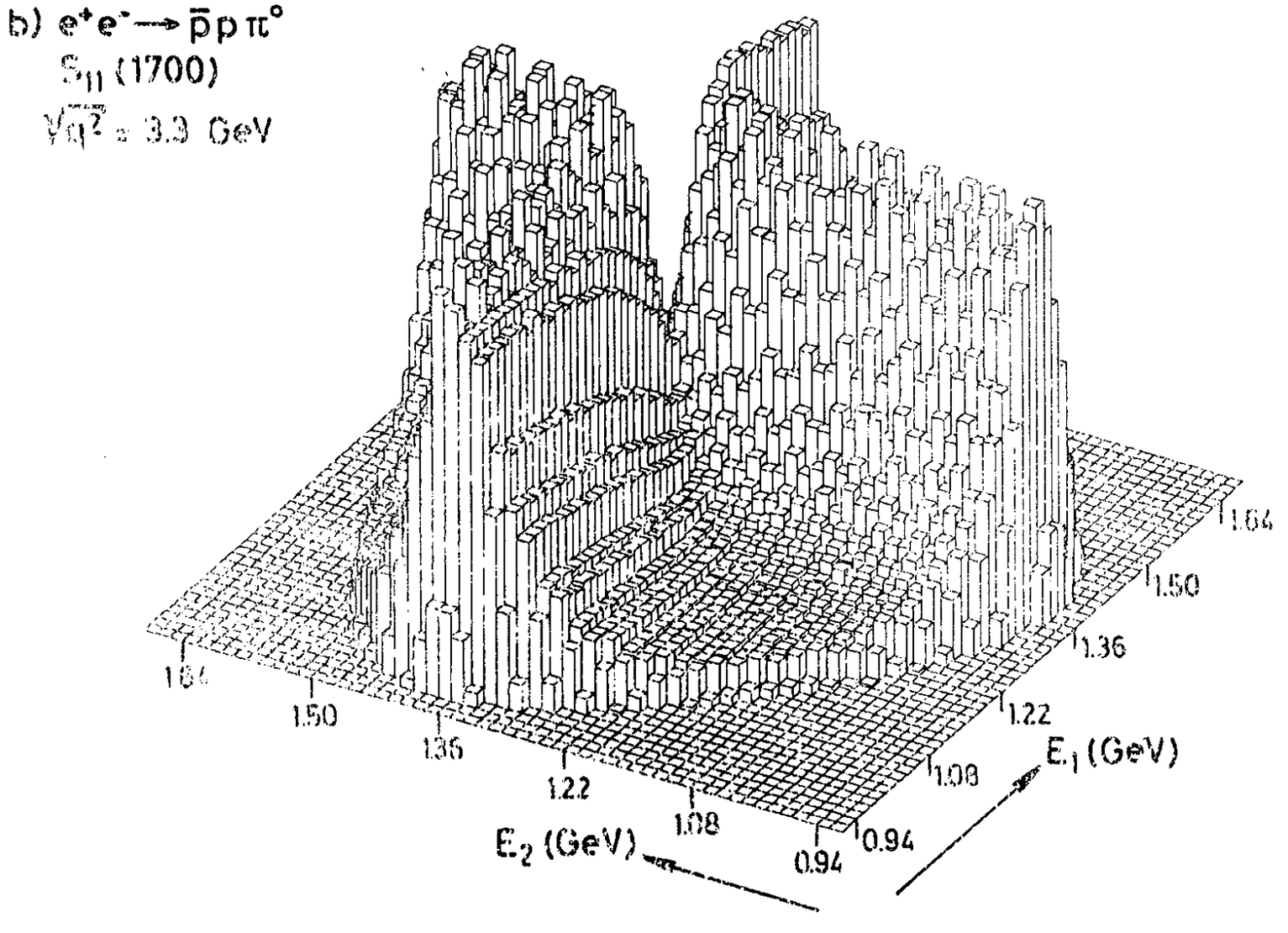
b) $e^+e^- \rightarrow \bar{p}p\pi^0$
$S_{11}(1700)$
$\sqrt{q^2} = 3.3$ GeV
1.64
1.50
1.36
1.22
1.08
0.94
E_2 (GeV)
1.64
1.50
1.36
1.22
1.08
0.94
E_1 (GeV)

Fig. 7

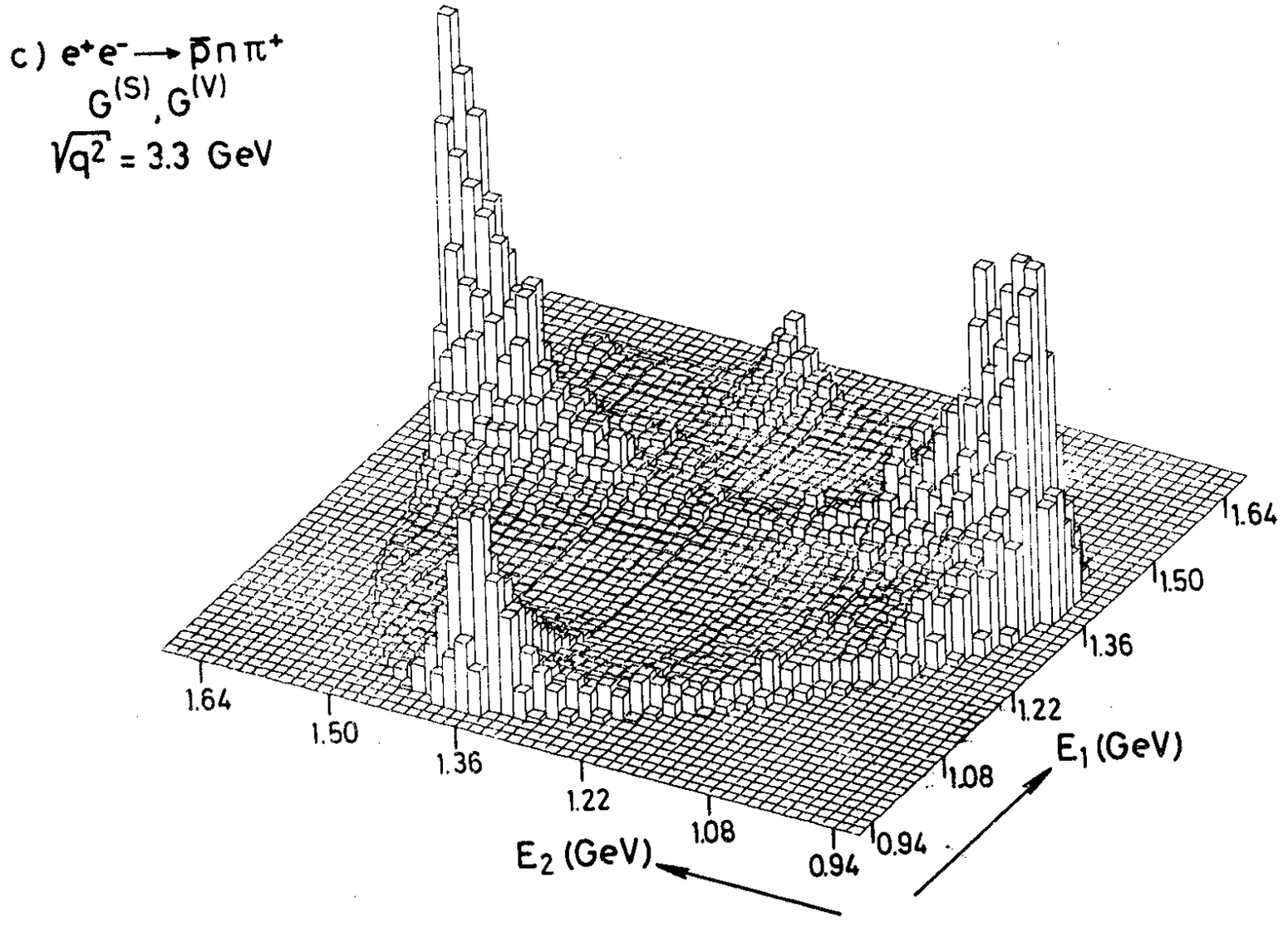
c) $e^+e^- \rightarrow \bar{p}n\pi^+$
$G^{(S)}, G^{(V)}$
$\sqrt{q^2} = 3.3$ GeV
1.64
1.50
1.36
1.22
1.08
0.94
E_2 (GeV)
1.64
1.50
1.36
1.22
1.08
0.94
E_1 (GeV)

Fig. 8

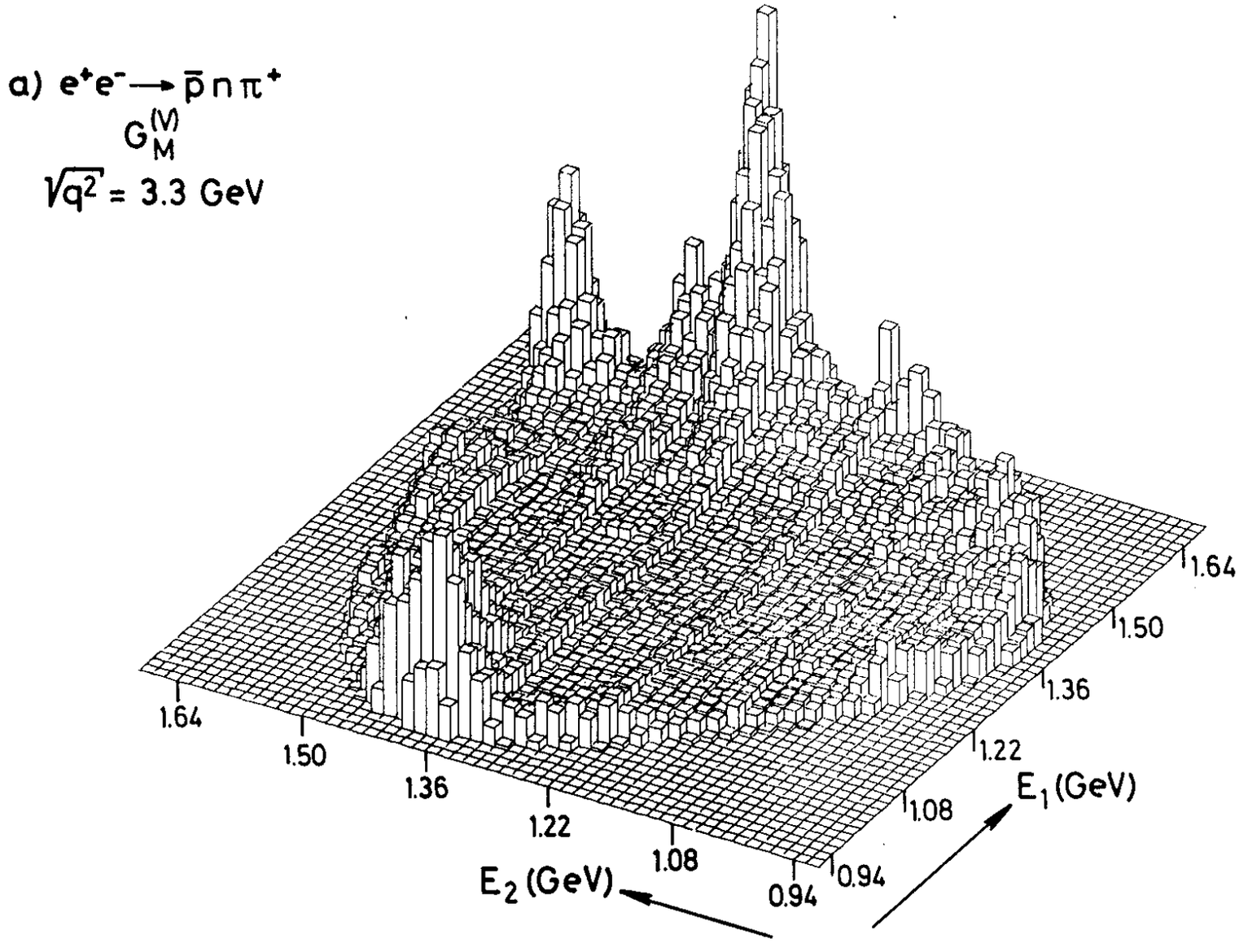
a) $e^+e^- \rightarrow \bar{p}n\pi^+$
$G_M^{(V)}$
$\sqrt{q^2}$ = 3.3 GeV
1.64
1.50
1.36
1.22
1.08
0.94
E_2 (GeV)
1.64
1.50
1.36
1.22
1.08
0.94
E_1 (GeV)

Fig. 8

d) $e^+e^- \longrightarrow \bar{p}p\pi^0$

$G^{(S)}, G^{(V)}$

$\sqrt{q^2} = 3.3$ GeV

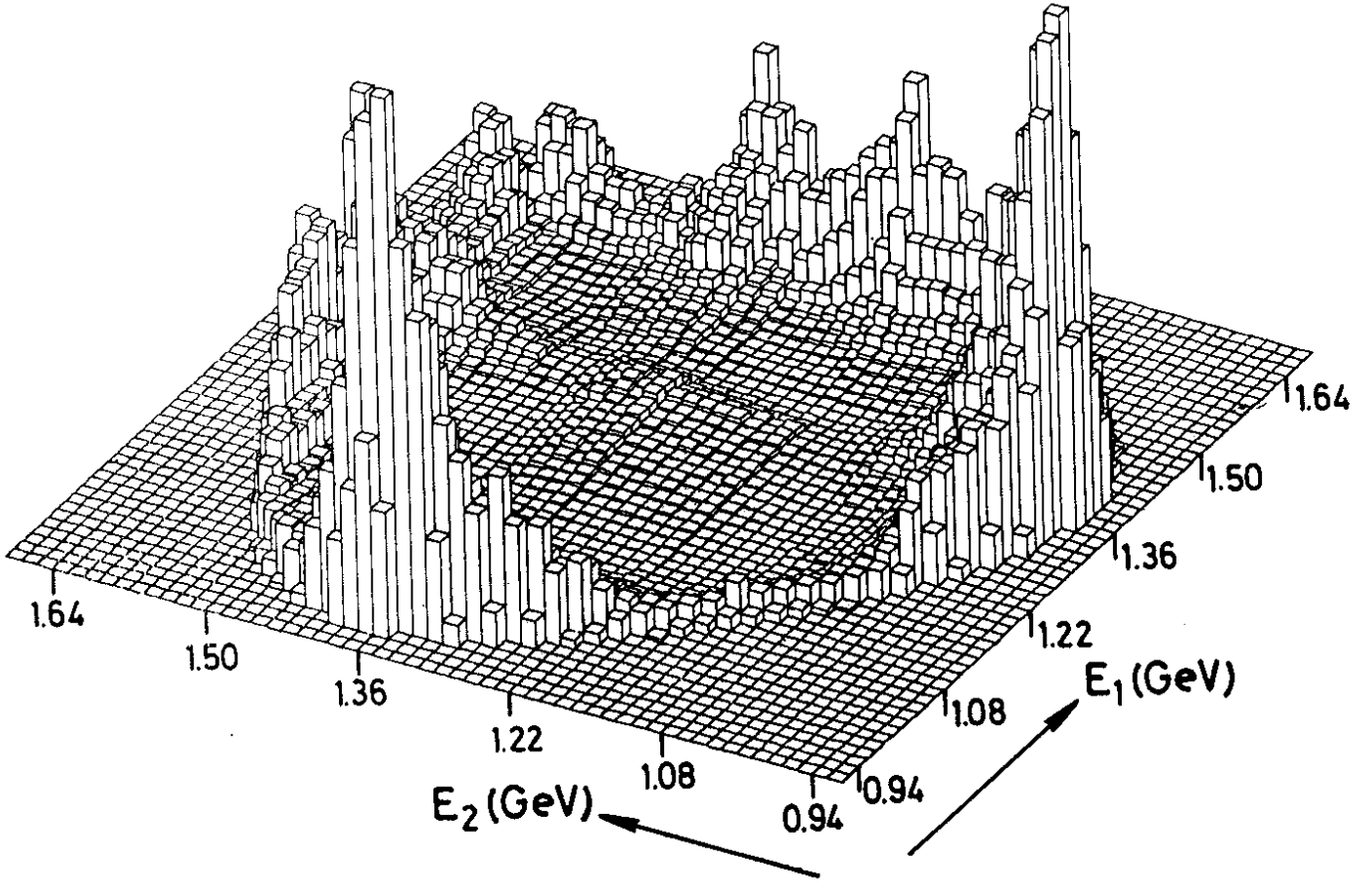

Fig. 8

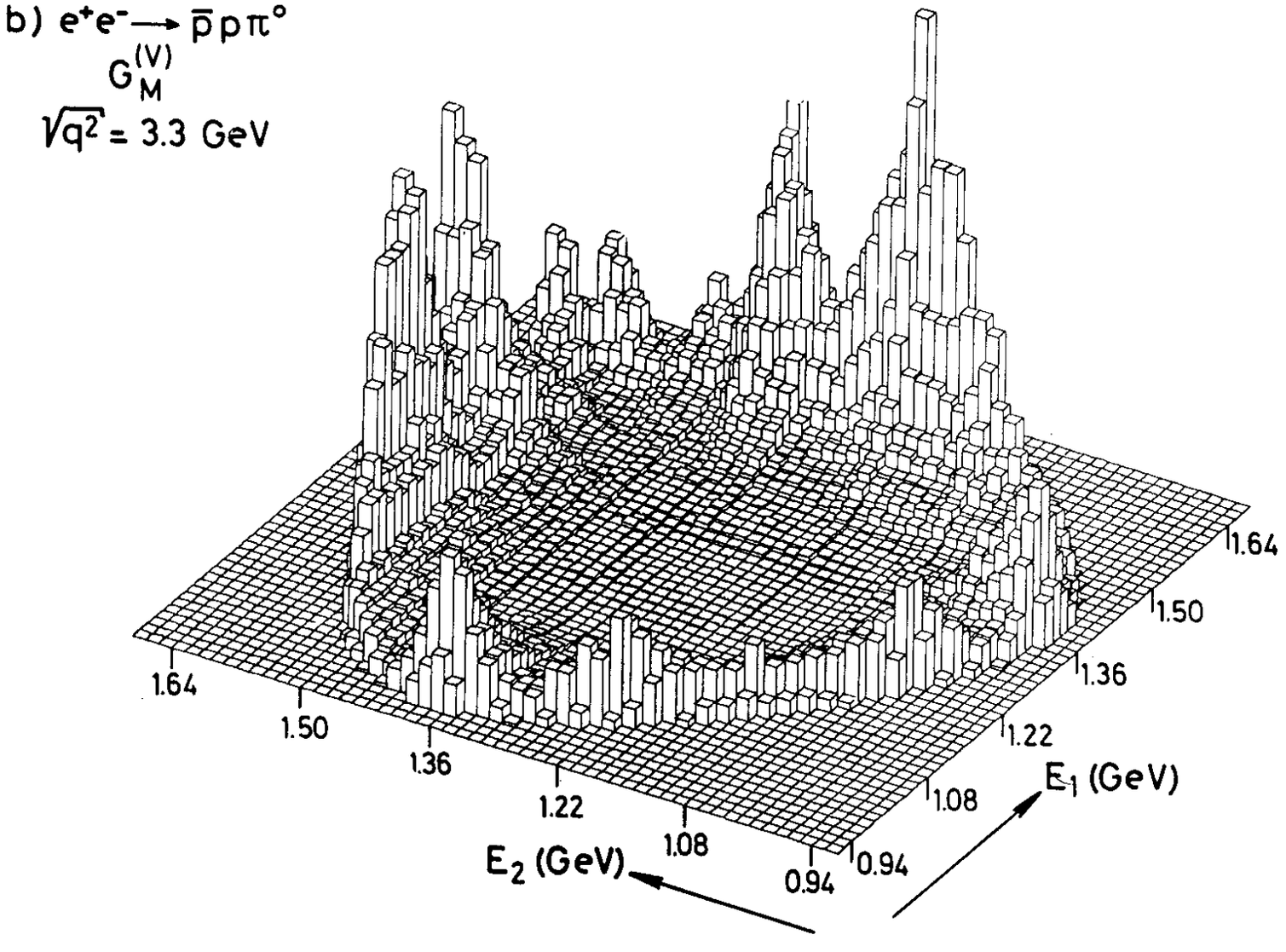
b) $e^+e^- \rightarrow \bar{p}p\pi^0$
$G_M^{(V)}$
$\sqrt{q^2} = 3.3$ GeV
1.64
1.50
1.36
1.22
1.08
0.94
E_2 (GeV)
1.64
1.50
1.36
1.22
1.08
0.94
E_1 (GeV)

Fig. 8

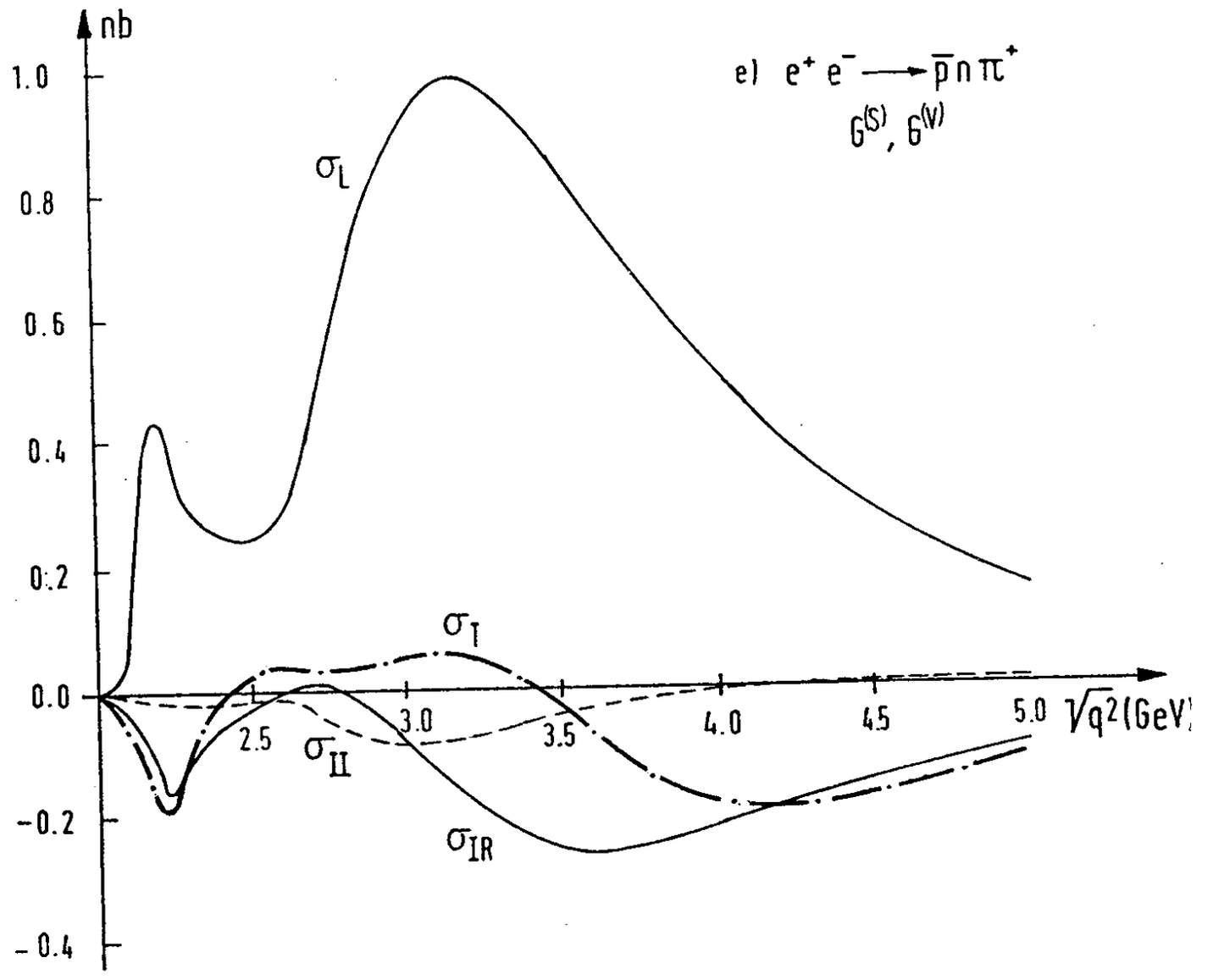
nb
1.0
0.8
0.6
0.4
0.2
0.0
-0.2
-0.4
e) $e^+e^- \longrightarrow \bar{p}n\pi^+$
$G^{(S)}, G^{(V)}$
σ_L
σ_I
σ_{II}
σ_{IR}
2.5
3.0
3.5
4.0
4.5
5.0
$\sqrt{q^2}$(GeV)

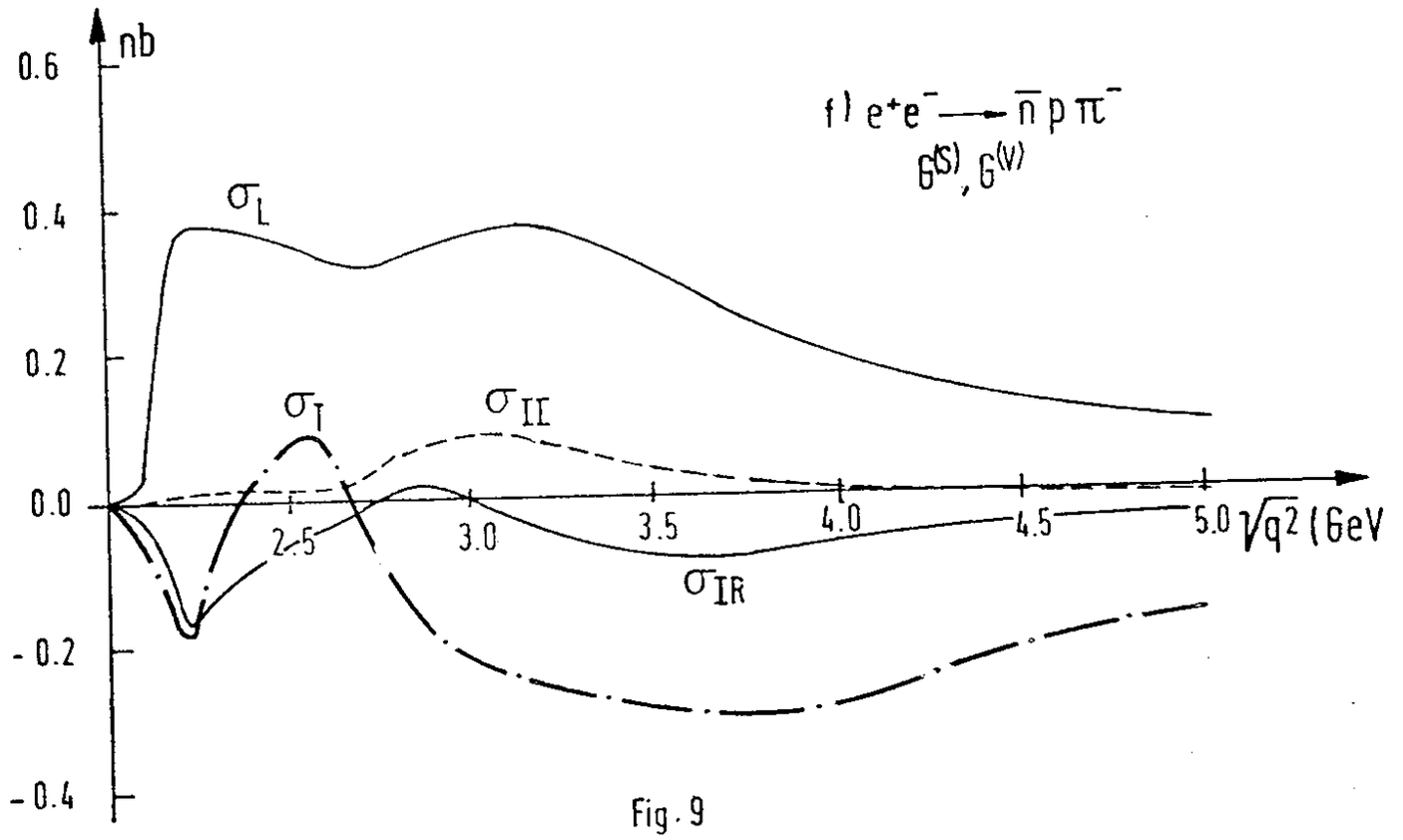
nb
0.6
0.4
0.2
0.0
-0.2
-0.4
f) $e^+e^- \longrightarrow \bar{n}p\pi^-$
$G^{(S)}, G^{(V)}$
σ_L
σ_I
σ_{II}
σ_{IR}
2.5
3.0
3.5
4.0
4.5
5.0
$\sqrt{q^2}$ (GeV

Fig. 9

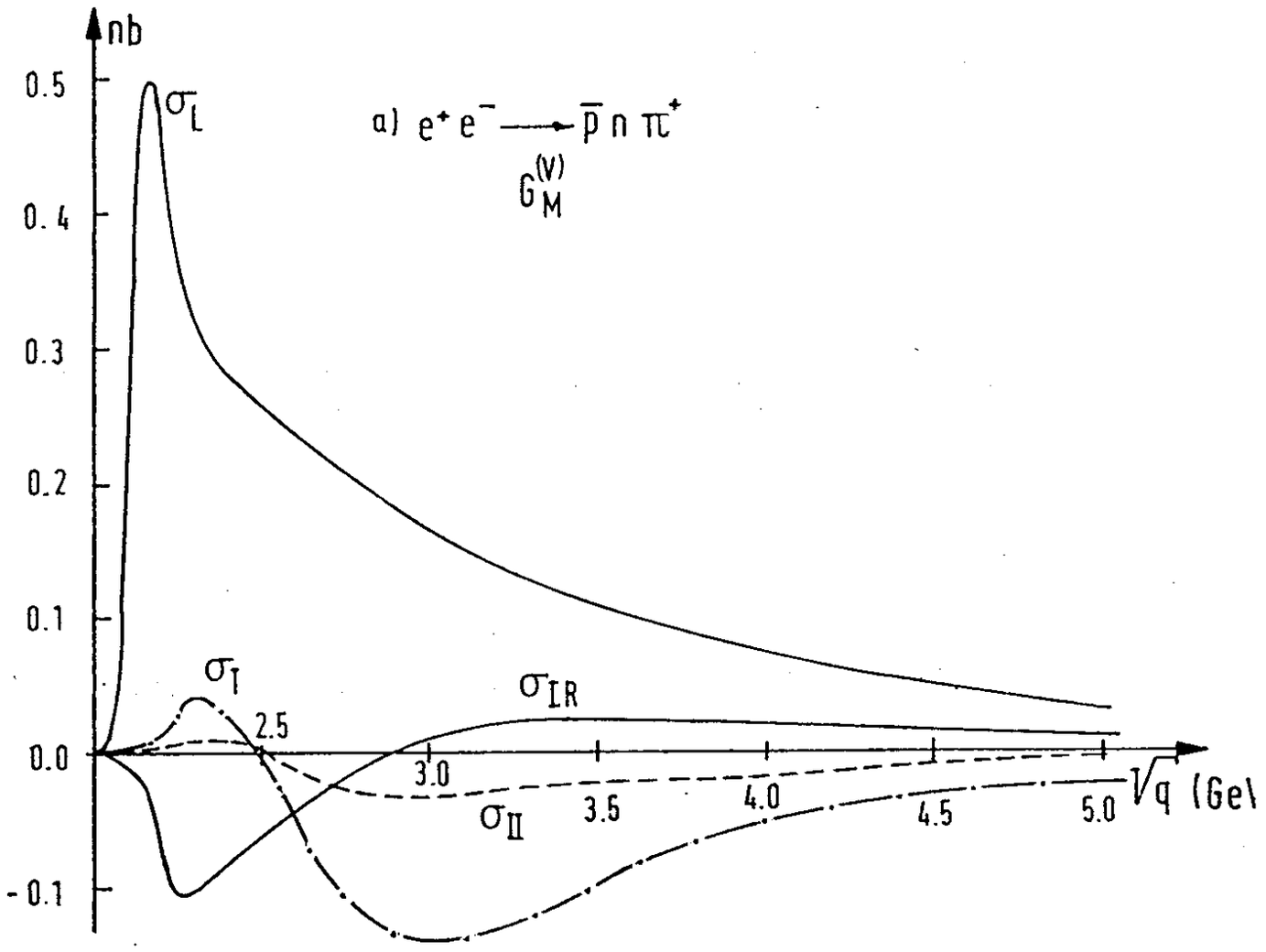
nb
0.5
0.4
0.3
0.2
0.1
0.0
-0.1
σ_L
a) $e^+e^- \longrightarrow \bar{p}\, n\, \pi^+$
$G_M^{(V)}$
σ_I
σ_{IR}
σ_{II}
2.5
3.0
3.5
4.0
4.5
5.0
$\sqrt{q}$ (GeV

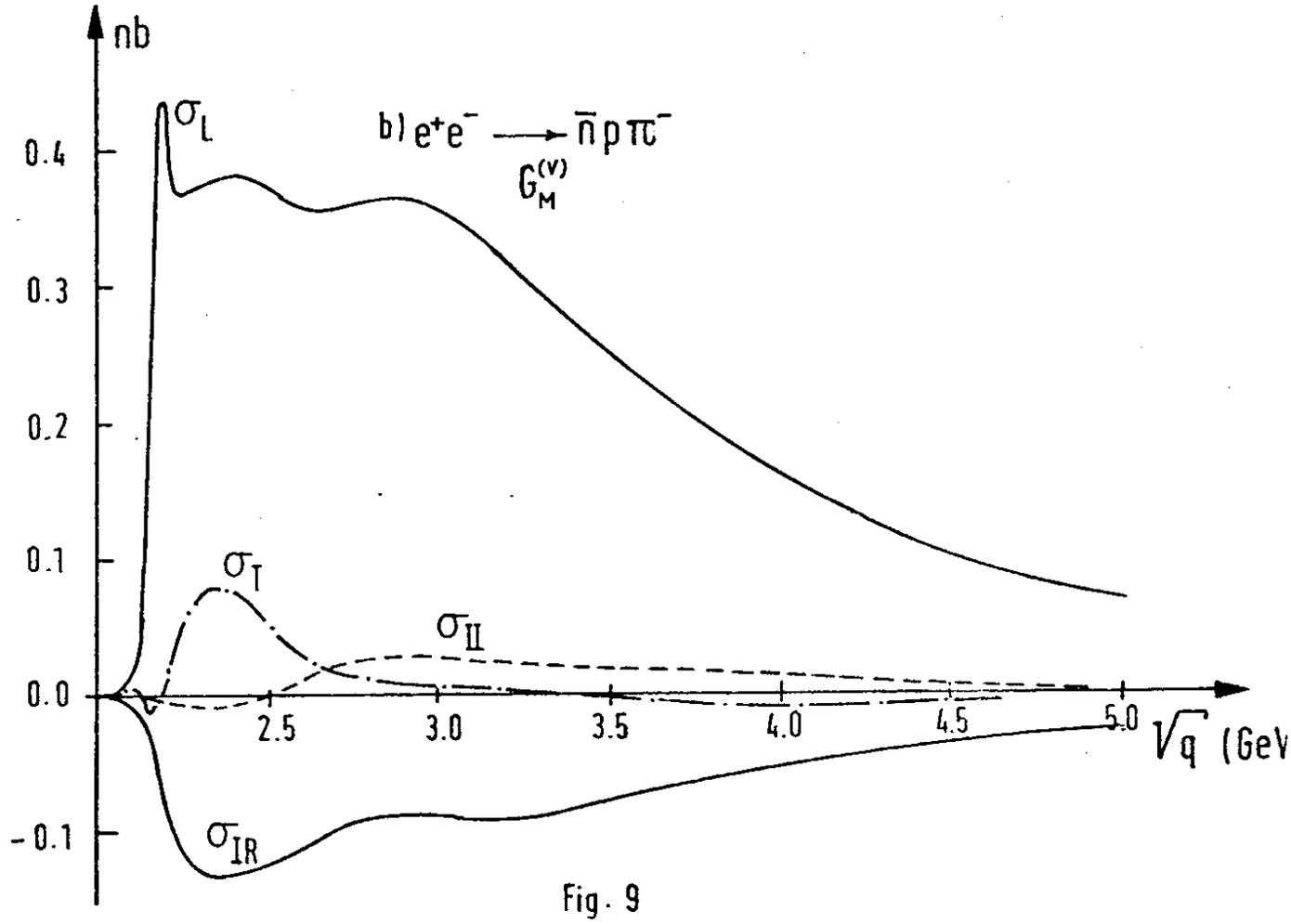
nb
0.4
0.3
0.2
0.1
0.0
-0.1
σ_L
b) $e^+e^- \longrightarrow \bar{n}\, p\, \pi^-$
$G_M^{(V)}$
σ_I
σ_{II}
σ_{IR}
2.5
3.0
3.5
4.0
4.5
5.0
$\sqrt{q}$ (GeV

Fig. 9

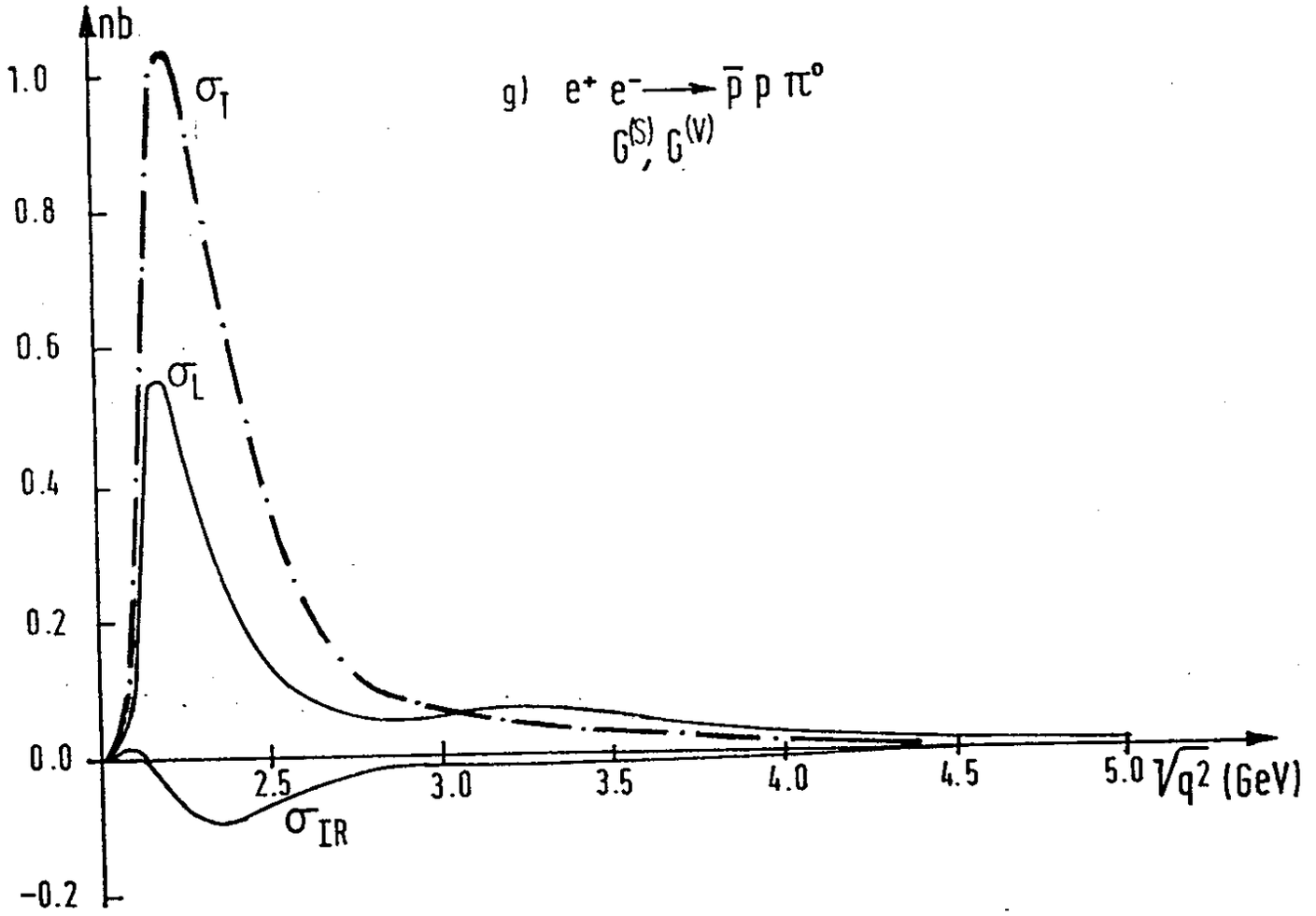
nb
1.0
0.8
0.6
0.4
0.2
0.0
-0.2
σ_T
σ_L
σ_{IR}
g) $e^+ e^- \longrightarrow \bar{p}\, p\, \pi^0$
$G^{(S)}, G^{(V)}$
2.5
3.0
3.5
4.0
4.5
5.0
$\sqrt{q^2}$ (GeV)

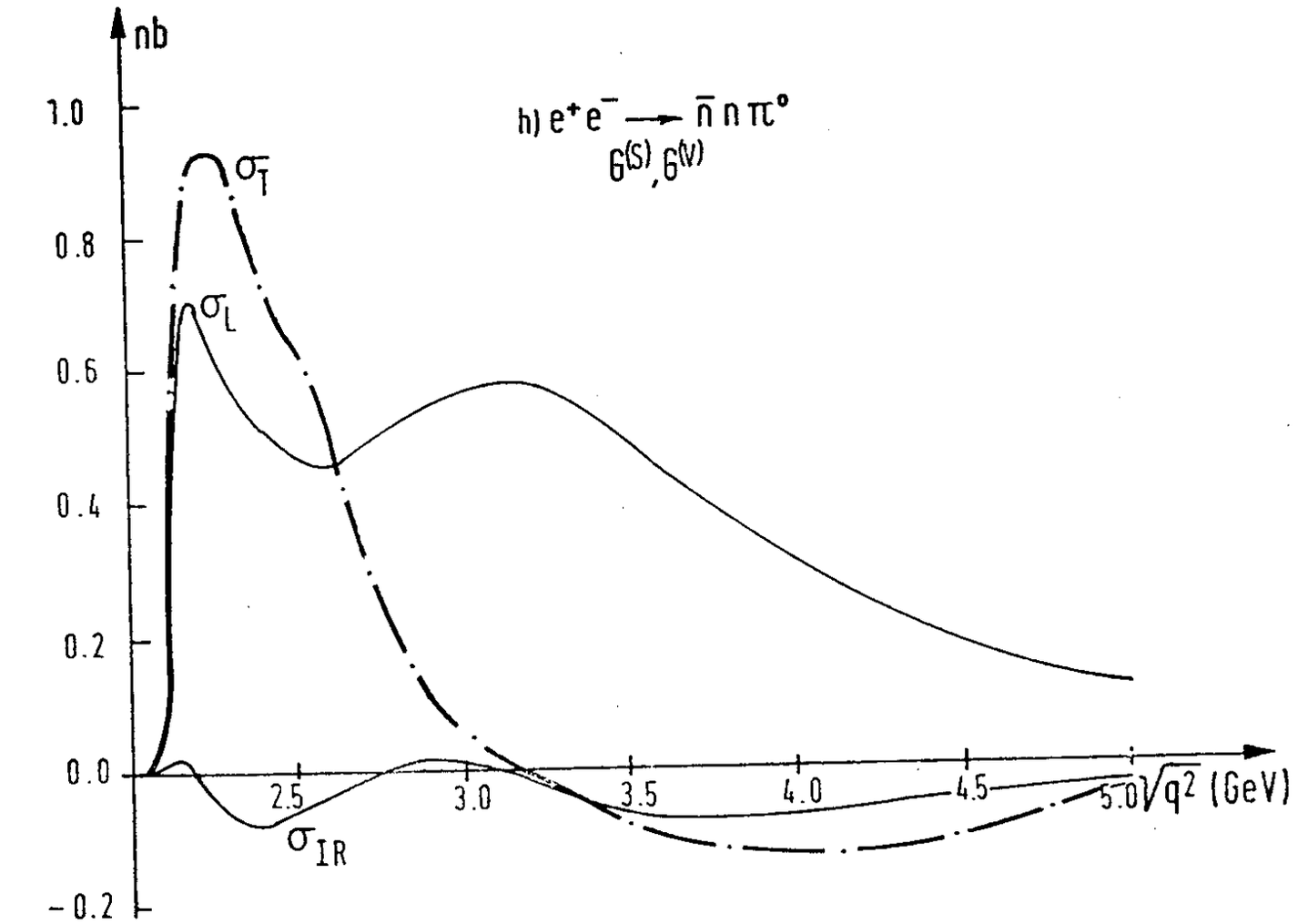
nb
1.0
0.8
0.6
0.4
0.2
0.0
-0.2
σ_T
σ_L
σ_{IR}
h) $e^+ e^- \longrightarrow \bar{n}\, n\, \pi^0$
$G^{(S)}, G^{(V)}$
2.5
3.0
3.5
4.0
4.5
5.0
$\sqrt{q^2}$ (GeV)

Fig. 9

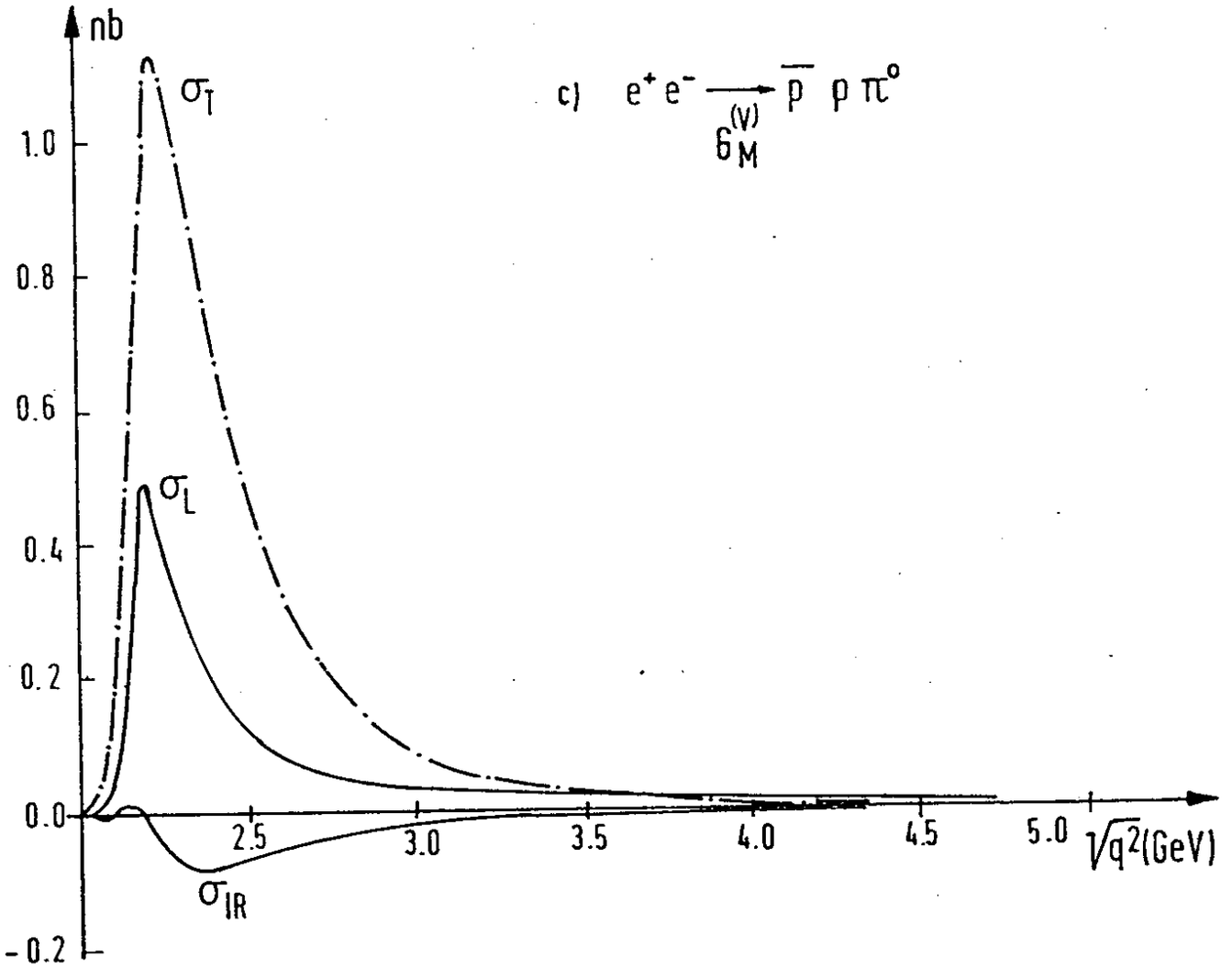
nb
σ_T
c) $e^+e^- \xrightarrow[G_M^{(V)}]{} \bar{p}\, p\, \pi^0$
1.0
0.8
0.6
0.4
0.2
0.0
-0.2
σ_L
σ_{IR}
2.5
3.0
3.5
4.0
4.5
5.0
$\sqrt{q^2}$(GeV)

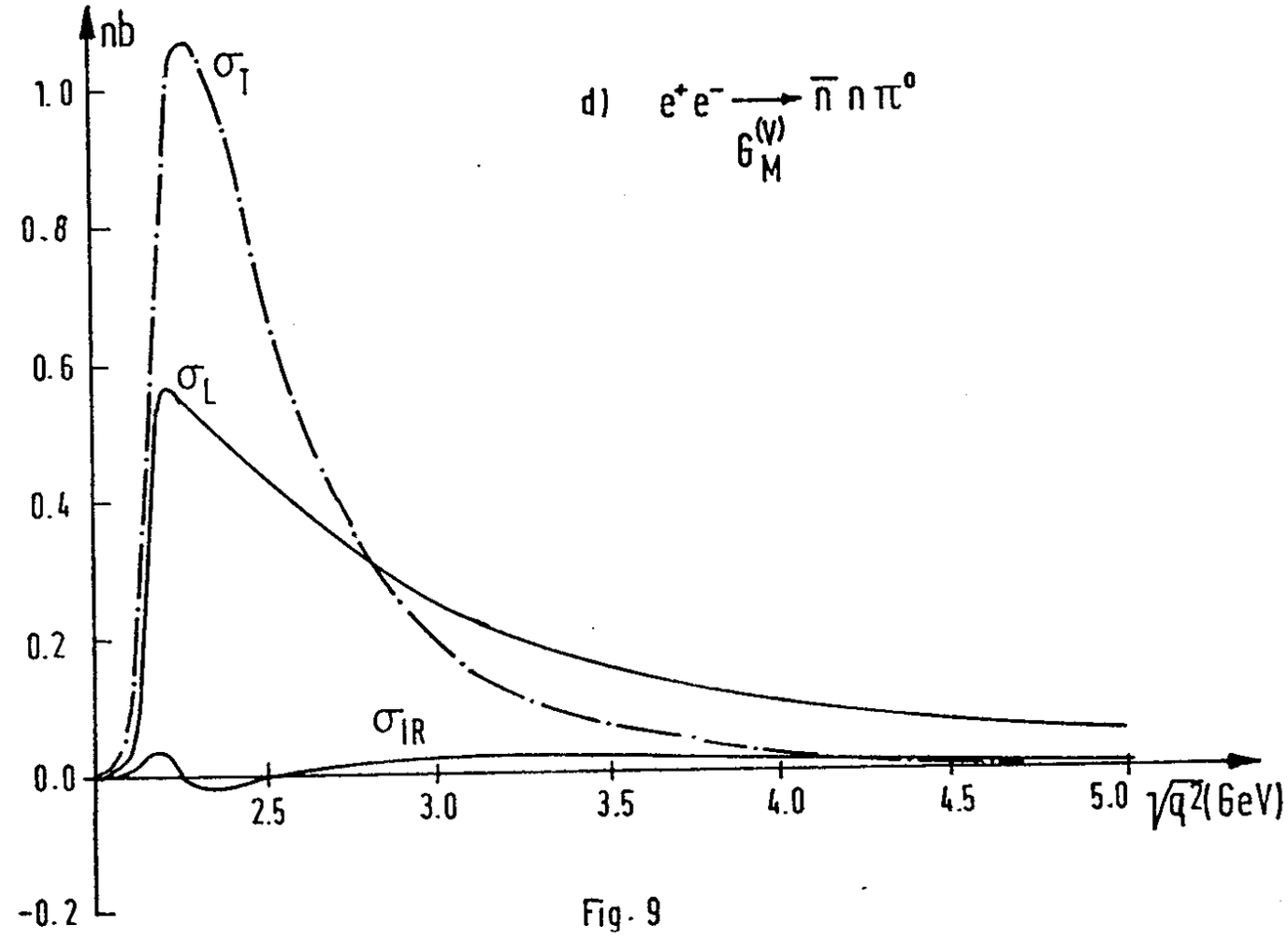
nb
σ_T
d) $e^+e^- \xrightarrow[G_M^{(V)}]{} \bar{n}\, n\, \pi^0$
1.0
0.8
0.6
0.4
0.2
0.0
-0.2
σ_L
σ_{IR}
2.5
3.0
3.5
4.0
4.5
5.0
$\sqrt{q^2}$(GeV)

Fig. 9